UNIVERSIDAD DE VALLADOLID

ESCUELA DE INGENIERIAS INDUSTRIALES

MÁSTER EN INGENIERÍA INDUSTRIAL

"Ray Trace Modeling in a Solar Secondary Concentrator with Various Inlet Shapes"

Autor:

Cerezo Aguado, David

María Teresa Parra Santos

San Diego State University

Valladolid, Julio 2018.

TFM REALIZADO EN PROGRAMA DE INTERCAMBIO

TÍTULO: "Ray Trace Modeling in a Solar Secondary Concentrator with Various Inlet Shapes"

ALUMNO: David Cerezo Aguado

FECHA: 22/06/2018

CENTRO: COMBUSTION & SOLAR ENERGY LABORATORY

TUTOR: Dr. Fletcher J. Miller

ABSTRACT

Renewable energies are turning into a necessity instead of an alternative, and solar energy is the major future source of inexhaustible free energy. This thesis is focused on Concentrated Solar Power plants, which use heliostats to concentrate solar radiation in a relatively small area to heat a fluid; finally, this fluid directly or indirectly drives a turbine to generate electricity. In the past, the radiation entered the receiver directly through a quartz window. In this research a secondary concentrator (SC) is added to the system to concentrate the sunlight through the Small Particle Heat Exchanger (SPHER) quartz glass window. The radius of the SC inlet is bigger than the domed window radius, so the receiver area for the solar irradiation is increased. Therefore, if the SC is added, the size of the window can be reduced (to obtain the same amount of energy incident in the window) and the heat losses will also decrease.

MIRVAL (a Monte Carlo Ray Tracing software) is used for the ray tracing from the sun to the Secondary Concentrator (SC), including the interaction with a real heliostat field. Once the rays reach the inlet of the Secondary Concentrator (SC), a FORTRAN code is used to study the interaction between the rays and the SC shape, which will be defined first as a shape in SOLIDWORKS and finally as a mesh in ANSYS. The FORTRAN output will be graphed in MATLAB in order to get the spatial distribution of the power absorbed in the SC. In addition, a new SC shape will be added to the code and tested in order to get a polyvalent code that can be used to test with different SC shapes for different heliostat field designs. With several SC shapes we will be able to optimize both parameters, SC shape and heliostat field design.

In this thesis a method to graph the distribution of power absorbed for different secondary concentrator shapes has been developed. The main variables in the simulations (number of rays and number of cells) will be studied and several simulations will be graphed at different times of the day and year.

KEYWORDS: Concentrated Solar Power (CSP), Secondary Concentrator (SC), Small Particle Heat Exchanger (SPHER), High Flux, Ray Trace, and MIRVAL.

ACKNOWLEDGEMENTS

DAVID CEREZO AGUADO

Table of contents

LIST OF FIGURES

LIST OF TABLES

ACRONYMS

C&SEL	Combustion and Solar Energy Laboratory
CPC	Compound parabolic concentrator
CSP	Concentrated solar power
GHG	Greenhouse gas
HEX-HEX	Hexagonal inlet & hexagonal outlet
HEX-ROUND	Hexagonal inlet & round outlet
HTF	Heat transfer fluid
MCRT	Monte Carlo ray tracing
PV	Photovoltaics
ROUND-ROUND	Round inlet & round outlet
SC	Secondary Concentrator
SDSU	San Diego State University
SPHER	Small Particle Heat Exchange Receiver

1. INTRODUCTION.

1.1 Solar Energy

Energy is a key in the society developing and is strongly linked to social and economic growth. The concern about finding a sustainable source of energy is increasing since the population has been increasing and the resources available in the world are getting depleted [1][2].

The renewable energies are turning into a necessity instead of an alternative. Currently the energy production is based on techniques and resources which endanger human health and are unsustainable. About 80% of carbon dioxide emissions and two-thirds of total greenhouse gas (GHG) emissions worldwide are caused by energy production and utilization [3]. The two ways to reduce these emissions are to increase energy efficiency and renewable energy [4][5].

In 2008, for first time, developed countries' GHG emissions were surpassed by the developing countries' GHG emissions. And in the last years, the developing countries CO_2 emissions keep growing constantly, since energy demand is proportional to economic growth [3]. Trying to cover this growing demand with non-renewable energy sources is an unsustainable solution since they are exhaustible and limited sources of energy. Some of these countries have perfect features to develop more solar energy facilities because of the great amount of solar irradiation that they receive [2].

Solar energy is the major future source of inexhaustible free energy. Every year 5×10^4 EJ ($EJ = 10^{18}$J) harvestable solar energy arrives on the earth. The energy that the earth receives from the sun each hour is equivalent to current yearly primary energy supply of the world [6].

1.2 Concentrated solar power.

The CSP technology concentrates the sunlight in a relatively small *target area* by mirrors or a lens. In this manner, a high temperature is achieved in a small area and the heat losses are decreased [7]. These types of facilities are postulated to be the one of the most

representative options in the change to renewable energies [8]. As a function of the geometry there are four generic CSP technology types [7][9][10]. They are shown in Figure 1. The parabolic trough and the Linear Fresnel Reflector are classified as '"Line focus type" since the receiver, typically a steel tube, is linear. Because of the same argument, the Central Receiver and the parabolic dish are classified as "Point focus type", where the radiation is focused on the receiver. The Point focus type facilities are able to get higher concentration ratios, but they need a more precise tracking [10].
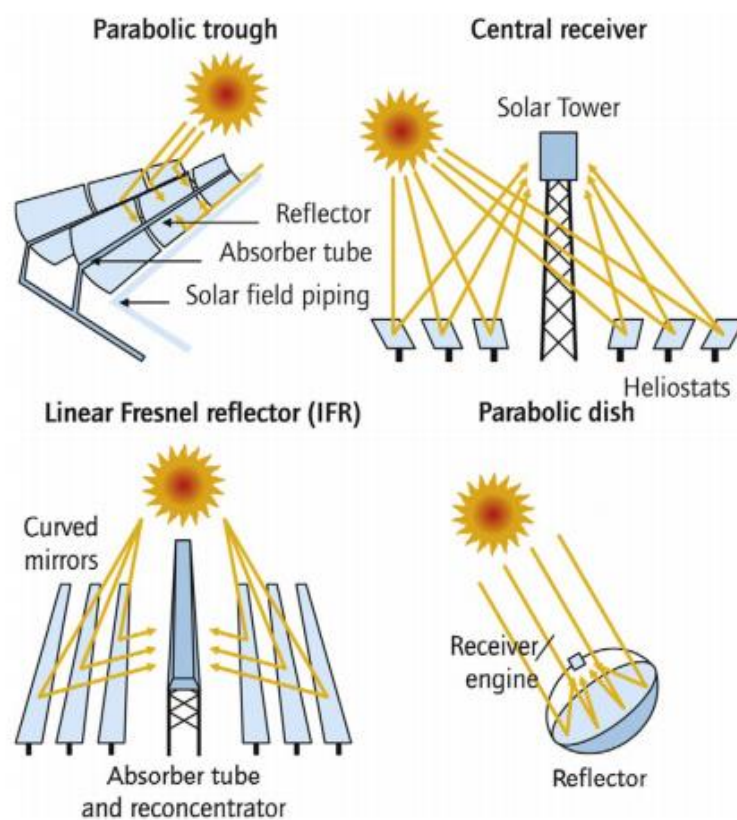
Figure 1. Typical solar concentrators in CSP plant: parabolic trough concentrator (top left), linear Fresnel reflector (bottom left), Central receiver (top right) and parabolic dish concentrator (bottom right). At the left the line focus type technology and at the right the point focus type technology. [7][11]

In this research, the Central Receiver CSP will be studied, and in Figure 2, a scheme of how one of these plants works is shown, specifically for the combined cycle (Brayton-Rankine). The heliostat field is formed by tracking mirrors, which reflect the sunlight and focus it on the target plane of the solar power tower, where the solar receiver is located. Then, the rays hit the solar receiver window and the heat is used to increase the temperature of a secondary fluid in a heat exchanger. Then that fluid is used in a power

cycle (Rankine, Brayton, Combined… depends on the temperature that it is possible to reach in each case) [10][12][13] where the turbine movement is used to obtain electricity.
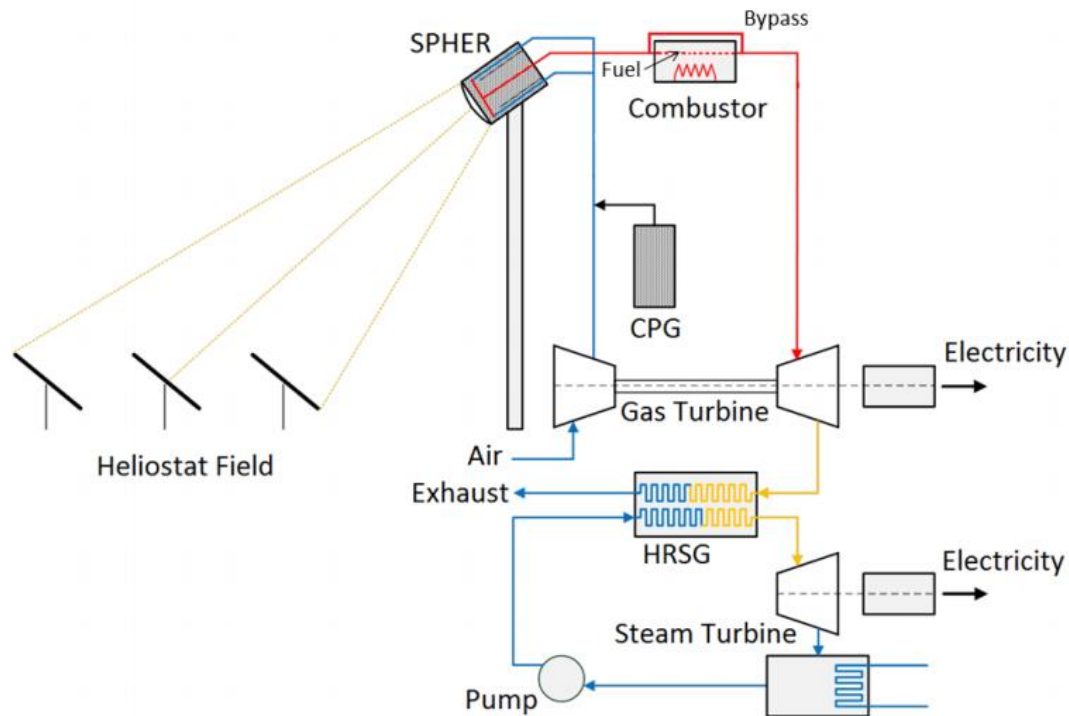
Figure 2. Combined cycle diagram with the Small Particle Heat Exchanger [14]

The solar power tower is faced to the North and the heliostat field is located in front of it (Figure 3, left), but the heliostat field, can be increased in the other directions (Figure 3, right). Several different distributions of the heliostat field were studied in previous researches for the SDSU C&SEL [15].

Probably the most important drawback of CSP, and solar energy in general, is the uncertain time when that energy can be used to obtain electricity. In addition, the price of the electricity, which varies as a function of the demand; it is usually more expensive when it is not possible to get it from the solar energy [5][16]. Therefore, if it is not a constant energy, and it is not possible to control the time to obtain it, a good storage system or a hybrid system, will offer a reliable and efficient electricity resource.
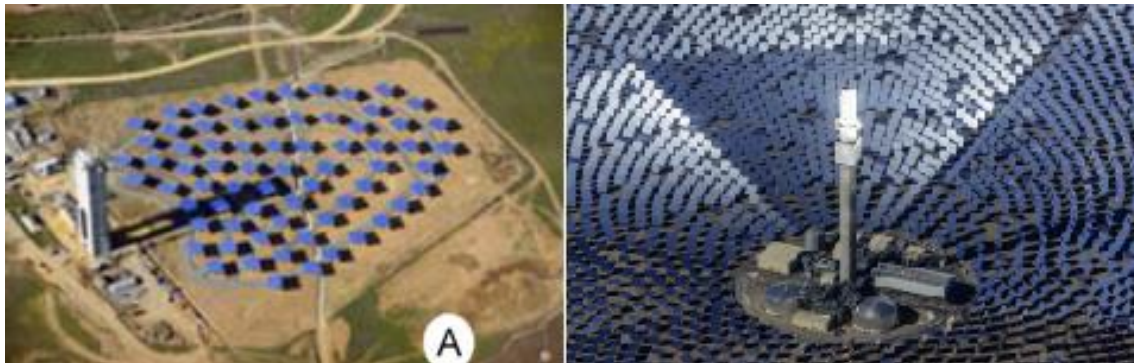
Figure 3. Solar Tower CSP facility with only one direction heliostat field. (SOLUGAS project at the Solucar Platform in Seville (left)) and heliostat field distributed in all directions at the Crescent Dunes CSP Plant(right) [9][10] (Modified)

The two main solutions to get this are: first, burning fossil fuel or biomass during periods of no sunshine. Second, using thermal energy storage (TES) systems to store the heat energy during the period of sunshine and use it when the solar irradiation is not enough to obtain electricity from the sunlight [5]. The San Diego State University (SDSU) Combustion and Solar Energy Laboratory (C&SEL) is currently researching these storage methods, specifically in the simulation and validation of a Single Tank Storage System. There are three types of TES (sensible heat storage, latent heat storage and thermo-chemical heat storage). The sensible heat storage systems are the most developed and there are already some CSP with this technology [5].
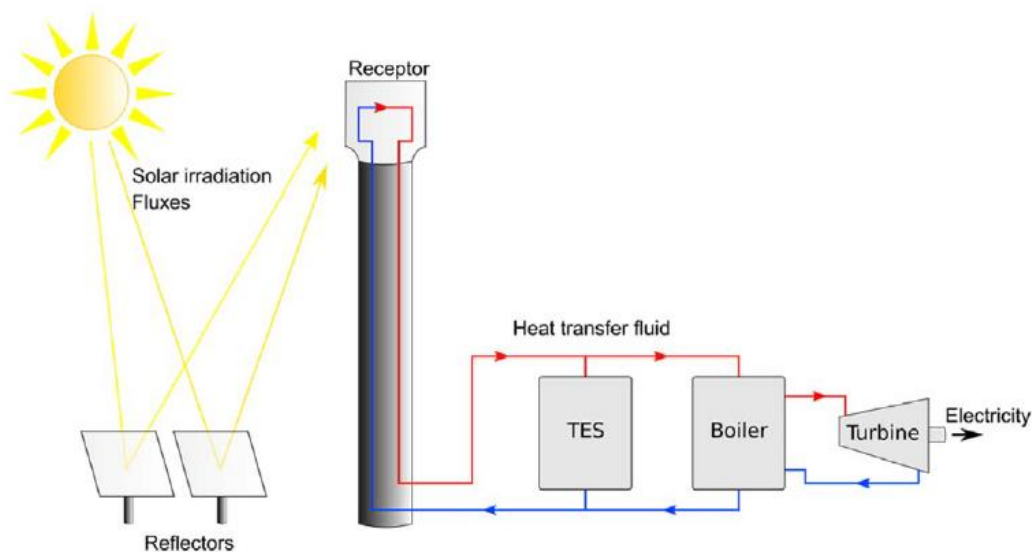
Figure 4.Scheme of a CSP plant with the thermal energy storage (TES) integrated [5]

DAVID CEREZO AGUADO

A scheme of how the TES works is shown in Figure 4. Part of the fluid, once it has been already heated, is used in the TES, instead of directing all of it to the power cycle.

CSP plants are turning into a good investment, since the price to obtain electricity from this technology is getting lower and lower every year, and the goal for the 2020 is set at 6¢/kWh [17] and 3¢/kWh for 2030. For this reason, countries like the US or China are planning to increase the number of CSP plants. Figure 5 shows the aspirational combined capacity planned for 2020. Spain has already a combined capacity greater than the U.S., however, since there has been an unstainable growth, there it is not objectives to add more capacity in the near future [10].
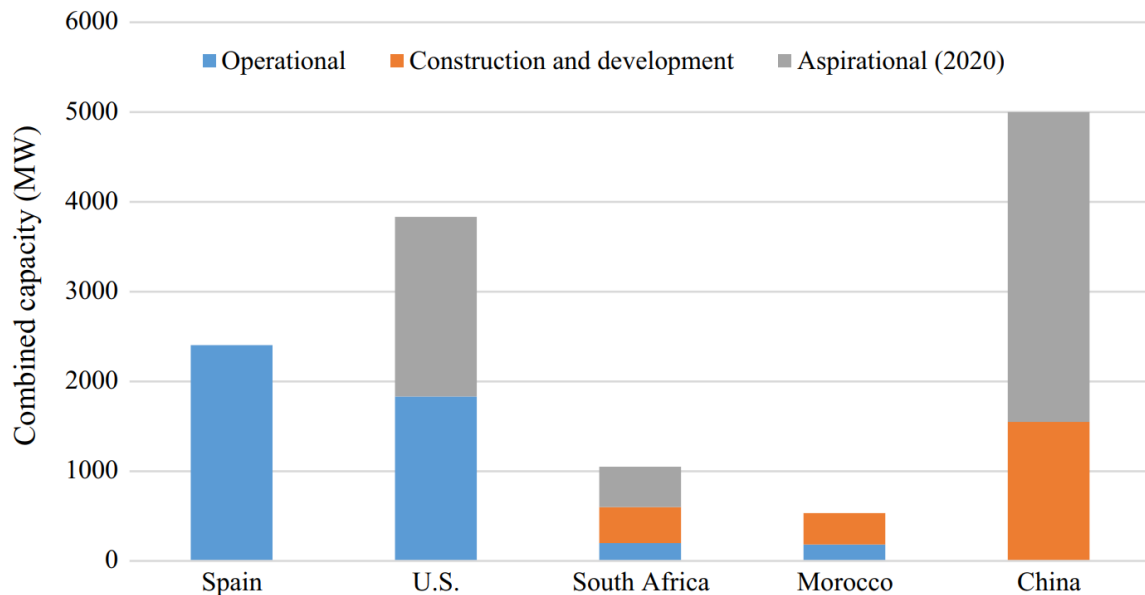
Figure 5. Combined operating, construction and development, and aspirational CSP capacities for selected countries. ''Aspirational (2020)'' capacities are subjectively estimated from announcements or planned projects at risk up to about 2020. [10].

Another alternative, in order to improve the global efficiency, consists on combining the CSP, with the PV and use TES in the system. The CSP plant will provide a stable power output to reduce the PV system fluctuations. [16]

.

1.3 Small Particle Heat Exchange Receiver

The fluids which are being employed currently in other CSP plants (thermal oil, molten salts, direct steam…), are used as heat transfer fluids (HTFs) [18]. The choice of the fluid will influence the performance of the facility. The HTFs are heated by the surfaces which contain them, specifically, by the solar irradiation reaching the pipes. This technology involves three main problems. First, because of the sequence of the heat exchange, the temperature at the pipe is always higher than the temperature at the fluid, increasing the thermal losses. Second, these materials have a degradation temperature around 800K, so the Rankine cycle of the CSP Plant has to work in temperatures below the optimum (the optimum temperature for the Rankine cycle is about 1000 K), decreasing the performance [12] [19]. Third, and linked to the second problem, the Rankine cycle requires a large amount of cooling water, and most of the CSP plants are located in dry regions [19] [20].
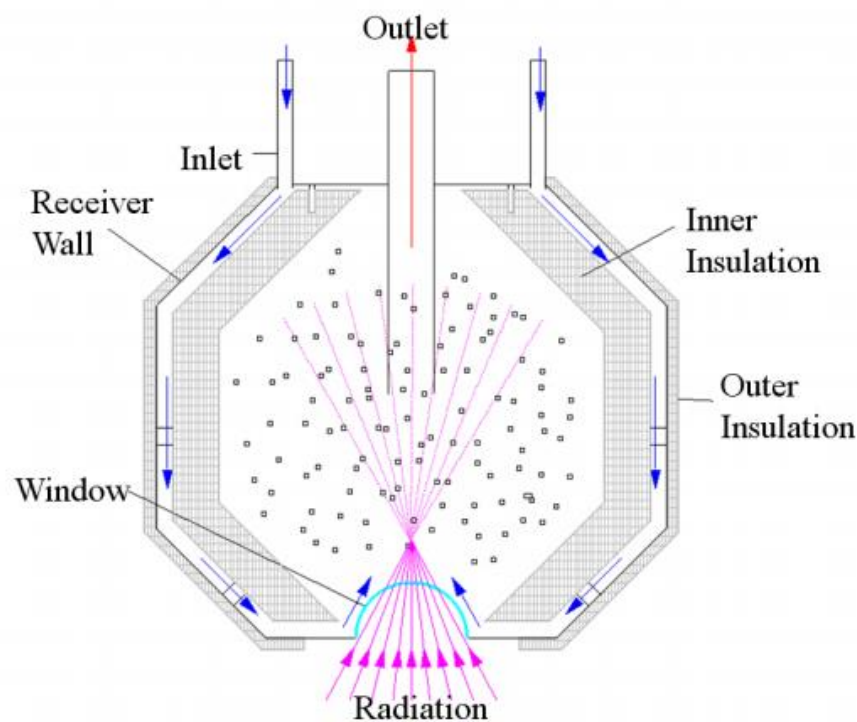
Figure 6. Particle solar receiver concept.[21]

Regarding these problems, a new method for the heat exchange was proposed [22][23].

The Small Particle Heat Exchange Receiver (SPHER), it is a pressurized vessel, which has a window, where the solar radiation enters and is used to directly heat a fluid [24].

This SPHER scheme is shown in the Figure 6. This method is based on heating a gas which will be used to power a Brayton cycle. The fluid is a mixture of air and carbon nanoparticles, which absorb volumetrically the solar irradiation. The particles at the inflow absorb the solar radiation and their temperature increases for heating, by conduction, the gas stream [24]. This mixture can be heated above 1300K, and can be used not only for a Brayton Cycle, but also for a combined cycle since the optimum temperature for both cycles are 1100 K and 1300 K respectively [12][25]. There are no degradation problems for the mixture in that temperature interval [19]. During the heating, the nanoparticles reach high temperatures and oxidize, and that is the reason there are no particles in the outflow [21].

During the last years, in addition to the research about Brayton cycles, supercritical CO_2 Brayton cycles have been studied. [10] [13]. Figure 7 shows the thermal conversion efficiency as a function of the turbine inlet temperature. It is clear how the efficiency is increased when it is possible to get higher temperatures at the inlet for the power cycle previously mentioned. The supercritical fluid has the best features of Rankine and Brayton since the exhaust heat is recovered. In addition, these fluids have a low compressibility, so the energy used to compress it is lower than others [13].

The SPHER method also offers the possibility to develop solar chemistry. With this technology a solar reactor for the steam-gasification of carbonaceous materials was simulated [19][26]. Moreover, a hybrid system can be created adding fuel injectors because of the simplicity of the receiver. Thus, the system is able to produce electricity in cloudy days or evening [23].
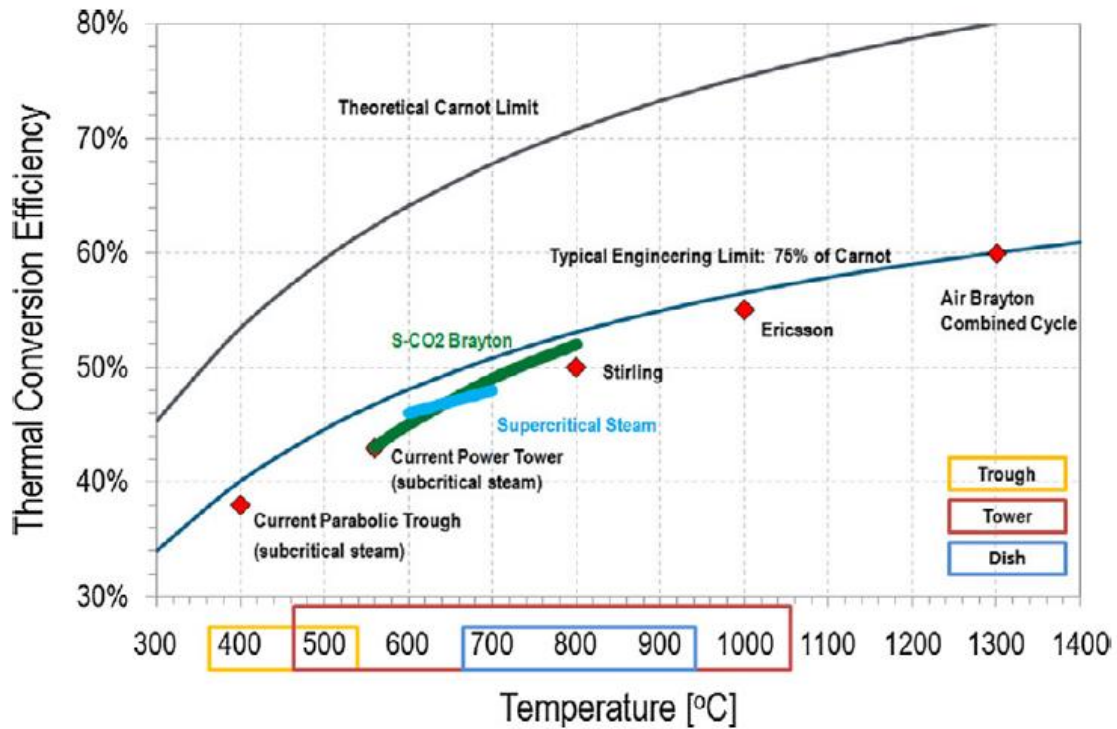
Figure 7. TCE in a CSP Plant for different power cycles in function of the temperature at the turbine inlet [13]

1.4 Secondary concentrator

The secondary concentrator (SC) is used to concentrate the sunlight through the SPHER quartz glass window. Figure 8 shows a scheme of the SPHER without and with the SC shown. The yellow arrows represent the sunrays hitting in the domed window. The SC used in CSP are non-imaging concentrators, where the rays entering to the SC are not reproduced in the distribution of rays at the exit, and these are simpler geometrically than the imaging concentrators used typically in telescopes [17][27][28][29].

The SC inlet is located at the target plane described in the section 2.4.1.1. The radius of the SC inlet is bigger than the domed window radius, so the receiver area for the solar irradiation is increased. The outlet is located in the plane of the edge of SPHER's quartz window, so all the solar rays exiting the secondary concentrator hit the window and (if they are not reflected) enter the receiver. An earlier study of the flux distribution was performed on the dome window for a very specific shape of secondary concentrator [29].
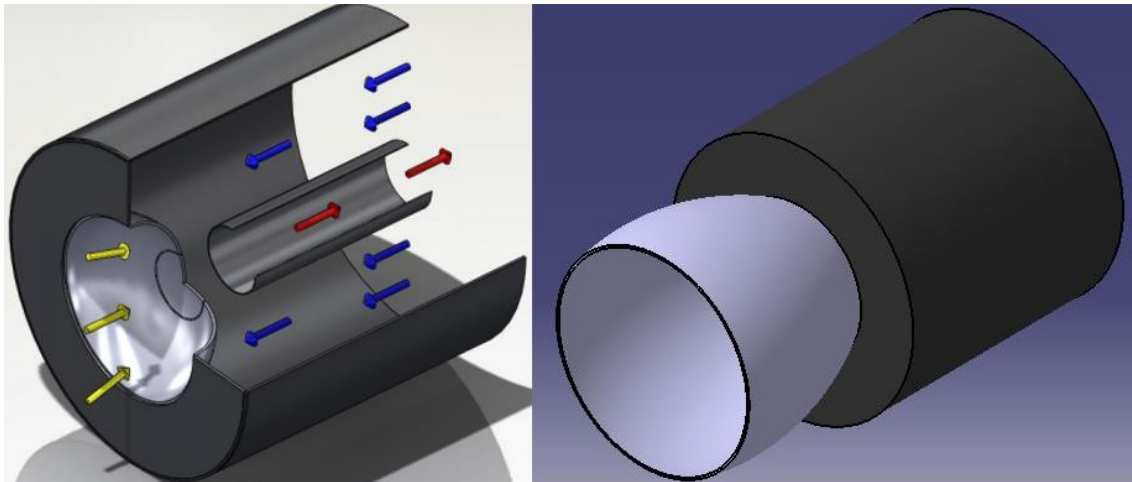
Figure 8. Small Particle Heat Exchanger Receiver (SPHER) with no secondary concentrator (SC) (left), where the rays (yellow arrows) are hitting the window to heat the fluid. At the right, the SC is already added. The SC outlet is located at the window, and now the SC inlet has a larger diameter than the window diameter. [19] (Modified)

In previous research, the Compound Parabolic Concentrator (CPC) was tested computationally, since it has been demonstrated theoretically that with this shape the maximum concentration ratio is obtained in 2D [30]. At the SDSU C&SEL the flux distribution from a 3D CPC was calculated; a FORTRAN code was developed for this calculation [29]. The CPC is the most efficient shape in 2D, but in 3D there is not a theoretical method to calculate the optimal solution. To test other shapes of interest, the code was improved in order to be able to include any SC shape that can be drawn in computer-aided drawing software (ANSYS method) [17]. The purpose of this improvement is not only to test different shapes and to obtain the most effective, but also to test shapes that can be located together in the target plane, without loss of space [31].

Previous researchers tested other SC shapes, but with physical models [32]. These SC shapes are shown in the Figure 9, and every time that it is necessary to accomplish a minimum change in the SC shape, a new SC must be manufactured. In addition, those 3D shapes cannot be defined by an equation. However, with the ANSYS method, for including different shapes, only the inlet and outlet shape must be added in the FORTRAN code. So for example, the curvature of the faces can be changed without changing the code, it is only necessary to change the input meshes; being able to run different shapes with the same code.
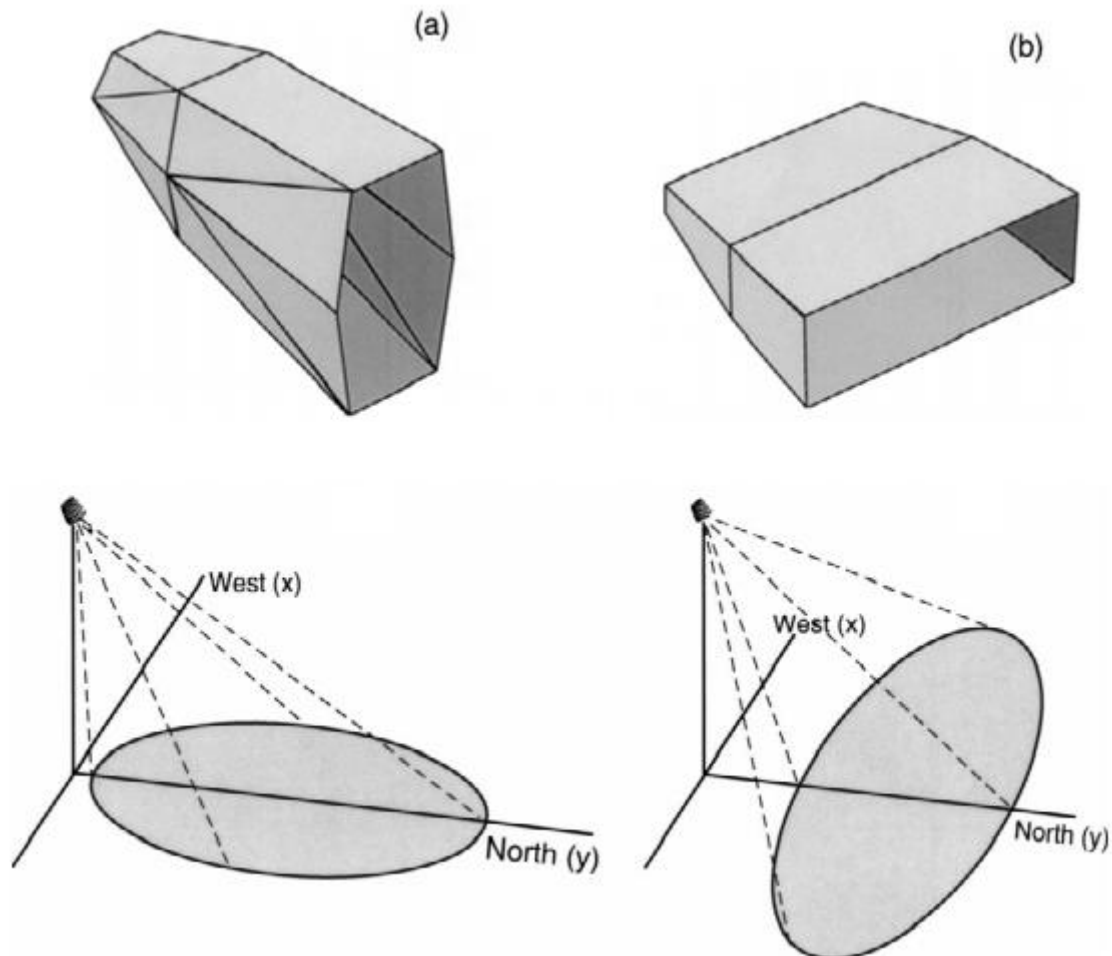
Figure 9. Secondary Concentrators (non-definable by equation) shapes tested physically. At the lef t(a), SC with a hexagonal irregular inlet and a hexagonal regular outlet designed for a north-heliostat field. At the right (b), SC with rectangular irregular inlet and outlet designed for an east-west wide heliostat field. [32] (Modified)

The Figure 9 shows the two different shapes that were tested for different heliostat field distributions. The first one (a), at the left, is designed for a north- heliostat field, and for this reason, the SC inlet is bigger in the vertical direction than the horizontal direction. The second one (b) is designed for an east-west wide heliostat field, and the horizontal length is bigger in order to adapt the SC inlet to the optimum shape, which can reach a higher ratio of rays reaching the window after entering trough the SC inlet. [32]

When the size of the heliostat field is increased progressively, it is necessary to include new SCs due to the spot size from the furthest heliostat. The CPC SC has round inlets, which cannot be put together without losing space between the respective inlets. A SC with hexagonal inlet and round outlet was tested for this reason since the inlets can be

DAVID CEREZO AGUADO

joined by the edges (Figure 10) and hexagonal inlet/hexagonal outlet because of the easier manufacturing compared to the previous configuration [17]; one example of this configuration in a real CSP is shown in the Figure 10. In this thesis a new non-axisymmetric inlet is proposed, in order to test new shapes that can provide a greater power reaching the window. The heliostat angular extent is different in the two orientations, for this reason, the new SC shape tested has different lengths in vertical and horizontal direction, similar to the one discussed above. In addition, it will give the possibility of testing computationally if the new SC shape can increase the power reaching the window in the case that a new or unusual heliostat field shape is designed. For example, if the heliostat field of a current CSP plant starts to be increased.
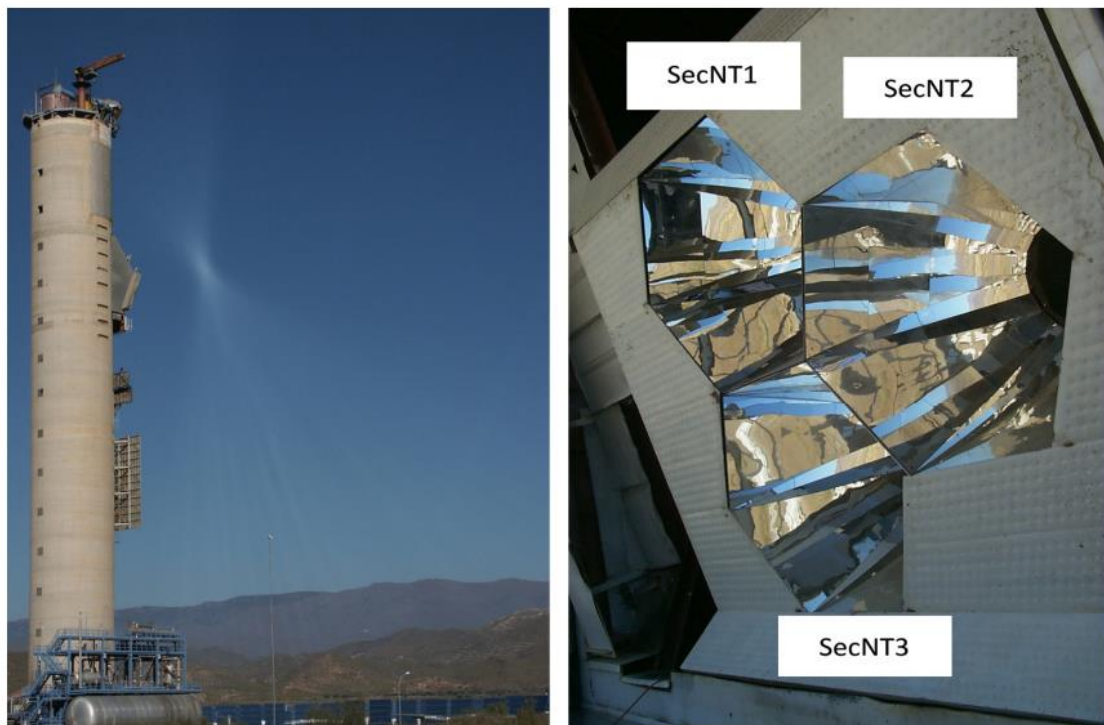
Figure 10. Secondary Concentrator with Hexagonal inlets to avoid the loss of space [31]

In order to check how the SC increases the power reaching the window several simulations are run. First, the simulations are performed without a SC and with a circular target plane with $\emptyset$ = 1.7m. Then, a CPC with $\emptyset_{OUTLET}$ ≈ 1.7m and $\emptyset_{OUTLET}$ ≈ 2.4 m is

added to the system and both powers reaching the windows are compared. The simulations time are 12 pm, 2 pm and 4 pm respectively. The Table 1 shows these results.

Table 1. Increase of power reaching the window when the CPC is added to the system, for March 21.

March 21, $3 \cdot 10^7$ rays	12pm	2pm	4pm
Total power reaching window without CPC (MW)	5.319	4.592	2.322
Total power reaching window with CPC (MW)	5.450	4.881	2.718
% Total power increase	**2%**	**6%**	**15%**

At 12 pm the power increases about 2% if a CPC is added. This value increases from 2% to 6% and 15%, at 2 pm and 4 pm respectively. This is the expected results, since at 12 pm the flux in the target plane will be more centered because the sun position is centered too. When the sun is moving from that position, the flux is not that centered and the CPC collected more rays in proportion, which otherwise, wouldn't reach the window. However, it will be demonstrated how the power reaching the window can decrease, if the SC shape it is not well designed. It is necessary to note that the size or the window without the CPC is sized previously to allow practically all the radiation from the given heliostat field. If the window were smaller, the differences would be greater. A interesting calculation that could be accomplished would be to calculate how much smaller the window could be (in the case that the CPC is added) for obtaining the same power than in the non-CPC case.

1.5 Objective of this Trabajo Fin de Master

In this chapter the characteristics of a CSP plant, and the main parts of them, have been explained. In addition, it is explained how the CSP is postulated to be one of the main technologies allowing us to reduce dependence on fossil fuels. The constant decrease of the cost to produce electricity with this technology is reflected in the aspirations of increasing the capacity of production of this renewable energy technology. However, it is necessary to keep researching to optimize every part of the CSP plant in order to increase as much as possible the efficiency, and therefore to decrease the cost of producing electricity with this technology.

DAVID CEREZO AGUADO

In the SDSU C&SEL several theses have been already done in various areas of CSP, and others are currently underway with the goal of developing a receiver capable of supplying a Brayton cycle with hot, pressurized air. This Trabajo Fin de Master is focused on one part of the CSP plant, specifically on the secondary concentrator. In previous research, the SC was added to the SPHER to determine the flux patterns on the window and additional gain of power, but the FORTRAN code first developed only permits the inclusion of a SC that can be defined by an equation [29]. Using the FORTRAN code, and the ray tracing software (MIRVAL), it is possible to get the power reaching the window in the SPHER for a defined heliostat field. The heliostat field can be increased, but the way it can be increased depends on the inlet size and the acceptance angle of the SC. Next, that FORTRAN code was modified to be able of include a SC with any shape [17]. In this method, the SC shape is designed in SOLIDWORKS and converted into an ANSYS mesh.

The objectives of this Trabajo Fin de Master are:

- The FORTRAN code will be modified so the target plane can be bigger than the SC inlet. Therefore, it will be possible to calculate the percentage of rays, which are hitting inside and outside of the SC inlet.

- To define the number of rays necessary to obtain a stable response in the simulation of the power absorbed in any SC shape. To verify if the number of rays used in previous researches is enough to consider the simulation as valid.

- To test if the number of surfaces used in the meshes can be decreased and how the results vary when that decrease is done, since a lower number of cells for the same shape, means a shorter simulation time.

- The main objective consists of modifying the code to calculate the spatial distribution of energy absorbed in any shape of SC during the course of the day. The program to generate the ray tracing is MIRVAL. The FORTRAN code will be used to calculate the power absorbed in the SC at different times of the day through "power runs", and after several simulations the curve of energy absorbed

during the day can be approximated. The Figure 11 shows a couple of these curves, in which is represented the total power absorbed in the SC at different moments of the day. As it will be demonstrated later, the curve is practically symmetric around 12pm. For this reason, data for the CPC are graphed at 8 am, 10 am, 12 pm, 2 pm and 4 pm, but for the hexagonal-hexagonal SC only data at 12 pm, 2 pm and 4 pm are graphed.

- The power distribution in the SC will be graph with MATLAB in 3D. This information will be calculated in order to obtain the parameters to design a cooling system if necessary.
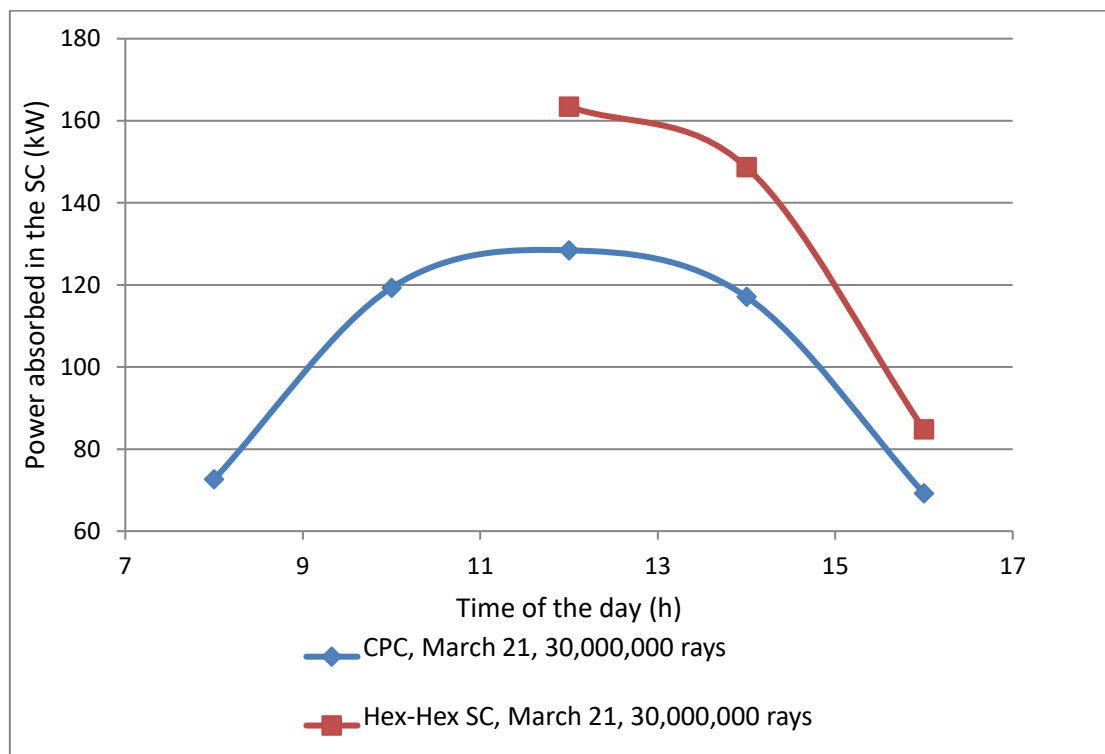
Figure 11. Energy absorbed in the SC curve obtained from several "power runs" at different moments of the day.

- Now that it is possible to test any shape, the second objective will be test a new non-axisymmetric inlet; to test if this shape can provide a greater power reaching the window. The heliostat angular extent is different in the two orientations, for this reason, the new SC shape tested with the new ANSYS method has different lengths in vertical and horizontal direction;.

2. SIMULATION

2.1 Monte Carlo Ray Tracing

Only a few problems of thermal radiation can be solved by exact solutions, and various numerical techniques are the alternative. For easy cases, it is possible to use conventional methods, but when the problem becomes complex, it is necessary to use Monte Carlo method [33]. The comparison of the effectiveness of these two methods when the complexity of the problem is increased is shown in the Figure 12.
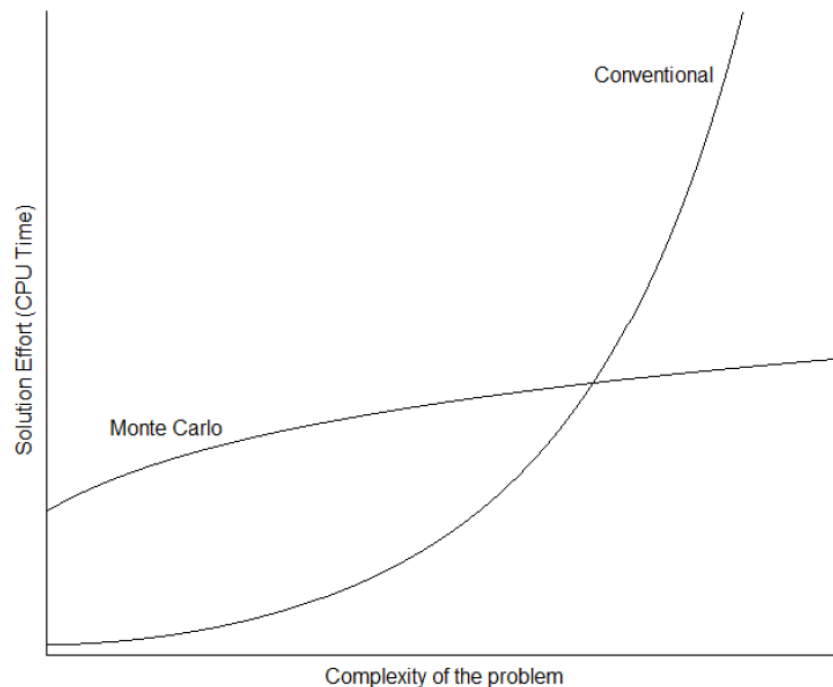
Figure 12. Comparison of Monte Carlo method and conventional solution techniques when the complexity of the problem is increased [33]

When the complexity of the problem increases, the CPU time for the conventional method grows exponentially while the MC method grows moderately. Since the previous studies accomplished at the SDSU C&SEL involve a great complexity, (using millions of rays, 3D shapes, participating media, etc…) the MC method is employed. The MC method generates *random* numbers by a probabilistic model to approximate a solution for a numerical problem, i.e. the inputs are represented by probability distributions. A clear

scheme was described in order to understand how the Monte Carlo method is used for the Ray Tracing [19], as shows Figure 13.
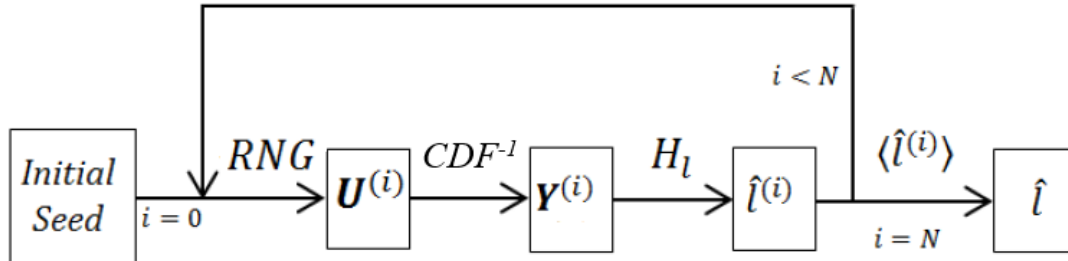
Figure 13. Schematic representation of a Monte Carlo Ray Tracing simulation [19]. (Modified)

The process of Figure 13 is repeated N times. N must be high enough to obtain an accurate estimate of the function $\hat{l}$, which can represent different parameters depending on the objective of the simulation. In this process, the Random Number Generator (RNG) generates random numbers $U^{(i)}$, which are used to obtain a set of variables $Y^{(i)}$, by inverting the Cumulative Distribution Functions (CDF) [12] which characterizes the emission and the interactions of a photon. H^l is the performance function and $l^{(i)}$ is the estimator of the objective value obtained for the ray i [12].

For the thermal radiation problem in the Small Particle Heat Exchanger Receiver, obtaining the solution by conventional numerical method can be extremely complicated or impossible, since the carbon particles, which were defined in the Section 1.3, have a strong spectral dependence. In this thesis and others in C&SEL [17][24][29][34], the MC method is specifically used for the Ray Tracing (MCRT).

MC is a method based on probability, and involves a statistical error [33]. This statistical error is demonstrated to be function of the number of rays traced in the next sections. Referring to the Figure 13, the parameter i represents the number of rays, and N, the number of rays used in the simulation, which must be enough to obtain an accurate estimate. The $Y^{(i)}$ is a vector for every ray, where it is defined by the parameter that describes it (Position in the target plane, direction, power and wavelength).

In spite of being called a Random Number Generator (*RNG*), actually it is impossible to create *"totally random number"* since a computer is used to run this simulation. In MIRVAL, the RNG used, [35] employs an initial value *"seed"* to start the series. If the "seed" value stays constant during several simulations, the results obtained will be the same. Therefore, the simplest way to obtain different random number series is vary manually the initial seed value. For this reason, the RNG used is a *pseudorandom* number generator**.**

2.2 MIRVAL

MIRVAL is a FORTRAN code, based on Monte Carlo method, used for the ray tracing in this research [36]. It is an open code, which permits to integrate new updates, like adding the CPC code [29], so the ray tracing can be calculated in only one step. In previous researches, this program was used to optimize the heliostat field shape [15], but in this research the heliostat field shape is constant and other variables are varied for the simulations (SC shape, time, day, number of rays, target plane…).
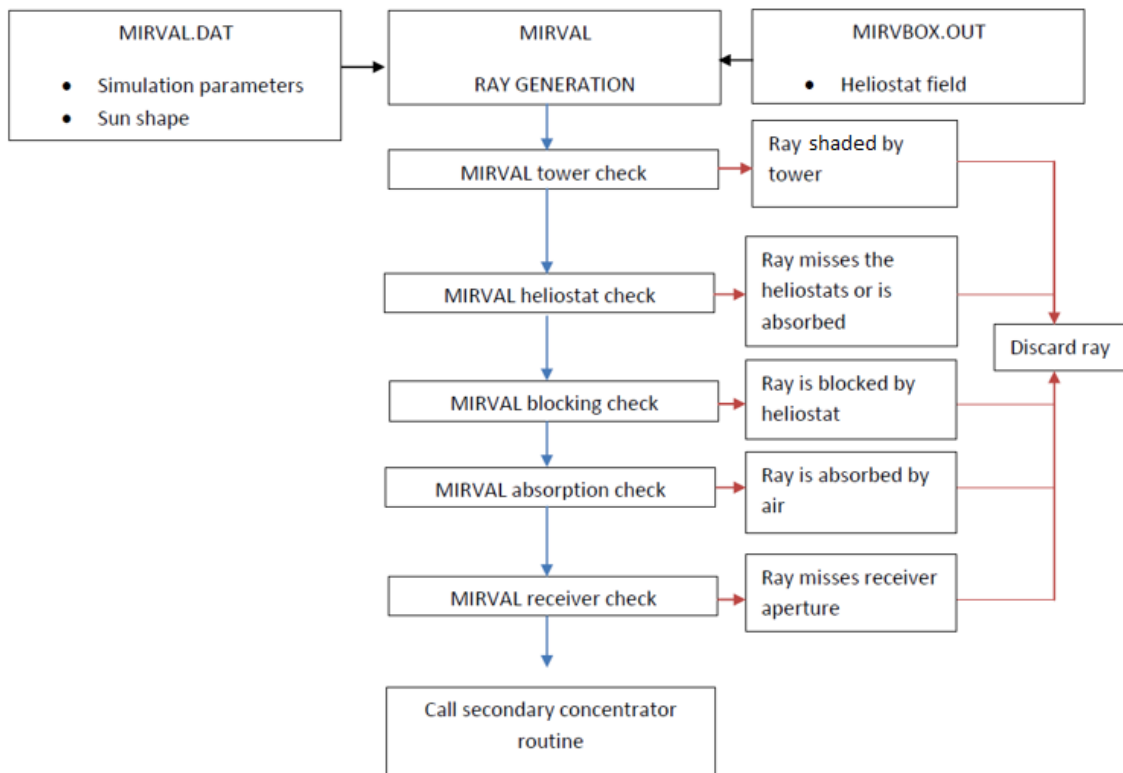
Figure 14. Schematic representation of MIRVAL procedures [15] (Modified)

The main program is about 12,000 lines of code in FORTRAN, but it is not necessary to modify the program to run MIRVAL. For that, the heliostat field and the other variables are read from two inputs files, which contain the main variables, as it is shown in Figure 14. This Figure shows the MIRVAL procedure including the input file (.DAT and .OUT), and the different steps where the ray can be discarded. In the ray tracing, before reaching the target plane, the ray can be shaded by the position of the tower, missed in the heliostat field, blocked in the heliostat field when it is reflected, or absorbed by the air. Although the MIRVAL simulation is done, for example, with 1,000,000 rays, only a portion of them (depending on the time and the day of the year) reach the target plane. A deeper explanation is given in the section 2.4.1.5.

2.3 Precedents

This thesis arises from a large trajectory in the SDSU C&SEL lab, the path followed by the research is explained in the paragraphs below. A flat window with an SPHER axisymmetric cylindrical was studied [24], and the ray tracing is developed by a MCRT, combined with the energy equation. This thesis [24] proposes, as a further work, to develop a similar method, but using MIRVAL. Also it proposes to improve the shape from a simple flat window, to a real window shape [37]. Then, the power reaching the window was studied; without the Secondary Concentrator; for a real geometry window and with MIRVAL [34]. It is also studied how the results change with the optical properties of the window, the material and the geometry (Figure 15).
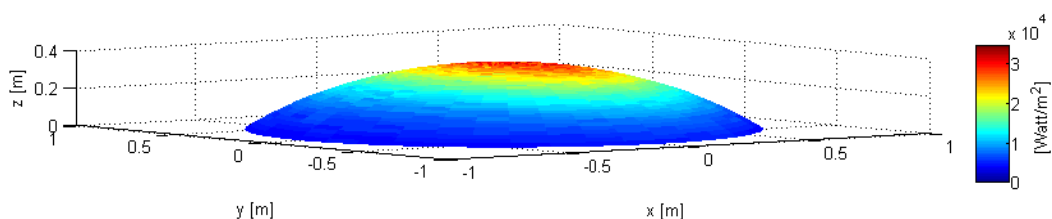
Figure 15. Absorption map for 45 degree spherical window without SC. March 21, 12pm. [34]

A FORTRAN code was created in order to be able to study the model with a SC [29]. The method is designed for shapes, which can be described by an equation. In this first research [29] the heliostat field was not varied, but in the next research [15] different heliostat field shapes were tested computationally with the SC added. The CPC is

demonstrated to be the most efficient shape for the 2D simulations, but in 3D the solution is not evident [17]. This fact involves that it is not possible to study other relevant shapes, like the SC hexagonal inlet, very appropriated for the possibility of increasing the number of concentrators. This is evaluated in order to increase the area of the heliostat field. For this reason, another alternative method is developed [17] in order to be able to study the power reaching the window for any secondary concentrator shape. It is based on discretizing the shape in a mesh generated by ANSYS.

In this thesis, the ANSYS method is used to calculate the power distribution in the Secondary Concentrator. Since the power absorbed in the SC is obtained, it is possible to design a cooling system in the case of being necessary. A FORTRAN code is used to calculate the power absorbed in the SC, and MATLAB is used to graph the results in 3D. In addition a new non-axisymmetric inlet is proposed, in order to test new shapes that can provide a greater power reaching the window.

2.4 Main variables

This section summarizes the main variables necessary to understand this thesis properly and to take into account in the simulations.

2.4.1 Heliostat field and geometry

2.4.1.1 Target plane:

It is mandatory to know this variable in order to understand the simulation steps. Among the different researches, it is called with different names Receiver (Target plane/aperture plane/ receiver opening) but all of them refer to the same concept. The target plane is illustrated in the Figure 16.

It is defined by the variables HEDMM1 and OEDMM1, which are set in the .DAT file. The inlet of the Secondary Concentrator is located in this plane. In the output .FLX file, the rays included, are the rays that hit in this target plane. At the command window, this concept is called "Receiver Dimensions", and the shape of this Target Plane can be

transformed by the variables RECOPROUND and SECONDARY[1] [29]. The Figure 17 shows part of the command window with the receiver dimensions.
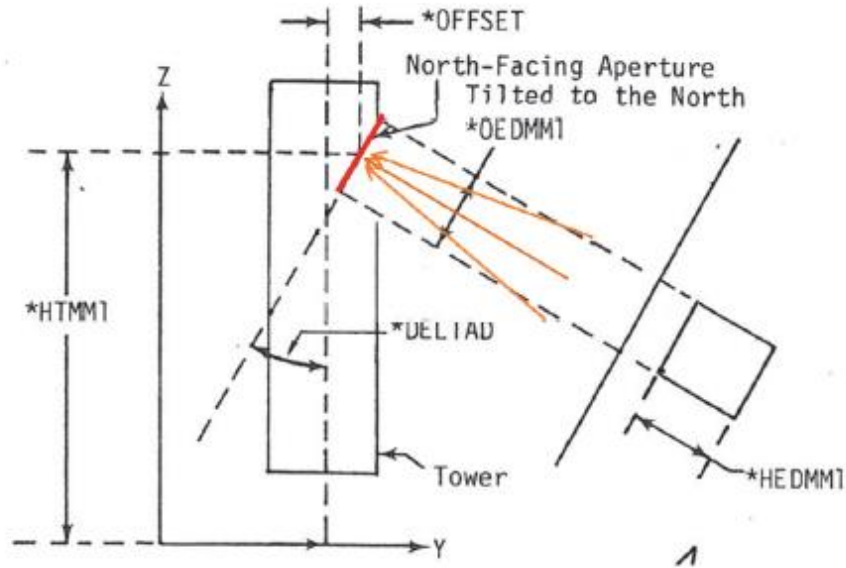
Figure 16. Scheme for the target plane [36]

Figure 17. Command window example with receiver dimensions

The variable RECOPROUND included in MIRVAL set the target plane as round when RECOPROUND=1. The variable SECONDARY activates in MIRVAL the SC. A resume of the Receiver Dimension output as a function of the values of those parameters is explained at the Table 2.

---

[1] Line 178 Berchtold's MIRVAL

DAVID CEREZO AGUADO

Table 2. Receiver Dimensions and Target Plane shape in function of RECOPROUND and SECONDARY

RECOPROUND	0	1	1	0
SECONDARY	0	0	1	1
TARGET PLANE	RECTANGLE	ROUND	ROUND	Not possible
Receiver dimensions output	HEDMMI X OEDMMI	2*CPCROUT X 2*CPCROUT	2*RECRIN X 2*RECRIN	Not possible

2.4.1.2 Slopes Error and CPCRECLIM

<u>DEVSLO: applied to the heliostat field</u>

With this parameter, an error is created to consider manufacturing and alignment imperfections in the heliostat field. This variable has a significant influence on the smallest possible projection radius and it is important to if the heliostat field is going to be increased. To test how the variation of DEVSLO affects to the results, the solar flux in a vertical (DELTAD=0 [26]) north faced target plane is studied. After several tests, this variable is set in 1.2mrad [29]. This parameter has a small influence for the case of the north field of heliostats, but it must be taken into account as important in the case of increasing the field of heliostats.

<u>CPCSLOPEERROR: applied to the SC</u>

This value is used to perform calculations within the SC. This parameter is included to take into account the manufacturing tolerances [19]. It generates an error for the reflection angle varying the normal vector at each point of reflection [38]. This error is used to calculate the new surface normal vector, and it is obtained as a function of the specularity error, the slope, alignment, shape and tracking errors. [39] The value is set in 3 mrad and it is only used if the parameter USESLOPEERROR=1. [29]

<u>CPCRECLIM: applied to the CPC</u>

The reflected rays in the CPC can be almost parallel to the concentrator slope, which involves the number of reflection before being rejected, absorbed or hitting the window can be a great number. For this reason, it is necessary to determine a maximum number of reflection in order to decrease the calculation time. The number of rays, which

overcome is usually less than 0.005% of the total. But if the comparison is done with the absorbed rays the proportion increase about 50 times. After several test, it is demonstrate that the number of trapped rays remain constant when the CPCRECLIM is around 20, and it can increase to around 30. This parameter is set to be 30, to ensure that the trapped ray's number is constant and since the simulation time is not practically increasing. These rays are taken as rejected for the global energy balance [Berchtold], but a counter is added in this thesis in order to know how many rays considered are actually "trapped" rays.

2.4.1.3 Heliostat Field

The heliostat field used to run the simulations in these and previous researches [17][29], is the Sandia National Laboratories Heliostat field at National Solar Thermal Testing Facility (NSTTF) located in Albuquerque, New Mexico. This facility provides a total power in excess of 6 MWth with flux levels of greater than 300 W/cm^2[40].
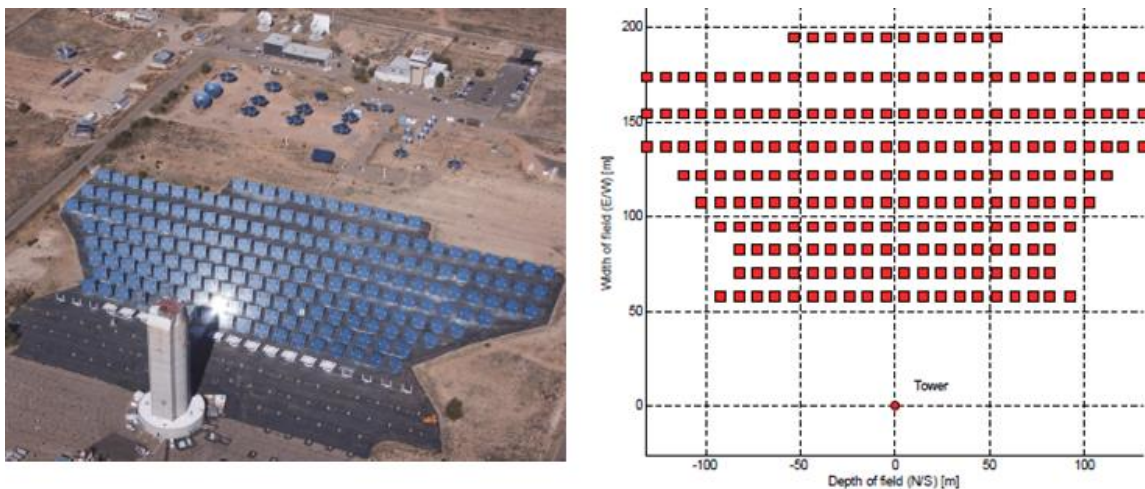
Figure 18. Sandia National Laboratories Heliostat field at National Solar Thermal Testing Facility (NSTTF) [40][29]

In Figure 18 the heliostat field is shown. At the left a real picture of the facilities in Sandia National Laboratories, and at the right the schematic layout created in MATLAB. The heliostat field is formed by 218 individual heliostats with 37m^2 of reflective area and an improved 96% reflectivity. Every of them have two motors and two degrees of freedom (azimuth and elevation) which permits to track the sun during the day. There is already four mirrors defined in MIRVAL's code: MM9, MD6, BNG and HW4. A scheme of the heliostat model developed in MIRVAL and used in this research is shown in the Figure

19. In the developed model, some assumptions are done as if that the axes of rotation for Azimuth and Elevation pass through O_m. The MM9 (Martin Marietta 9-facet) heliostat guidance is defined in the subroutine MM9 in MIRVAL. The motors are used in order to set an azimuth and elevation that makes a sun ray from the center of the sun ,which strikes the center of the center facet (where the origin O_m is set), shall be reflected through the objective point [36].

The variables DEVAZ and DEVEL are include as input variable for MIRVAL since the mirror guidance will not be perfect. Since the calculated *correct* values will not represent the real guidance, DEVAZ and DEVEL represent the standard deviation used to calculate the actual values employing a random selection according to normal distributions [36]. These values are set in DEVEL=0.0004 and DEVAZ=0.00045 by default.
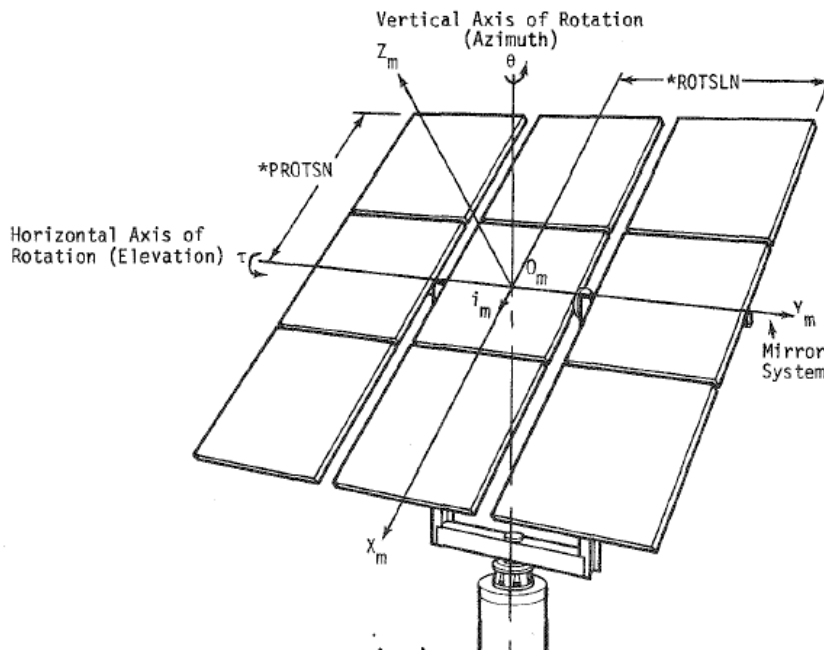
Figure 19. MM9 type Heliostat model in MIRVAL [36]

2.4.1.4 Theoretical model (RTE)

One of the greatest advantages of MIRVAL is that it allows the user to combine the *Radiative Transfer Equation (RTE)* in participating media and the possibility of including an incident solar flux distribution simulating a *heliostat field*. The simplest radiative

systems are defined for nonparticipating medium, when the surfaces are separated by vacuum or by a transparent medium. When the *medium* involves absorption, emission and/or scattering, it has to be taken into account [33]. The participating media can be any glass, liquid or gas and in the current case, the medium is the atmosphere. The RTE in participating media (which defines the atmospheric transfer of radiation in our model) is defined by the Equation 1 below[2] [41].

$$\frac{dI_\lambda(\bar{r}, \lambda, \hat{s})}{ds} + \beta_\lambda I_\lambda(\bar{r}, \lambda, \hat{s}) = \kappa_\lambda I_{\lambda,b}(\bar{r}, \lambda) + \frac{\sigma_{s,\lambda}}{4\pi} \int_{\Omega_{i=0}}^{4\pi} I_\lambda(\bar{r}, \lambda, \hat{s}) \, \Phi_\lambda(\bar{r}, \lambda, \hat{s_\iota}, \hat{s}) d\Omega_i \quad \text{Eq. 1}$$

Where the different terms represent:

The term $\beta_\lambda I_\lambda(\bar{r}, \lambda, \hat{s})$ represents the total attenuation caused by absorption and scattering (known as *extinction* as well), the extinction coefficient is defined by $\beta_\lambda = \kappa_\lambda + \sigma_{s\lambda}$.

The term κ_λ is the (linear) absorption coefficient and $\sigma_{s\lambda}$ represents the (linear) scattering coefficient. The linear absorption coefficient is the inverse of the mean free path for a photon. The first term to the right of the equal is the emission term $\kappa_\lambda I_{\lambda,b}(\bar{r}, \lambda)$. The emission rate will be proportional to the magnitude of the volume [33].

The last term $\frac{\sigma_{s,\lambda}}{4\pi} \int_{\Omega_{i=0}}^{4\pi} I_\lambda(\bar{r}, \lambda, \hat{s}) \, \Phi_\lambda(\bar{r}, \lambda, \hat{s_\iota}, \hat{s}) d\Omega_i$ represent the in scattering and it is calculated by integration over all solid angles since it has contributions from all directions. Φ_λ represents the scattering phase function, and if Φ_λ is constant (it means isotropic scattering) then $\Phi_\lambda \equiv 1$ and for this reason the factor 4π is included, since an integration over all solid angles yields 4π steradians.

2.4.1.5 Theoretical model applied to MIRVAL

A scheme of the model used in programs like MIRVAL, is shown in the Figure 20. The sunrays hit on the heliostat field and some of them are reflected to the Receiver Inlet

---

[2] In MIRVAL, only the absorption coefficient is used for the calculations [36]. The terminology wavenumber (η) is normally more convenient to use for gases instead of wavelength (λ). However, the terminology is kept in wavelength since the necessary Figures are illustrated with that terminology [41]. In other resources [33] the terminology is defined in function of wavenumber.

DAVID CEREZO AGUADO

located in the Target Plane. The original MIRVAL only calculated the power hitting in the Target Plane. In this and previous researches, a FORTRAN code is used to simulate the SC in order to know the power hitting the window when the SC is added.
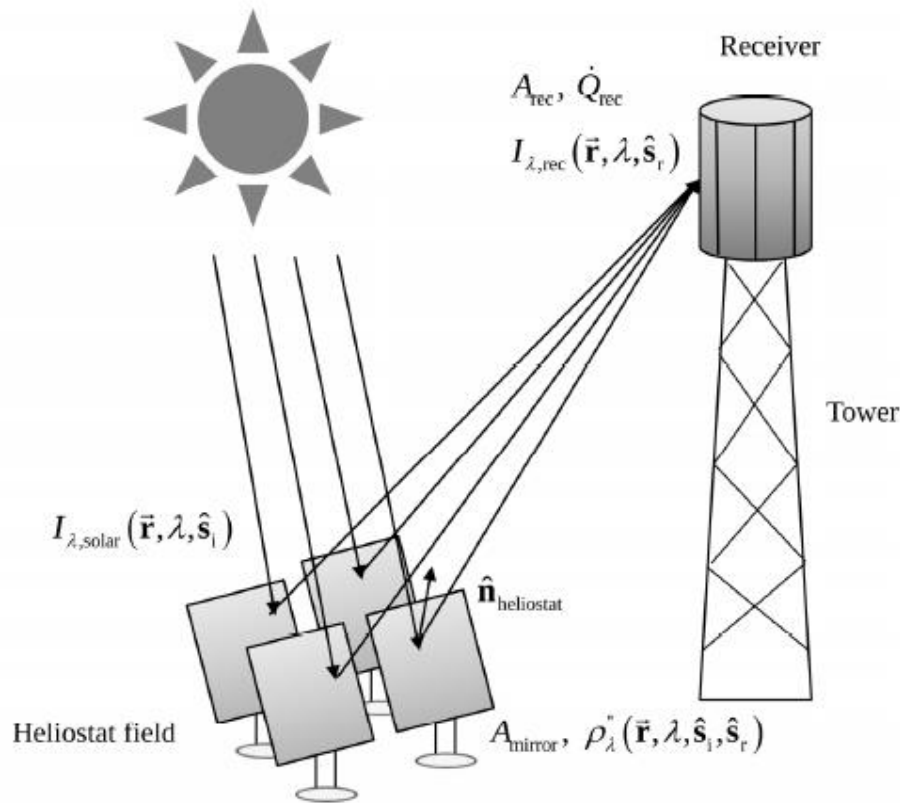
Figure 20. Simplified scheme of MIRVAL model [41]

So first the power hitting the Target Plane is calculated and with that file, the power hitting the window after going through the SC is calculated. Since the FORTRAN code is included in the latest MIRVAL [29], these two-steps could be done in only one step. An example of the data obtained by MIRVAL of the power hitting the Target Plane is shown in Table 3.

Table 3. MIRVAL output file for the rays hitting the Target Plane

Position $\bar{r}$ (m)		Direction $\widehat{S}_r$ (m)			Power (W)	Wavelength λ (μm)
XVAL	**YVAL**	**X**	**Y**	**Z**	**POWER**	**WAVELENGTH**
-1.28085	0.3666	0.31448	-0.87871	0.35913	105.5368	0.86191
-0.47613	0.37177	0.23974	-0.82555	0.51087	105.5368	0.41004
-0.36396	-0.26175	0.27996	-0.89612	0.34437	105.5368	1.24801

In the first two columns, there is the point where the rays are hitting in the Target Plane (defined by XVAL and YVAL). In the next three columns, there is the direction of the ray when hits the Target Plane, based on a normal to the target plane (X,Y and Z). In the sixth column there is the power of the ray. By last, the wavelength defined in μm, this parameter was added to MIRVAL by SDSU C&SEL. The irradiation depends on the *position*, *wavelength* and *direction* of every ray as it was shown in the Equation 1 and the Figure 20.

In MIRVAL the insolation can be set as constant or dependent on the path length of the ray through the *atmosphere*, which depends on time of the day and day of the year, as well as the latitude. The first MIRVAL version used at SDSU C&SEL only permitted to set the parameter IABTAB to 0 or 1 to deactivate or activate this function. Then, if IABTAB was set to one, other variables (SOLKON, TRANS…) were set in the input file MIRVAL.DAT to simulate in function of the time. The Equation 2 shows the formula used to define the insolation in function of the time (t).

$$I(t) = SOLKON * (TRANS)^{R(t)} \qquad \text{Eq.2}$$

Where R(t) is the ratio of the mass of air traversed by the incoming light ray at time *t* to the mass of air that would be traversed by a vertical ray. SOLKON is the exoatmospheric insolation (W/m^2) and TRANS is the clear atmosphere transmissivity for sunlight that shines directly down (vertically) on the site [36].

In order to get data more representative, previous research in the C&SEL [29] used real insolation data, obtained from National Renewable Energy Laboratory (NREL) and processed it to obtain a single table where the insolation is calculated for every month and daily hour (The latitude used for the simulations is 34.9633º). This data is shown in Table 4. To activate the subroutine INSOL5, where this table is defined, the IABTAB parameter must be set in IABTAB=5 in the input file MIRVAL.DAT.

Table 4.Insolation data saved in new subroutine INSOL5 in W/m^2 , data collected at Southwest Solar Research Park in Phoenix Arizona [29]

	Jan	Feb	Mar	Apr	May	Jun	Jul	Aug	Sep	Oct	Nov	Dec
5:00	0	0	7	59	166	109	39	36	27	10	0	0
6:00	8	57	113	246	448	376	183	176	174	159	69	7
7:00	126	281	375	495	667	644	359	372	399	453	284	80
8:00	401	534	616	680	794	768	481	512	567	661	533	303
9:00	635	692	731	765	863	840	586	587	664	756	687	517
10:00	744	749	791	811	907	885	688	653	733	815	740	612
11:00	778	756	819	842	936	912	749	714	769	852	746	671
12:00	770	760	825	842	942	926	772	746	756	861	754	686
13:00	744	762	815	824	918	928	779	750	732	830	741	690
14:00	699	722	778	781	878	908	742	724	713	779	679	650
15:00	630	642	710	713	805	859	693	686	671	683	557	565
16:00	460	497	587	622	696	798	599	603	550	479	322	386
17:00	209	241	362	455	513	701	452	440	329	206	84	129
18:00	36	48	120	212	262	489	277	220	106	37	4	4
19:00	0	0	12	41	62	196	105	50	8	0	0	0

Finally, with all of the effects taken into account the overall optical efficiency can be defined by the Equation 3:

$$\eta_{optical} = \eta_{cosine}\eta_{shading}\eta_{reflection}\eta_{blocking}\eta_{spillage}\eta_{atmosphere} \qquad \text{Eq. 3}$$

The Figure 21 is attached in order to give an intuitive idea of the terms shown in Equation 3. The cosine term is a reflection of the fact that only a part of the radiative power intercepted by the heliostat because of the cosine of the angle between the heliostat surface normal and the direction of incident solar rays. The radiative power intercepted is proportional to the cosine of this angle. If part of one heliostat is in shadow of a preceding heliostat, the tower, or the receiver, it is considered as a shading loss. The reflection loss occurs when reflectivity of the heliostat surface is less-than-unity. When the ray is reflected by the heliostat and it hits in the back surface of another heliostat, it is considered as a blocking loss. When the ray is reflected by the heliostat and it misses the SC inlet (even if it is hitting the Target Plane), is considered as a spillage loss. The atmospheric scattering and absorption cause the atmosphere loss. It is proportional to the

distance between the heliostat and the receiver, and the water vapor or aerosol content in the atmosphere.
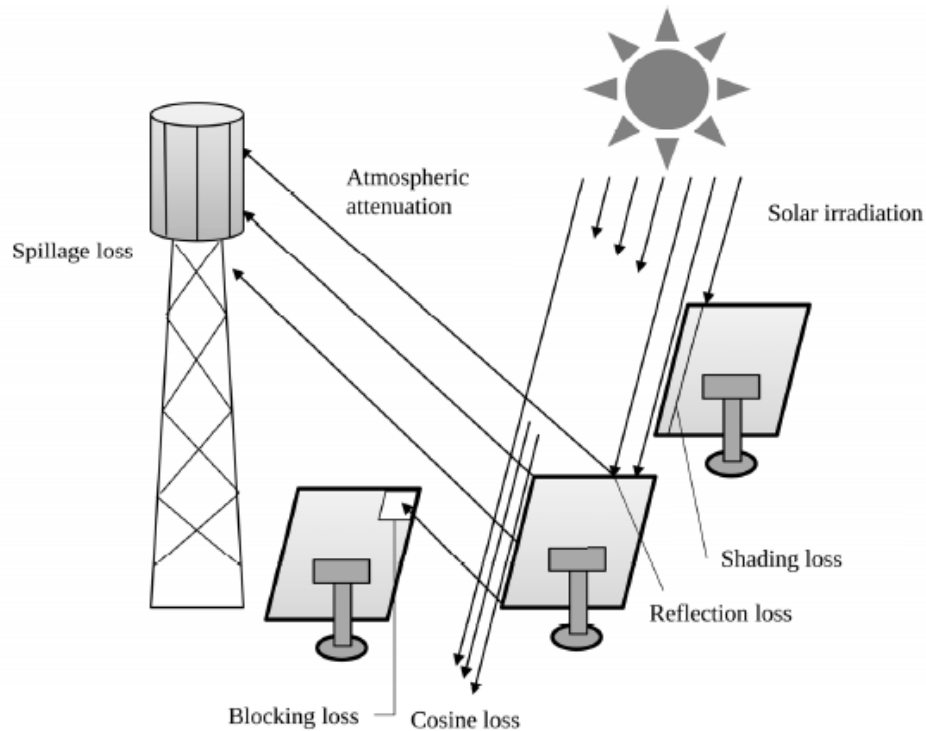
Figure 21. Optical losses in the system necessary to calculate the optical efficiency [41]

2.4.2 ANSYS Method.

The first FORTRAN code version only offered the opportunity of calculating the ray trace in the secondary reflector using a shape which can be described by an equation, for example the CPC [29]. Later, an alternative method was proposed in order to be able to study any shape [17]. In the ANSYS method which does not require an equation describing the shape, the desired shape is designed in SOLIDWORKS. With the shape, an X-surface mesh is generated in ANSYS, and ANSYS permits the export of that mesh to a .txt file, which can be processed in FORTRAN.

As was explained paragraphs before, the simulations cannot be accomplished by only adding the mesh as an input to the FORTRAN code (.txt file). It is also necessary to add the conditions of the new inlet/outlet shape to the code. A review of the FORTRAN code used to add the new geometrical conditions is exposed in APPENDIX A.

2.4.3 Meshes

The meshes used in previous research have been tested, and there are three issues that must be highlighted and corrected.

First, the number of surfaces indicated in the simulations is a larger number than indicated by the author. A deeper explanation about the method becomes necessary to understand why. As is described in the last section, the shape is first designed in SOLIDWORKS and then converted into a mesh in ANSYS. In previous research, these were the steps followed to get a .txt file from a SOLIDWORKS shape [17].

Steps:

1. Build SOLIDWORKS shape.
2. Save in the format *.igs.*
3. Open Workbench ANSYS, file *final.wbpj.*
4. Import geometry, geometry, replace geometry, browse.
5. Thin/surface, select outer faces (value cero).
6. Mesh, refresh mesh, update refresh.
7. Change Target System to STL.
8. Open Model, write solver file.
9. Save it in .txt format with the name *shape.txt.*
10. Run FORTRAN.

The meshes created in step 6 from the SOLIDWORKS shape, are automatically adjusted by ANSYS. If in the Mapped Face Meshing, the variable "Method" (where the geometry of elements is defined) is not set in "Triangles: Best split", ANSYS will use quadrilaterals and triangles to create the mesh. Finally, the Target System is changed to STL and the .txt file is written through the option Write Solver File. In this .txt file, the mesh is described by planes formed by 3 nodes i.e. triangles. Therefore, although the mesh was defined with quadrilaterals and triangles, ANSYS creates a shape.txt file where there are only triangles. The Figure 22 shows at the left the mesh formed by quadrilateral and triangular cells, and at the right part of the .txt file obtained from ANSYS where all the planes are triangles. For this reason the number of cells, which really are used in the

calculations, is the number of triangular cells contained in the .txt file, and not the number of elements given previously by ANSYS. The number of cells indicated by the author for the previous research was 13,230 for the round-round SC, 10551 for the hex-hex SC and 25372[3]. But the real number of surfaces used for the calculations were 26520, 21095, and 78350 respectively.
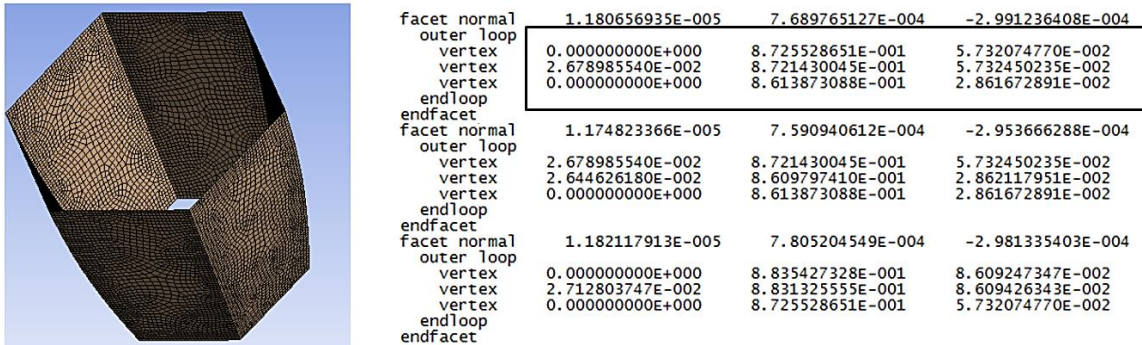
Figure 22. At the right, hexagonal inlet – hexagonal outlet SC mesh formed by quadrilateral and triangular cells. At the right part of the .txt file obtained from ANSYS with .STL system formed by triangular planes.

It was tested too, that for some shapes, even when in ANSYS the variable "Method" is set to "Triangles: Best split", ANSYS creates a mesh with some quadrilaterals. One alternative is proposed in order to avoid this problem.
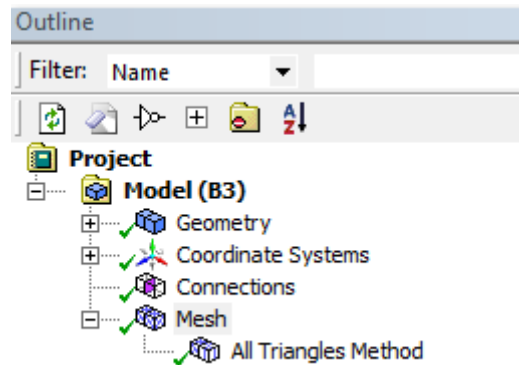
Figure 23. ANSYS menu with All Triangles Method displayed

Instead of using the option Mapped Face Meshing, a mesh formed by triangular cells can be created by the "All Triangles Method" option. Figure 23 shows the scheme of where this option has to be used.

---

[3] This value must be wrong since the real number of surfaces is 78350. Therefore, the real value has to be about 40000 surfaces.

DAVID CEREZO AGUADO

Second, if the power absorbed in the SC is graphed for the meshes used in the last research, the power distribution obtained is not correct or "realistic".
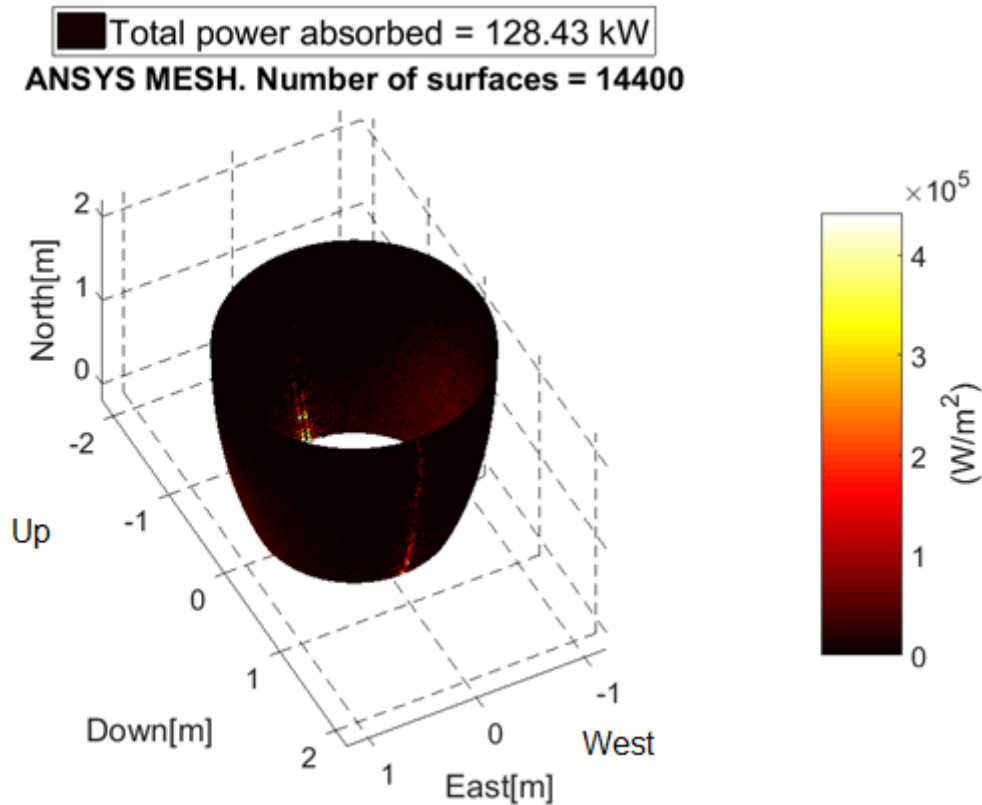
Figure 24. Power absorbed in the SC with the old type of meshes. CPC shape March 21, 1200pm.

The Figure 24 shows this power distribution for 12 pm on March 21. Almost all the power is absorbed in both extreme sides, with a homogenous distribution in the other SC parts. This is not the real behavior of the SC, so there is a problem in the mesh that must be corrected. The main variable which can influence the graphs is the area of the cells. Then, the area of every cell is calculated with MATLAB, and Figure 25 shows the results. There is a large variation in the cell area, with a minimum of $1.98 \cdot 10^{-1}$ cm^2 and a maximum of 12.2 cm^2. That means that there are cells about 60 times bigger than other cells. This distribution with a large standard deviation implies that if only one ray reaches one of the smallest areas, the power absorbed per unit of area will be very high since the area is in the denominator. Therefore, a large difference in cell area has been demonstrated, even when MATLAB displays the areas as apparently the same.
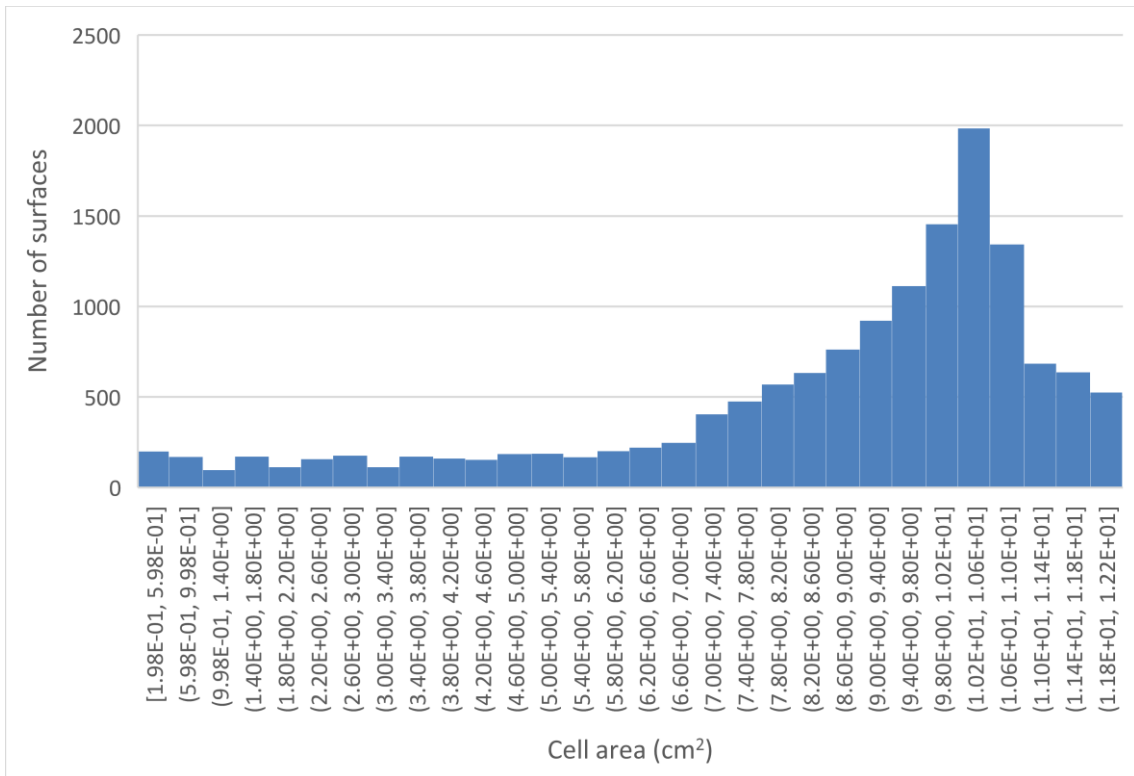
Figure 25. Area distribution in the 14400 cells mesh created from 7200 quadrilaterals by ANSYS

Figure 26 shows the grids for the old mesh (at the left, formed by quadrilateral cells) and for the new mesh (at the right, formed by triangular cells).
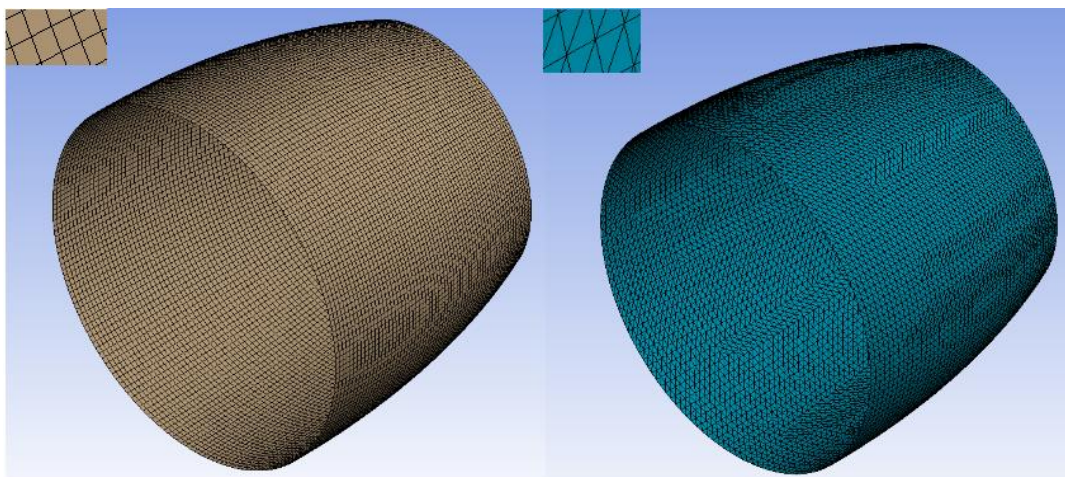
Figure 26. CPC shape meshes. At the left, old mesh formed by quadrilateral cells. At the right, new mesh formed by triangular cells. In both images, the top left shows a zoom of both grids.

In the new method, where the cells are directly defined as triangles, the number of cells is still the same but the distribution is more homogenous. With a minimum of 5.88 cm^2

DAVID CEREZO AGUADO

and a maximum of 12.1 cm^2, now the biggest difference in size is a factor of two (Figure 27).

Finally, when both mesh are obtained, the same MIRVAL input file (March 21, at 1200pm) is run, and the results are graphed in MATLAB. The Figure 28 shows these results. At the left, the results obtained from the old mesh (formed by quadrilaterals) which was already shown and commented in this section.
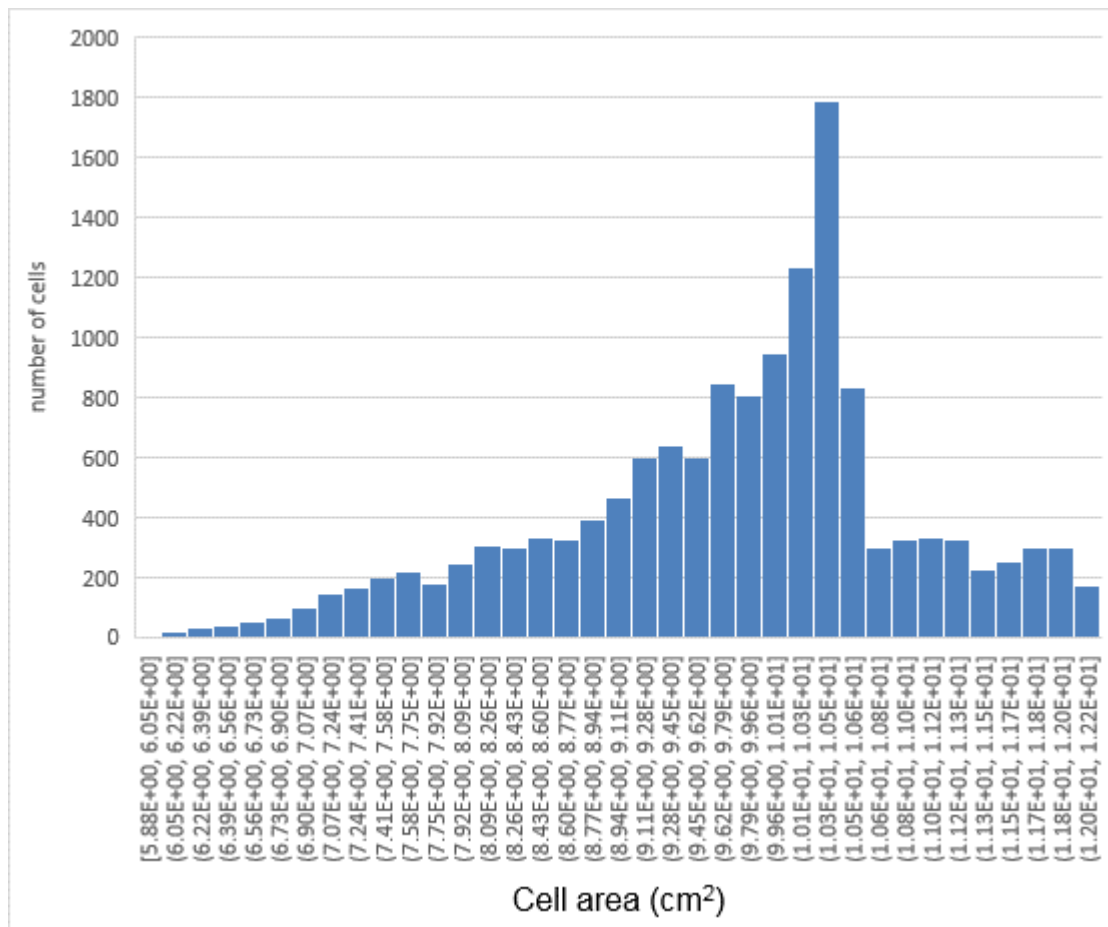
Figure 27. Area distribution in the 14400 cells mesh created directly from 14400 triangular planes by ANSYS

At the right, the power spatial distribution in the CPC looks more real when the new mesh, formed by triangular and with lower difference in the cells size, is used. So it has been demonstrated how even when the same global results are obtained (≈128.5 kW in both cases), the mesh area distribution affects strongly to the power spatial distribution.
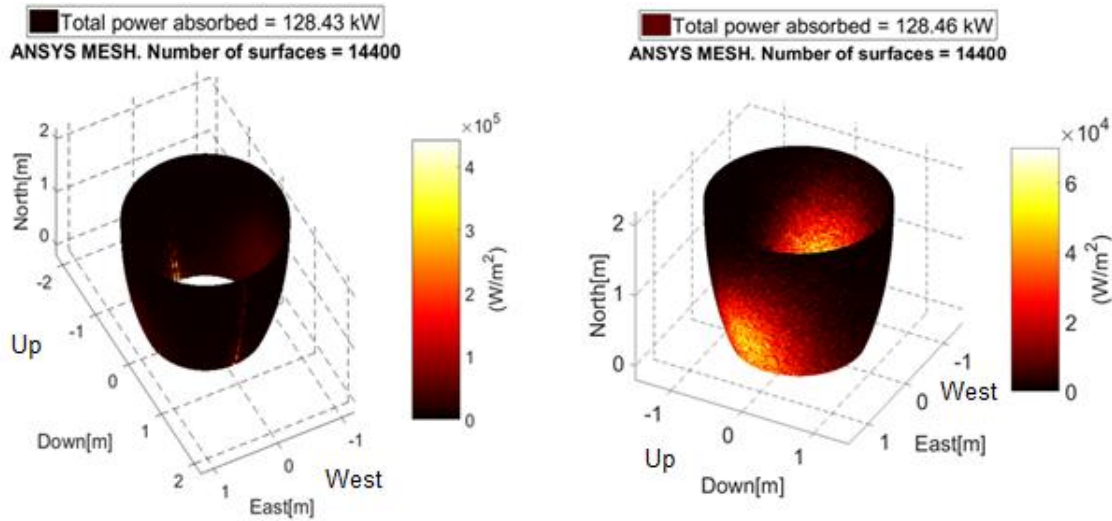
Figure 28. CPC power absorbed, March 21, 1200. At the left, the "old" mesh formed by quadrilateral cells is used. At the right, the new mesh formed by triangular cells and a lower difference in the cells size.

Third, after making new shapes in order to test them, an improvement to the ANSYS method used before, is proposed. When the shape is being designed, the first thing to create is the solid. Then, in the solid, the function shell is performed to obtain a "real" shape of the SC. The new method consists of clicking in the solid's surface before saving the shape as an .IGS file, and SOLIDWORKS will give the option of exporting only the selected faces as is shown in the Figure 29.

Then, the "Selected face(s)" option is chosen, and only that surface will be imported to ANSYS. Therefore, with the new method:

1. It is not necessary to use the function "shell" in SOLIDWORKS, since only the external surface is going to be imported, and the solid does not need to be modified.

2. It is not necessary to modify the thickness in ANSYS. (Step 5)
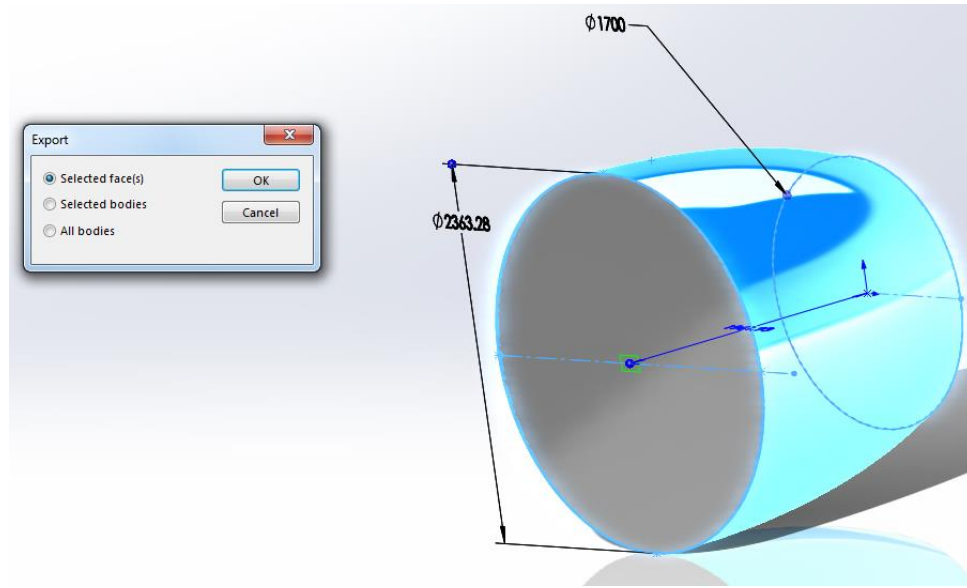
Figure 29. Export option for the shape's surface when Selected faces(option) is used.

2.4.4 Number of rays

The accuracy of the MCRT depends on the number of rays as was explained in the section 2.1. On one hand, the stability and accuracy of the solution is increased as the number of rays is increased. On the other hand, the computation time is increased proportionally too. This fact makes necessary to find the best compromise solution that results in sufficient accuracy in a reasonable time.

2.4.4.1 Theoretical Model

Previous researchers [42][43] have observed the error in the result caused by the fluctuations is proportional to one over the square root of the number of emissions. This approximation is fulfilled for radiation heat exchange between surfaces and for participating media. The Equation 4 was developed for the single case of surface exchange only [44]:

$$e = \pm 1.96 \sqrt{\frac{n-1}{N}}$$

Eq.4

Where e is the percent error, N is the number of emissions per element, n is the number of surfaces and 1.96 corresponds to a 95 percent confidence interval from Student's t-statistic for an infinite number of degrees of freedom [45].

The theoretical errors calculated by Equation 4 for the different meshes with the number of rays chosen are shown in Table 5.

Table 5. Error calculated for the different meshes by Mahan formula

Number of rays (N)	Number of surfaces (n)	Error (e)
$3 \cdot 10^7$	14400	0.043 %
$3 \cdot 10^7$	21240	0.052 %

This and other approximations were used to calculate the View Factor in the case of two circular diffuse black disks. (The view Factor is the proportion of the radiation, which leaves one surface and hits in other one).
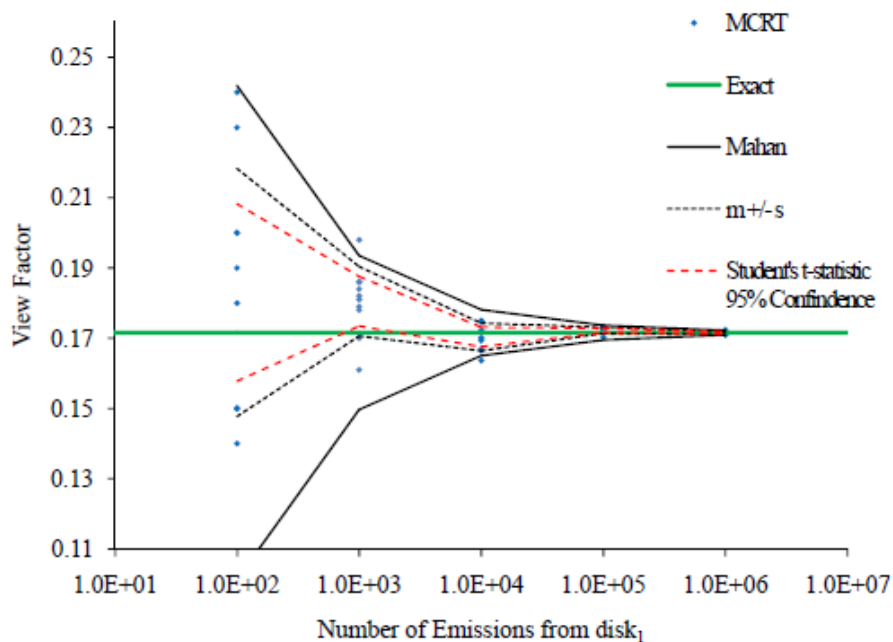
Figure 30. Error analysis for view factor calculation [24]

In Figure 30, every blue dot, represents one MCRT simulation. The green line represents the exact solution for the view factor [42]. The dotted black line represents the m±s solutions (the m±s method is based on running the MCRT several times and calculating

the mean (m) and the standard deviation(s) of the results.) [24][46]. The error has also been evaluated with Student's t-statistic by other authors [44][47] with a 95 percent level of confidence for each set of MCRT runs. All of them demonstrate the solution convergence when the number of rays (emissions) is increased.

2.4.4.2 Previous practical generic test

Based on the theoretical model, later researches at SDSU determined the number of rays necessary to obtain a stable response in the power reaching the target/aperture plane [34]. The asymptotes are calculated for different times on the day assuming the target/aperture plane as one surface; the graph obtained is shown in Figure 31.
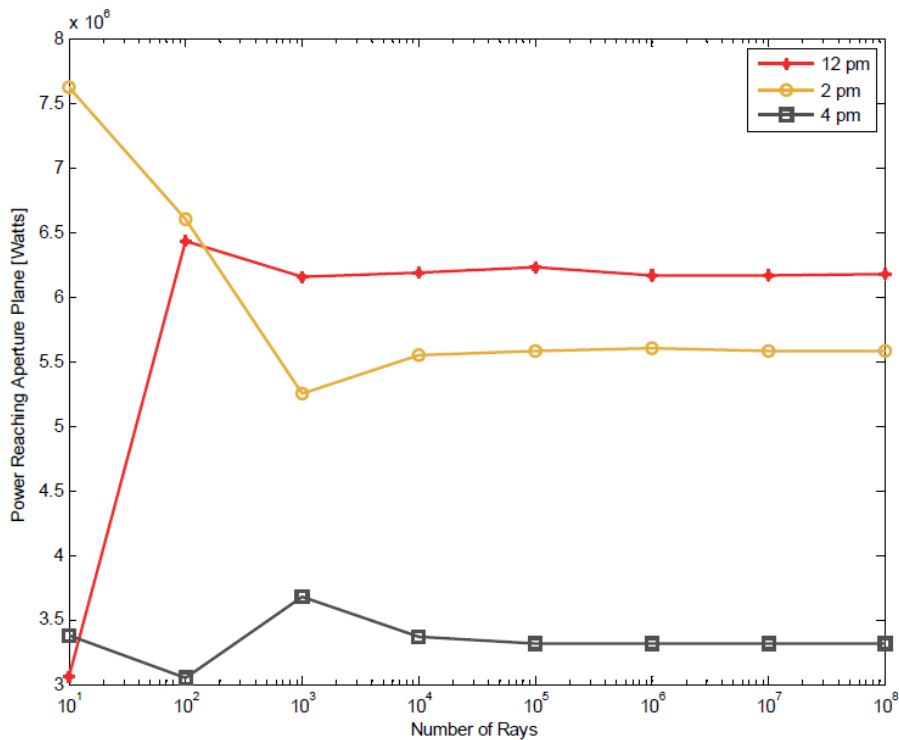
Figure 31. Power reaching the Aperture Plane for different times on the day [34]

It is necessary to remember the asymptotes are calculated for the target plane, and not for the window surface, which was included in the code later [34]. Once the asymptotes are obtained and the necessary number of rays obtained for one cell, a linear extrapolation is done. According to these calculations 10,000 rays need to reach every surface to obtain a stable response. In previous researches the number of rays used in the simulations are estimated with this supposition [29][34], which is a very conservative solution, but

plausible because the simulation time is shorter. However, in the ANSYS Method, the simulation time is increased hundreds of times (depends on the number of surfaces). To illustrate the importance of an optimal choice of this variable, one example of this relation is explained for the conservative method to calculate the rays. Remembering the mesh used for the round-round shape which has 14,400 surfaces. Selecting this mesh, and taking into account that around 2.5% of the MIRVAL file rays are absorbed, a 400,000 rays per cell MIRVAL file is needed. This means for a mesh with 14400 surfaces mesh a MIRVAL file with $5.76 \cdot 10^9$ rays is needed.
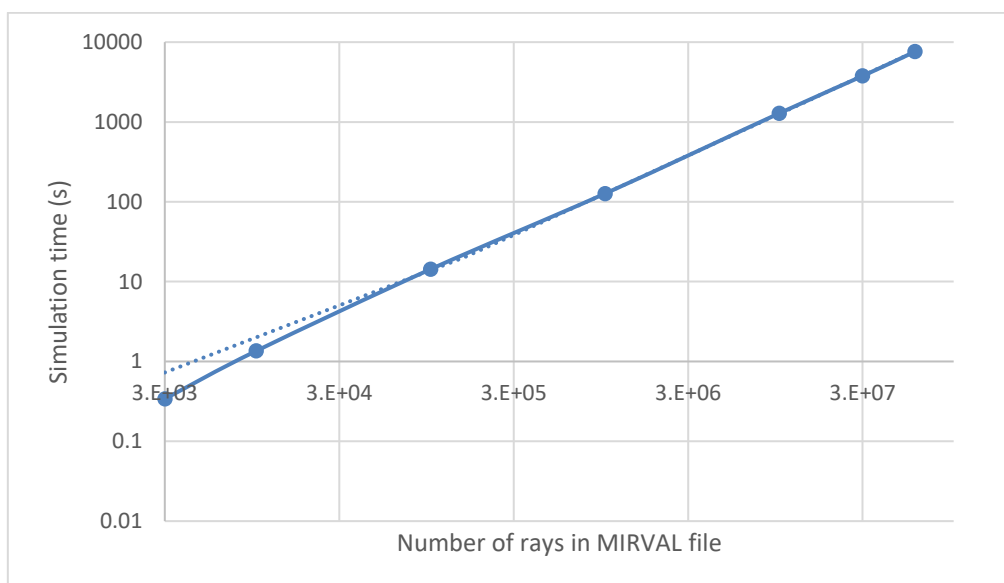
Figure 32. Simulation time versus number of rays for the 14400 surfaces ANSYS mesh (CPC shape)

With that number of rays, the estimated time for each simulation is about $6 \cdot 10^5$ seconds, i.e. almost 6.6 days for each simulation (Figure 32).

2.4.4.3 Specific study

For the reason explained in the last section, it is worth it to look for the asymptote in every case, instead of assuming that conservative solution. In the previous research [17], the FORTRAN input .FLX files run contains $3 \cdot 10^6$ rays. This variable was assumed as big enough since the results obtained from both codes (Equation and mesh) were similar enough. But using only that verification it is not possible to know if the solution is already stable. That is, the same results can be obtained with both methods, but if the number of rays is increased, the solution (the power absorbed and the total power hitting the window,

in this case) are going to vary until they reach the asymptote. For that, several simulations at different times of the day are done, starting with the CPC with 14,400 surfaces.

First, the CPC shape is studied for five different moments during the day (8am, 10am, 12pm, 2pm and 4pm), with a simulation day of March 21. Results are shown in Figure 33 and Figure 34.
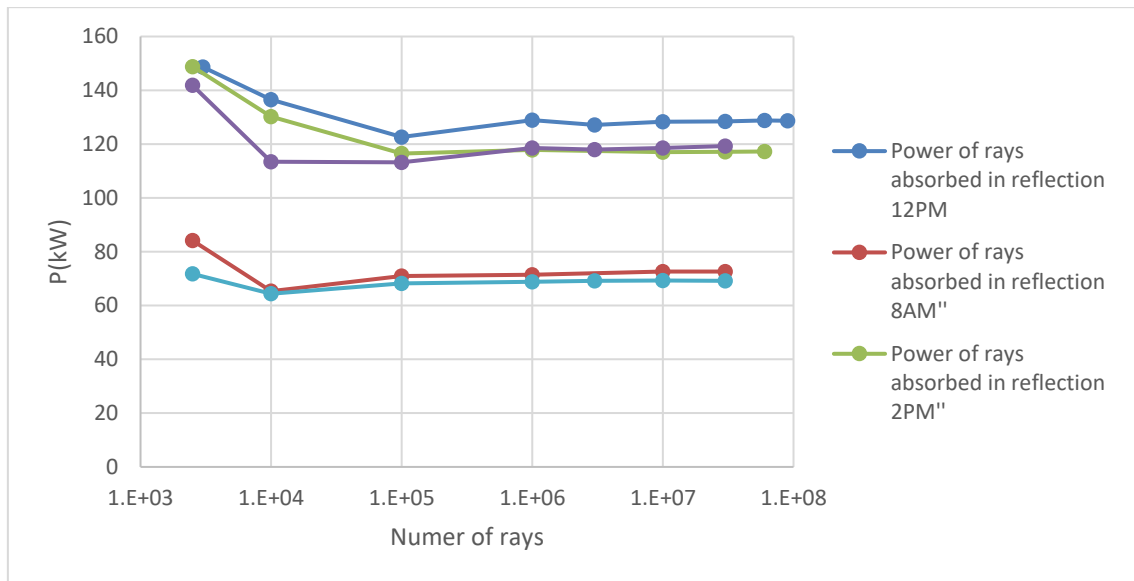
Figure 33. Power absorbed in the CPC for the 14400 surfaces ANSYS mesh vs number of rays. March 21

The number of rays is increased until a difference smaller than 0.5% between the consecutive points in the power absorbed is obtained. For example, the difference between 10^4 and 10^5 in the power absorbed at 12 pm is 4.84%. Therefore, the number of rays is increased again until decreasing that difference to a smaller value than 0.5%. In all the cases, that difference is reached with $3 \cdot 10^7$ rays or a minor number of rays, except of at 10 am. At 10 am, with $3 \cdot 10^7$ rays, the difference is 0.60%. It is just a 0.1% of deviation, so the number of rays to do the simulations is set in $3 \cdot 10^7$ in order to simulate all the cases with the same number of rays.

In order to verify the results presented in previous research [17], the same results applied to the power reaching the window are studied. It is clear the similarities in both Figures for the power in the cases 8 am & 2 pm and 10 am & 4 pm. Although the difference at the beginning of the graphs, when the number of rays is increased, both cases start to converge because of the sun symmetric position at that times. In the power reaching the window, the stabilization is obtained with a smaller quantity of rays than in the case of power absorbed in the window. With 1 million rays the error is smaller than 0.5% in every case.
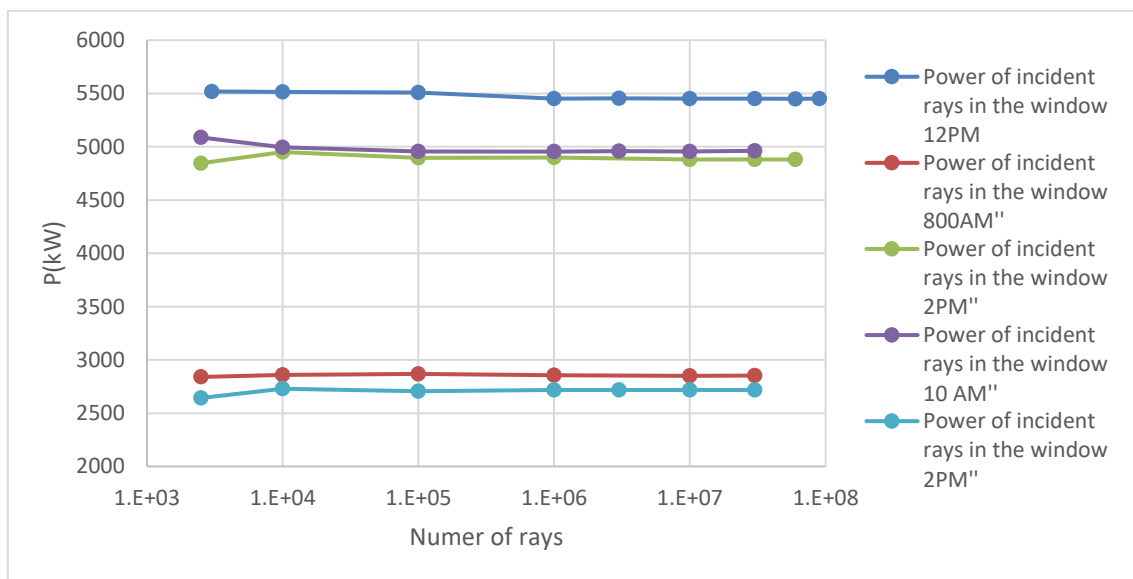
Figure 34. Power reaching the window for the 14400 surfaces CPC vs number of rays. March 21

Once the CPC shape has been studied, the other two shapes are tested too. First, in the hexagonal inlet-hexagonal outlet the similarities in the behavior have been tested for the symmetric position of the sun at 8 am & 2 pm and 10 am & 4 pm. For this reason, only three cases are studied, 8 am 12 pm and 2 pm. Similar results are obtained, being the 2pm case, which the power absorbed in the CPC needs more quantity of rays to get the stabilization (Figure 35 and Figure 36).

DAVID CEREZO AGUADO
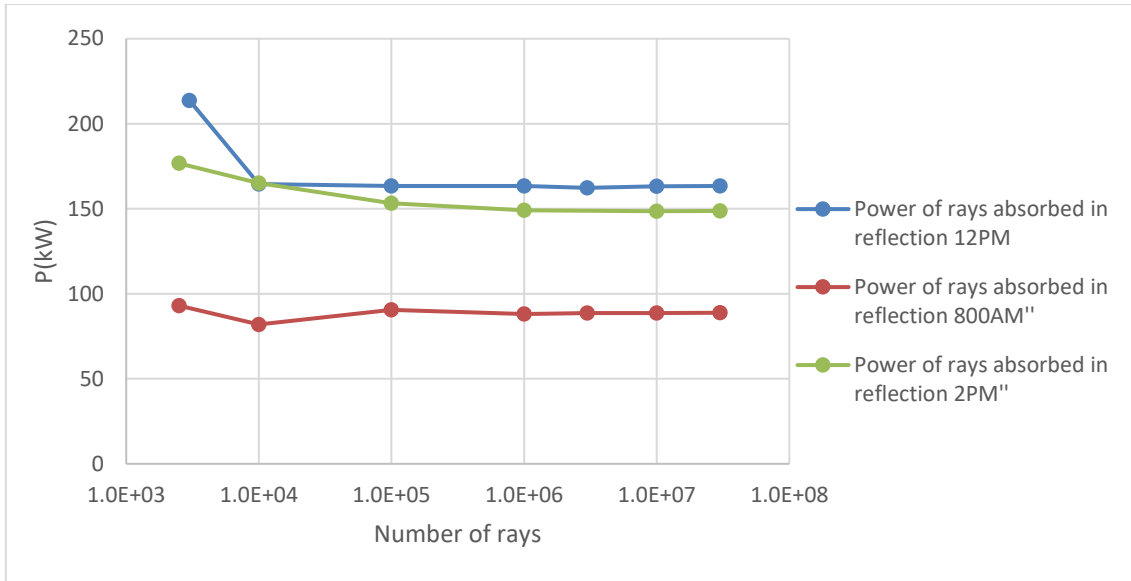
Figure 35. Power absorbed in the SC for the 21095 hexagonal inlet-hexagonal outlet vs number of rays. March 21
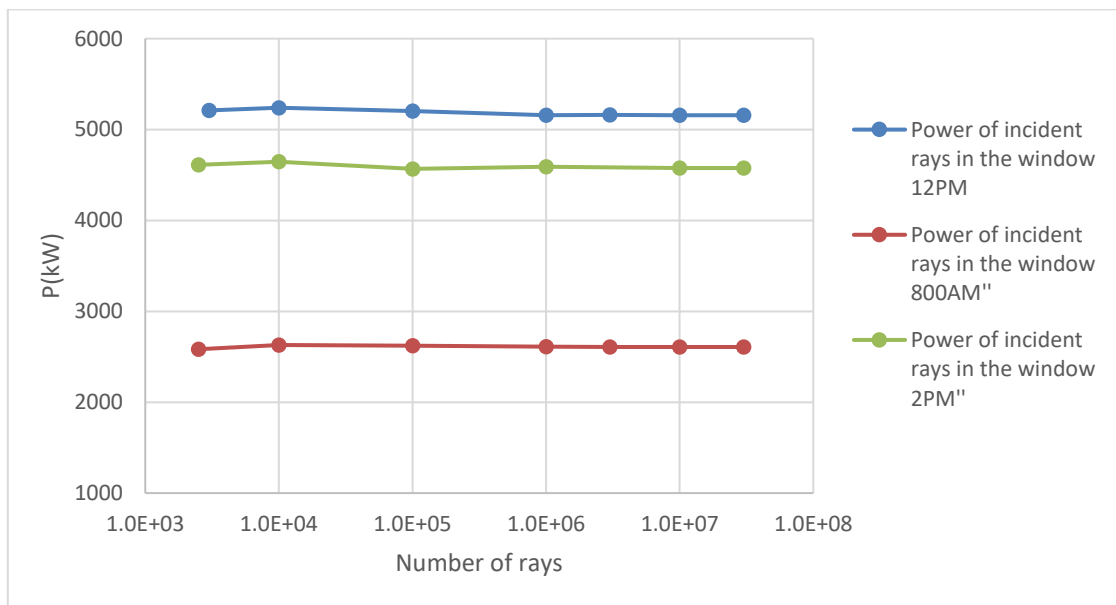
Figure 36. Power reaching the window for the 21095 hexagonal inlet-hexagonal outlet vs number of rays. March 21

The last case is the hexagonal inlet and round outlet. It has been demonstrated how both previous cases, despite having completely different geometries, the behavior in the parameters studied is the same. For this reason, only one time (12pm) is checked. All the parameters, studied for this time, are added in one single Figure (Figure 37) since can be clearly do for this case, which only one time on the day is included.

As in the CPC and the hexagonal inlet-outlet, the power reaching the window get stable with a smaller quantity of rays than the power absorbed in the SC.

Finally, since the "old" meshes (with a larger difference of areas) have been used for calculating the number of rays necessary to get a stable response, it is necessary to test if with the new redistributed meshes, the same solutions are obtained. Therefore, the round-round shape is tested at 12 pm, March 21 for the new 14400 cells mesh, and the differences in the main variables are 0.003% for the power incident in the window and 0.17% for the power absorbed in reflection. In addition, the hex-hex shape is tested at 12 pm, March 21 for the new 21240 cells mesh, and the differences in the main variables are 0% for the power incident in the window and 0.12% for the power absorbed in reflection.
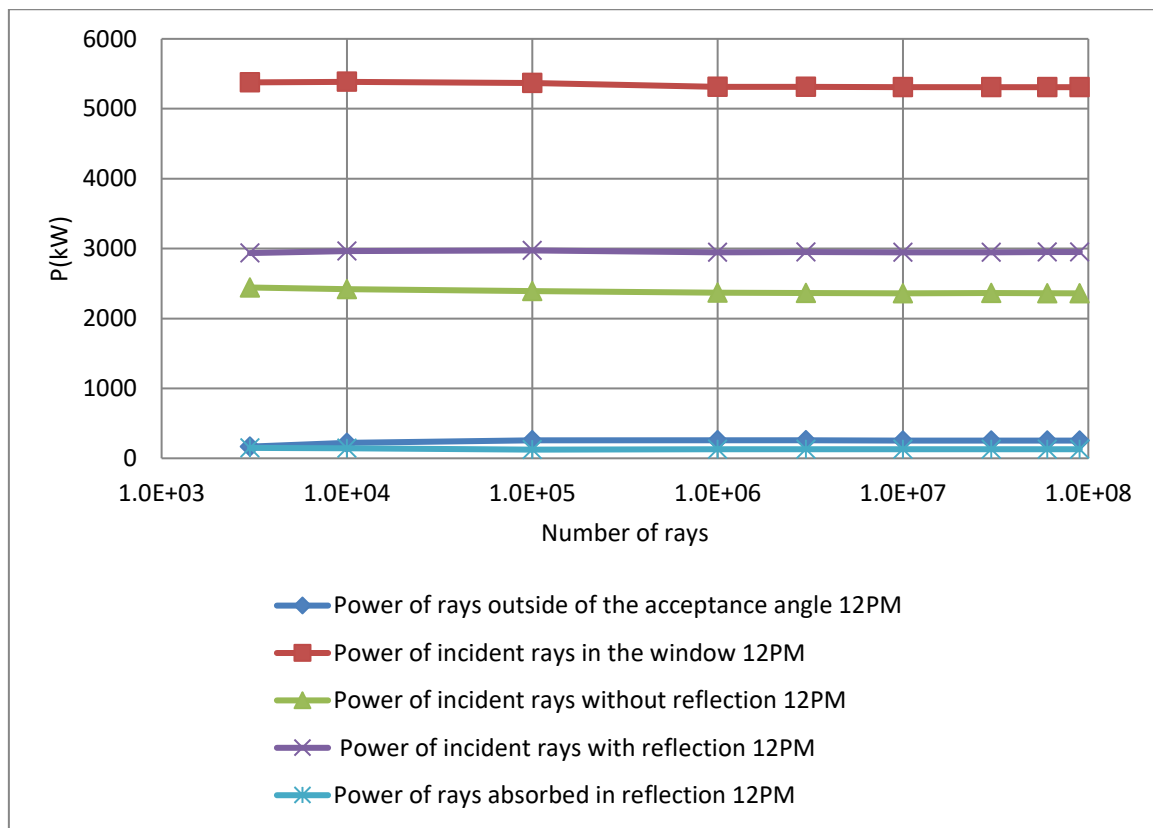
Figure 37. Main powers in the case of SC: hexagonal inlet-circular outlet vs number of rays. March 21

Conclusions:

- Inspecting the different tables obtained, it has been decided to use 3×10^7 rays for the simulations, making sure that the convergence is obtained with less than 0.6% of variation for any case.

- The mesh can be "redistributed" to get a more homogenous cells area proportion, and the solutions obtained are enough similar to consider the verification done above to be valid.

- The parameter "power reaching the window" converges with a smaller quantity the rays than the power absorbed in the window. That means that it has been demonstrated how the simulations for the power reaching the window, made in previous research [17], with $3 \cdot 10^6$ rays, have a convergence with less than 0.5% of variation.

- The value of $3 \cdot 10^7$ is set for the study of the power absorbed in the SC. If the objective is comparing several types SC, the size of Target Plane can be smaller as it was demonstrated in previous research and therefore the number of rays can be decreased [17].

- The variation of the percentage rays rejected after reflection it is not studied since this percentage is a relatively small percentage. Previous research studied the behavior of these rays [48]

2.5 Method scheme

Now that the background necessary to understand the method used has been explained, in order to clarify exactly how the simulations are done, Figure 38 is included. This Figure summarizes all the steps followed to obtain the power absorbed in the SC; also, the power reaching the window is included since the method used is the same and to clarify the difference between them. In order to make it easier to identify the parts of the SPHER a scheme of it is included at the bottom left. The FORTRAN input files are colored in green, they are the shape file defined by a mesh in a .txt file and the rays reaching the

target plane, obtained from MIRVAL. After running the FORTRAN code where the SC calculations are accomplished, the power hitting the window (.ALJ file) and the power absorbed by the SC shape (.txt file) are obtained (colored in orange). Once the output files have been saved, MATLAB is used to graph the results. Both Figures show the power striking the window distribution for the window shape (left) and the power absorbed in the CPC case (right).
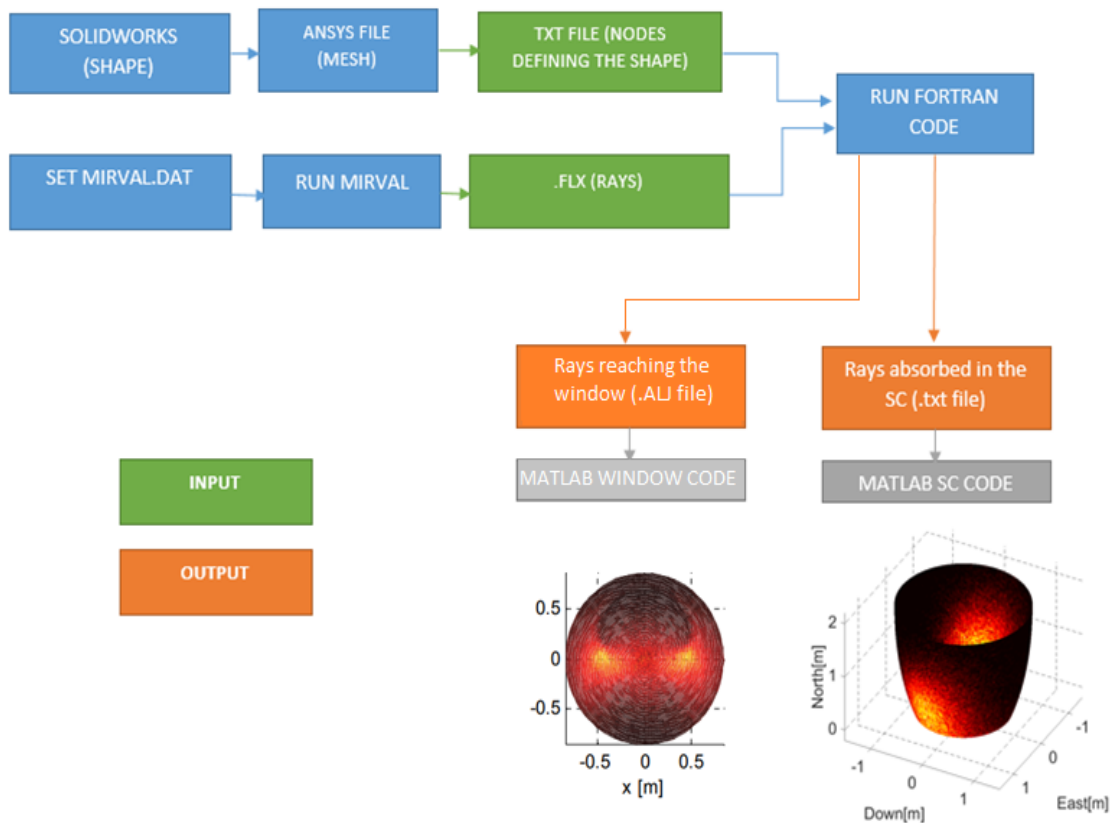
Figure 38. Scheme of the simulation steps necessaries to get the power reaching the window (at the left) and the power absorbed in the SC (At the right) with the ANSYS method. March 21, 1200pm.

2.6 Verification

In section 2.4.4 the necessary number of rays to obtain a stable response with the ANSYS method was calculated. In this section the results obtained with both (ANSYS and exact equation) methods will be calculated and compared. In previous research [17] the code was verified since there is no generated curvature in the ANSYS surfaces, but with several differences.

DAVID CEREZO AGUADO

▪ First, the power absorbed in reflection was annulled since the parameter CPCREFL was set to 1. Therefore, that means the absorbed power in the SC will be always 0. In the current research, since it is mandatory to take into account the power absorbed in the SC results, instead of setting that CPCREFL=1, data from THORLABS is used for a lab spec protected silver coated manufactured mirror (Figure 39) CPCUSEREFLCALC = 1. The function was included in the code through polynomials, which are split into four wavelength bands in order to run faster since there is an exact value for each wavelength.
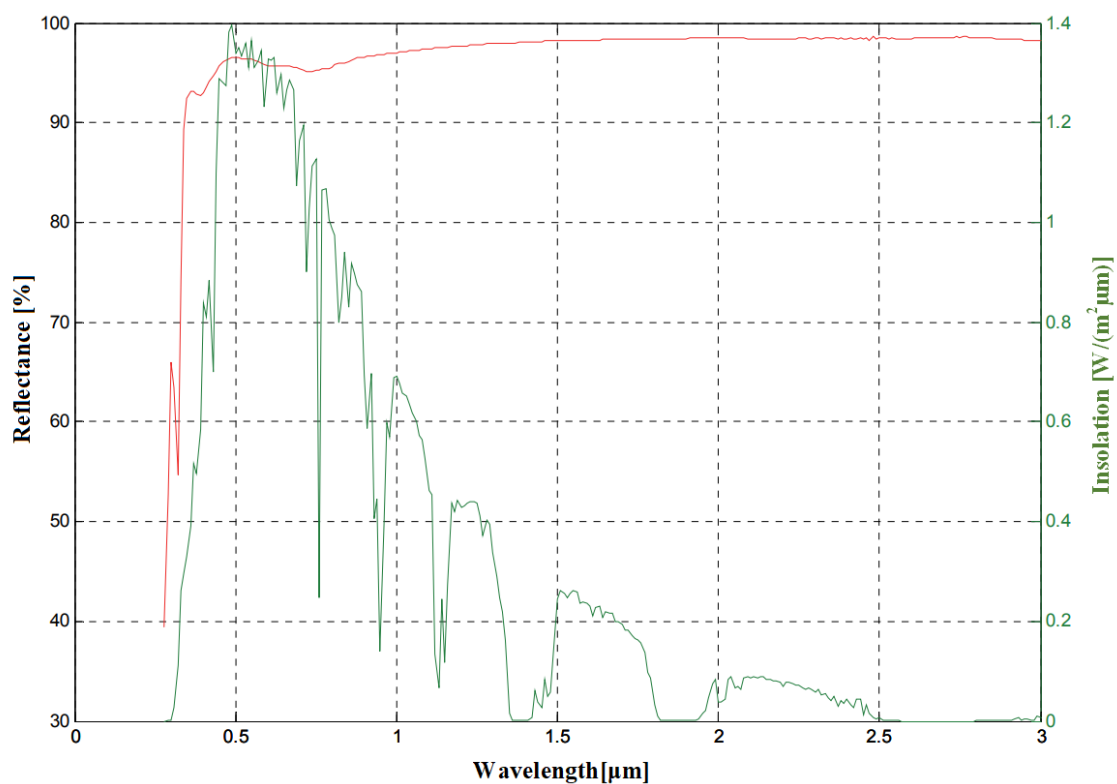
Figure 39. Reflectance for THORLABS mirror with protected silver coating [29] and solar spectrum from NREL.

▪ Second, the FORTRAN code was designed for a target plane which was always smaller or the same size than the SC inlet. The code has been modified to be able to set a target plane bigger than the SC inlet. So that means it is possible to do further research about the SC inlet shape taking into account the power missing the SC inlet. The proportions of power absorbed in the SC, reaching the window…etc. are calculated with respect to the total power and the power

entering in the CPC as well. An image of the command window for one of the simulations is shown in Figure 40

Figure 40. Command window interface with the [percentages referred to the number of rays hitting inside the inlet and the total amount of rays

- Third, in the user guide of the FORTRAN code for the perfect shape [29], it is stated that the trapped[4] rays are going to be considered as rejected. However, it has been found in both codes that rays were being counted as absorbed in the SC because of a counter error. Both codes have already been modified. It is necessary to clarify this concept to be precise but the proportion of trapped rays is really low, less than 0.005% of the total usually so the error had no practical effect on previous [29] results.

- Fourth, the verification was done with a number of rays, which is enough for an accurate determination of the power reaching the window, but not enough to obtain a stable power absorbed in the SC, as has been demonstrated in the section 2.4.4.

---

[4] Related with the CPCRECLIM explained in the section 2.4.1.2

- Fifth, the ***number of surfaces*** of the ANSYS shape ***has been decreased*** from ***26520 to 14400.*** A calculation of how the decrease in the number of surfaces influences the results is done in this section.

The parameters, which are not modified for the verification, are:

- The error in the shape is set in 0 in both cases.

- The error in the heliostat field is set in 1.2mrad in both cases.

- The random number is set as a constant since in this way is possible to compare the files ray by ray. In the MIRVAL.FLX file every ray is numbered. The RANDOMGEN (random number generator) subroutine is called repeatedly during the reflection when the code is running, and it influences in the slope error and the how the rays is classified. So in order to be able to perform an exact comparison ray by ray, it is necessary to cancel it. The values set for this subroutine are chosen to obtain logical results, close to what it will be obtained with the subroutine activated. For example, if the value of power accepting the window is 128kW with the subroutine activated, the random number will be set in a constant value which provides a value close to that number.(So the percentages of the different powers (incident, absorbed…) will remain almost constant respect the values that we would obtain if the subroutine was activated.)

Once the differences and similitudes in the verification are exposed, the results for different times in the day are calculated. The summary of the relative error between the results obtained for the perfect shape and the 14400 surface shape is shown in the Table 6.

Even when the number of surfaces is decreased in the mesh from 26520 to 14400, the results are practically the same when the perfect shape or the mesh are used for the calculation. The greatest difference is 0.079% for the rays incident with reflection at 10AM. In the case of interest, rays absorbed in reflection, both methods give the same solution with 0% difference.

Table 6. Relative error between the results obtained with the perfect shape and the 14400 surface shape. March 21

TIME	10AM		
NUMBER OF RAYS	106	$3 \cdot 10^6$	107
RAYS OUTSIDE OF THE ACCEPTANCE ANGLE	0.00%	0.00%	0.00%
RAYS INCIDENT IN THE WINDOW	0.04%	0.04%	0.04%
RAYS INCIDENT WITHOUT REFLECTION	0.00%	0.00%	0.00%
RAYS INCIDENT WITH REFLECTION	0.08%	0.07%	0.07%
RAYS ABSORBED IN REFLECTION	0.00%	0.00%	0.00%
TIME	12PM		
NUMBER OF RAYS	$3 \cdot 10^6$	107	$3 \cdot 10^7$
RAYS OUTSIDE OF THE ACCEPTANCE ANGLE	0.00%	0.00%	0.00%
RAYS INCIDENT IN THE WINDOW	0.04%	0.04%	0.04%
RAYS INCIDENT WITHOUT REFLECTION	0.00%	0.00%	0.00%
RAYS INCIDENT WITH REFLECTION	0.07%	0.07%	0.08%
RAYS ABSORBED IN REFLECTION	0.00%	0.00%	0.00%
TIME	2PM		
NUMBER OF RAYS	107	$3 \cdot 10^7$	$6 \cdot 10^7$
RAYS OUTSIDE OF THE ACCEPTANCE ANGLE	0.00%	0.00%	0.00%
RAYS INCIDENT IN THE WINDOW	0.04%	0.04%	0.04%
RAYS INCIDENT WITHOUT REFLECTION	0.00%	0.00%	0.00%
RAYS INCIDENT WITH REFLECTION	0.07%	0.07%	0.07%
RAYS ABSORBED IN REFLECTION	0.00%	0.00%	0.00%

The number of surfaces have been decreased in this thesis from 26520 to 14400 for studying the power absorbed. It is also checked how the results vary when the number of surfaces is modified. As a last test, the code is tested with different number of rays and the results obtained from 14400 and 26520 mesh are compared to those from the perfect shape at 8:00 AM; the results are shown in Table 7.

Table 7. Relative errors between both methods when the number of rays is increasing.

TIME	800am				
NUMBER OF SURFACES	14400-PERFECT				
NUMBER OF RAYS	2500	10^4	10^5	10^6	10^7
RAYS OUTSIDE OF THE ACCEPTANCE ANGLE	0.00%	0.00%	0.00%	0.00%	0.00%
RAYS INCIDENT IN THE WINDOW	0.00%	0.08%	0.05%	0.03%	0.04%
RAYS INCIDENT WITHOUT REFLECTION	0.00%	0.00%	0.00%	0.00%	0.00%
RAYS INCIDENT WITH REFLECTION	0.00%	0.13%	0.09%	0.06%	0.06%
RAYS ABSORBED IN REFLECTION	0.00%	0.00%	0.00%	0.00%	0.00%
NUMBER OF SURFACES	26520-PERFECT				
NUMBER OF RAYS	2500	10^4	10^5	10^6	10^7
RAYS OUTSIDE OF THE ACCEPTANCE ANGLE	0.00%	0.00%	0.00%	0.00%	0.00%
RAYS INCIDENT IN THE WINDOW	0.00%	0.08%	0.00%	0.03%	0.02%
RAYS INCIDENT WITHOUT REFLECTION	0.00%	0.00%	0.00%	0.00%	0.00%
RAYS INCIDENT WITH REFLECTION	0.00%	0.13%	0.00%	0.05%	0.04%
RAYS ABSORBED IN REFLECTION	0.00%	0.00%	0.00%	0.00%	0.00%

From Table 7 we notice that the number of surfaces can be decreased and the results obtained are practically the same, even with a small quantity of rays in the MIRVAL.FLX (as low as 2500). The differences between them are less than 0.1% in the most unfavorable case. However, it is necessary to remember that even when the results obtained with both methods is the same; it does not mean that the result is valid, since the number of rays has to be increased until the convergence is reached. In addition, the results obtained with a relative small quantity of rays (10^4 - 10^5) can be used to compare the power hitting the window using different SC since it is a variable with a very low variation.

2.7 MATLAB Program used to graph the power absorbed spatial distribution in the SC

MATLAB is used to graph the power distribution in 3D on the surface of the SC. The inputs are the shape file, with the planes which formed it and the AbsorbedPlane.txt file with the number of rays absorbed, the power of each ray and the plane where that ray is absorbed. The MATLAB program reads the shape file and it is stored in 3 arrays X, Y and Z. The AbsorbedPlane.txt is read and stored in an array too. Then, the planes in both files are compared, and if they are the same, the power associated for that ray is stored in the power of the plane where the ray is. Since the results are verified for the ANSYS code with the number rays set, now it is mandatory to test if the MATLAB program is working

correctly. In the FORTRAN code for the ANSYS method, these steps are followed: The intersection point is calculated for every absorbed ray, and then, that point is compared with all the planes in the shape file, in order to find which plane contain that point. Then, that plane is written in the Absorbed Plane file. That means that the MATLAB program is not comparing directly the planes from the shape file. For this reason, it was demonstrated how in the execution of the FORTRAN code, when that planes are written there is a very low difference in them because of the round-off error. That difference is about 10-18 in the studied cases. Therefore it is not possible to use the MATLAB function "Determine equality", which compares directly both planes, because not all rays will be stored because they are not recognized as equals. Instead of that, the 9 nodes which form each plane are subtracted from both files and a tolerance is set for that difference. That part of the code is shown in the Figure 41. The tolerance is set to $1 \cdot 10\text{-}12$ for the number of surfaces used and all the rays are correctly stored.

```matlab
TOL=1e-12;
for j=1:n_rays4
    for h=0:(n_rays(1,2)-2)/4
            h;
            if abs ( values(1,(2+h*4))- (X(1,j)) )<TOL
            if abs ( values(1,(2+h*4+1))- (X(2,j)) )<TOL
            if abs ( values(1,(2+h*4+2))- (X(3,j)) )<TOL

                if abs ( values(2,(2+h*4))- (Y(1,j)) )<TOL
                if abs ( values(2,(2+h*4+1))- (Y(2,j)) )<TOL
                if abs ( values(2,(2+h*4+2))- (Y(3,j)) )<TOL

                    if abs ( values(3,(2+h*4))- (Z(1,j)) )<TOL
                    if abs ( values(3,(2+h*4+1))- (Z(2,j)) )<TOL
                    if abs ( values(3,(2+h*4+2))- (Z(3,j)) )<TOL


                    power(1,j) = double(power(1,j))+double(values(3,2+h*4-1));
                    power(2,j) = double(power(2,j))+double(values(3,2+h*4-1));
                    power(3,j) = double(power(3,j))+double(values(3,2+h*4-1));
```

Figure 41. MATLAB code comparing the values in both files. (Absorbed Plane and Shape File)

DAVID CEREZO AGUADO

2.8 Tilt angle and acceptance angle.

These variables influence directly the results and have to be set for the simulation. Both angles have been studied by a previous researcher [29], but it is necessary to study how these variables have to be set as a function of the different inlet-outlet shapes.

The tilt angle is represented by the parameter "DELTAD", which is shown in Figure 16 (section 2.4.1.1). This angle is assumed to be fixed once the SC is positioned, so the optimum angle has to be calculated. The case studied is for Rout=0.85m and the most efficient disposition for that window radius is set in 26 degrees, using the results of several simulation series [29].
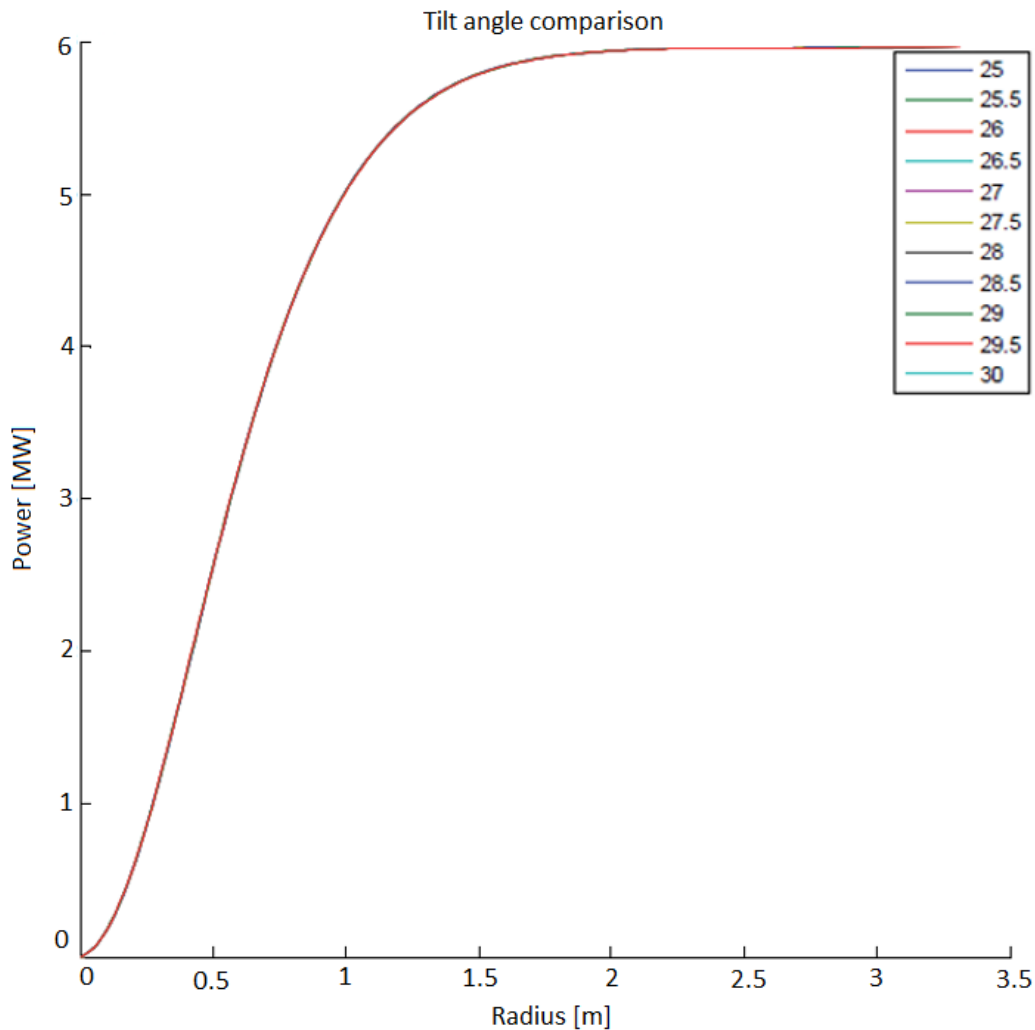
Figure 42. Power incident in the window, function of the outlet radius and the tilt angle in the CPC case. March 21 12pm. [29] (Modified)

The results obtained show the small variation between the power hitting the window when this parameter is varied. For example, if the tilt angle is set in 22 or 30 degrees instead of 26, the difference between them is about 0.1%. A review of this idea is shown in Figure 42. For the entire Rout interval, the angle varies progressively from 25 to 30, increasing 0.5 degrees every time, and the results obtained are practically identical.

So in one hand the optimum tilt angle for the CPC case was calculated using several simulations, and in the other hand, the low influence of this parameter over the power absorbed in the window has been demonstrated. Due to the presented result, this angle will be set in 26 degrees for all the simulations.

The simulations run so far in this thesis are for the March 21 and the tilt angle optimum calculated before [29] is only applicable for that specific day. During the course of the year the sun position is changing and therefore the optimum tilt angle is changing too, being neccesary to calculate it every certain interval time. This task was done for 12 different days during the year for an *alternative CPC with wings* [49], and the results are shown in the Figure 43. The optimum tilt angle at March 21 is close to 25, but the Figure is attached to realize how the optimum tilt angle varies during the year.
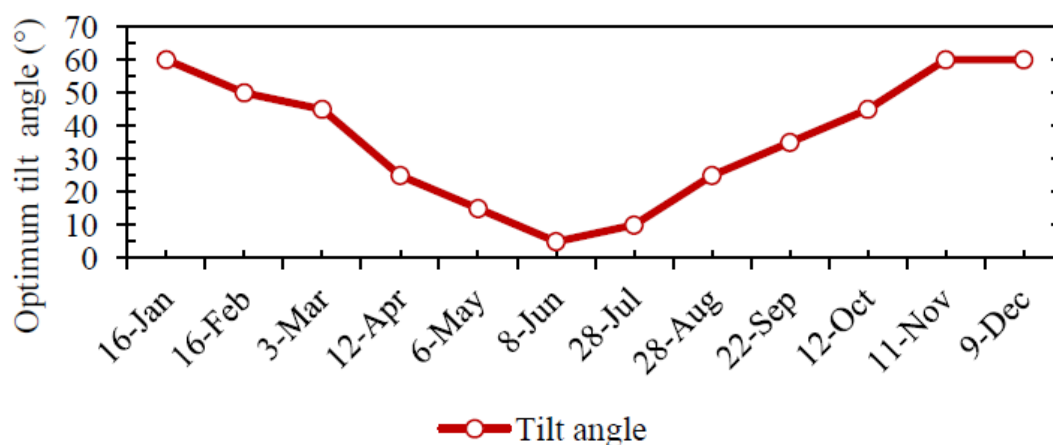
Figure 43. Optimum tilt angle calculated for the central part of the CPC with wings by month. [49]

Two simulations are performed in order to test if the graph above can be used to approximate the optimum tilt angle already calculated for an *alternative CPC with wings* to a *regular CPC*. All the parameteres are the same in both simulations (December 21, 1200pm, Rout=0.85m..) except for the tilt angle, which is set in 26⁰ (the value used so

far) and 60⁰ (approximately the value show in the Figure above). The table 8 shows the results:

Table 8. Power incident in the window when the tilt angle is modified from 26 to 60 degrees. Dec 21, at 12pm.

Tilt Angle (⁰)	Power incident in the window (MW)
26	4.43
60	3.16

When the tilt angle is set in the value shown in the Figure 43, the power incident in the window decreases about 30% compared to the case when the tilt angle is set to 26⁰. So the tilt angle calculations performed for the *alternative CPC with wings* cannot be extrapolate for the *regular CPC*. In any case, it is recommended to study the optimum tilt angle for different moments of the year in order to test if it is worth it to track the SC for increasing the power incident in the window.

The variance of the acceptance angle has a great influence too. In order to understand what is the acceptance angle, the Figure 44 is included. The acceptance angle is named by θ_c, the CPC radius are defined by *Rintlet=a* and *Routlet=a'*. Physically θ_c represents the maximum angle that the rays can have in order to be incident by the concentrator and it is defined by the Equation 5:

$$\theta_c = tg(\frac{a + a'}{h})$$

Eq.5

For the CPC case, previous researches defined the optimum acceptance angle for a specific case, on March 21 at 12:00pm. This value was set in $\theta_c=46°$, since the incident rays start to decrease when this value is larger. These tests were run with the concentrator mirror surface reflectivity set to 100 % [29].
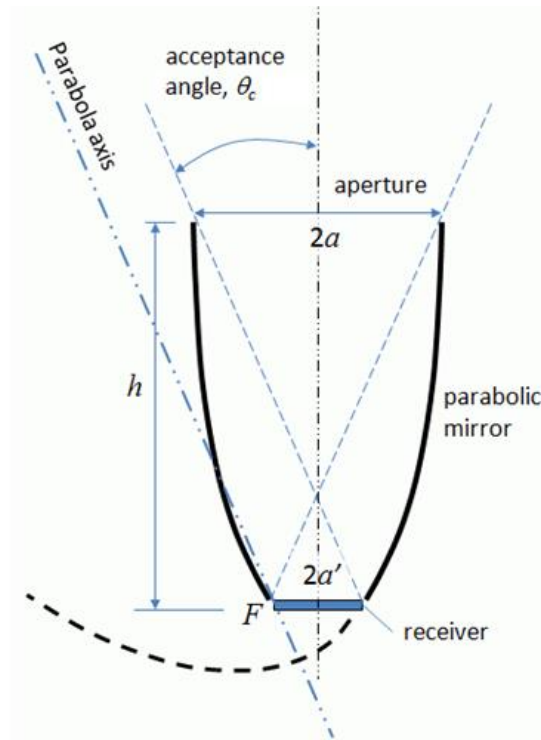
Figure 44. Geometry of the CPC (modified) [50]

In the case of the CPC, every vertical 2D projection of the 3D shape is always the same, since the inlet and the outlet are circumferences, so a and a' will be constant in any case, therefore the θ_c will be constant too.

However, for the hexagonal-round and the hexagonal-hexagonal cases, the value of a and a' depend on which plane the impact point of the rays. In Figure 45 an intuitive diagram is included for a better understanding of this idea, with the hexagonal inlet and the circumference at the inlet. In the Figure below, A and B represent the impact point of two random rays. In the case A the acceptance angle is defined by the a=Rinlet and the a'=Routlet. But this is the only single case when these values are coincident. If the impact point is located in B (for example), the Rinlet (a) depends on the impact angle of the ray. The Routlet (a') in this particular case is constant since the outlet is a circumference. If the hexagonal inlet-hexagonal outlet it is simulated, both values a and a' depend on the impact point.
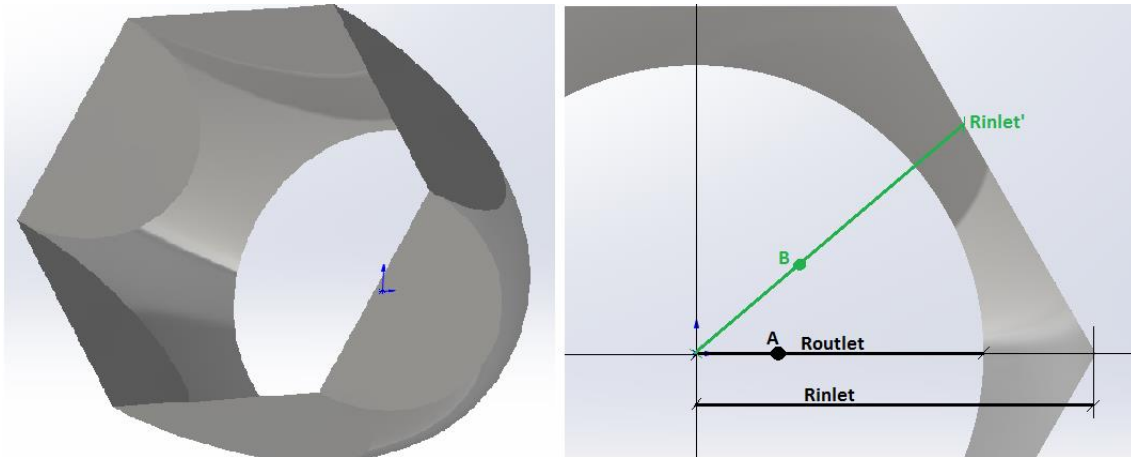
Figure 45. Rinlet and Routlet in function of the impact point for the hex-round case. The impact points of the rays area A and B respectively.

These variables were not taken into account in the previous research [17], so the code has been modified in order to include them. In the modified code the impact point in the target plane and the outlet plane is read for every ray, and used to calculate the variables *a* and *a'* for obtaining the acceptance angle in every case.

Both codes (with and without this Acceptance Angle subroutine) are executed with same inputs and the results are compared, in order to check the variation of them. The random subroutine was deactivated to run these simulations. In the Table 9 below, as a review, the main variable (power incident in the window) is shown for four different input files.

Table 9. Difference between the old and the modified code for the incident power with hex-inlet and round-outlet

HEXAGONAL INLET - ROUND OUTLET (MARCH 21)						
ACCEPTANCE ANGLE USED		AccAngle	46	RE	AccAngle	46	RE
Number of rays		12pm, 10^5 rays		%	12pm , 10^6 rays		**%**
RAYS INCIDENT IN THE WINDOW	%	93.23	94.05	0.88%	93.13	94	0.93%
	(W)	5360159	5407263		5308929	5358486	
Number of rays		8am, 10^4 rays		%	10am, 10^4 rays		**%**
RAYS INCIDENT IN THE WINDOW	%	93.94	94.63	0.73%	93.68	94.41	0.78%
	(W)	2714507	2734442		4834325	4872148	

If at the top of the column there is written "AccAngle" the modified code with the correct acceptance angle, when there is written "46" the Acceptance Angle is set in 46 for all the cases. The differences, represented by the Relative Error, in both results vary between

0.78% to 0.93% for the hex-inlet and circ-outlet. In all cases, as is logical, the power of rays incident in the window decrease since the acceptance angle is decreasing too. Several times of day were tested: 8am, 10am and 12pm. In addition, for the M case (12pm) the number of rays is increased to test that the solution does not vary much, and it is shown how the result varies 0.05%.

Table 10. Relative error between the old and the modified code for the incident power with hex-inlet and hex-outlet

HEXAGONAL INLET - HEXAGONAL OUTLET (MARCH 21)						
ACCEPTANCE ANGLE USED	AccAngle	46	RE	AccAngle	46	RE
MIRVAL INPUT FILE	12pm, 10^5 rays		%	12pm , 10^6 rays		%
RAYS INCIDENT IN THE WINDOW	%	91.38	93.21	2.00%	91.34	93.12	1.95%
	(W)	5253686	5358765		5206943	5308232	
MIRVAL INPUT FILE	8am, 10^4 rays		%	10am, 10^4 rays		%
RAYS INCIDENT IN THE WINDOW	%	92.49	93.87	1.49%	92.35	93.68	1.44%
	(W)	2672422	2712292		4765770	4834325	

In the case hex-inlet and hex-outlet (Table 10), the differences are greater and vary from 1.44% to 2%. This fact is normal, since now both (inlet and outlet) distances are decreasing, and therefore the acceptance angle is decreasing proportionally. The same input files were used as for the hex-inlet and round-outlet.

The newly calculated acceptance angle varies now from about 41.8 to 46 degrees depending on the position of the ray. Therefore, it is not possible to set an "optimum *single* acceptance angle" (since it will be varying in function of the ray impact point) as it was done with the perfect CPC case. One possibility is to set the "reference" acceptance angle in the R_{inlet} case (46 in this case). Another possibility is to calculate the average acceptance angle for every simulation. However, it is necessary to remember that these optimum angles in all the cases are calculated for a specific day and time.

In the annexes it is shown that the other variables vary (power absorbed, rays incident with reflection…) too, except the rays incident without reflection, with exactly the same percentage. It makes sense since the rays incident in the window directly must have a small angle at the inlet. The largest difference is in the rays rejected after reflection, but

they only represent a small percentage from the total (Less than 1%). These calculations have been performed using the acceptance angle, which is an approximation for the optimum CPC case. The percentages of the rays rejected after reflection have decreased when the new subroutine has been added, being still a low percentage of the total rays (decrease from 0.13% to 0.03% for hexagonal-round case and decrease from 0.76% to 0.18% for hexagonal-round case). Other researchers have studied the behavior of the rays rejected after reflection [48] and it would be interesting to test how the results can vary when the percentage of rays rejected after reflection increases for the new SC shapes.

2.9 Elliptical inlet

Since the ANSYS method allows the user to test any shape, and taking into account that the inlets tested so far are axisymmetric, a new shape for the inlet will be tested, specifically an ellipse, while the outlet will remain circular. The ellipse in the code is defined by the two main parameters the semi-major axis "a" and the semi-minor axis "b". The point "C" is centered in the target plane's origin (0,0) and "c" represents the focal distance (Figure 46).
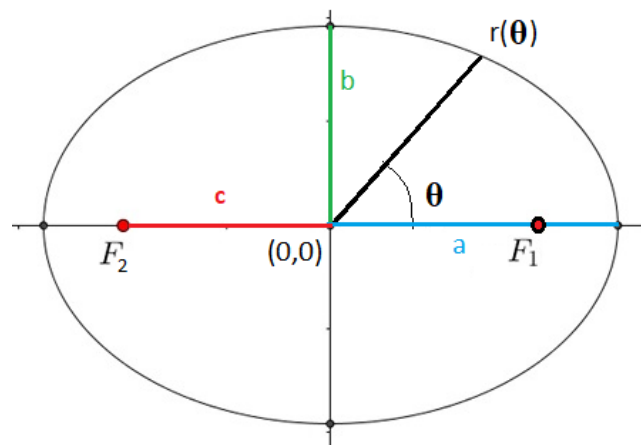
Figure 46. Ellipse shape with its main parameters

The new shape is implemented in the code by polar coordinates, with the Equation 6:

$$r(\theta) = \frac{b}{\sqrt{1 - \varepsilon^2 cos^2(\theta)}}$$

Eq.6

Where the ε represents the ellipse eccentricity and it is given by the equation 7:

$$\varepsilon = \sqrt{1 - \frac{b^2}{a^2}}$$

Eq.7

The eccentricity is calculated since it is related with the focal points, which are interesting for the future work (Section 4) and because is a variable which could be vary to study how the results change.

$$\varepsilon = \frac{c}{a} \; with \; (0 \le \varepsilon \le 1)$$

Eq.8

If in the future it is decided that the eccentricity is a "unimportant variable", the distance r can be calculated directly with the known values "a", "b" and the angle "θ ":

$$r(\theta) = \frac{1}{\sqrt{\frac{cos^2(\theta)}{a^2} + \frac{sin^2(\theta)}{b^2}}}$$

Eq.9

In the FORTRAN code the semiminor axis "b" is defined by the variable CPCRIN (which can be modified), and the semimajor axis "a" is directly an input variable "SEMIMAJOR". Therefore, the three inlets implemented so far (all of them are represented in the Figure 47) are defined by only two parameters "CPCRIN" and

DAVID CEREZO AGUADO

"SEMIMAJOR" since the hexagon is inscribed in the CPC circumference, making easier the code and the modification of the values for these variables.
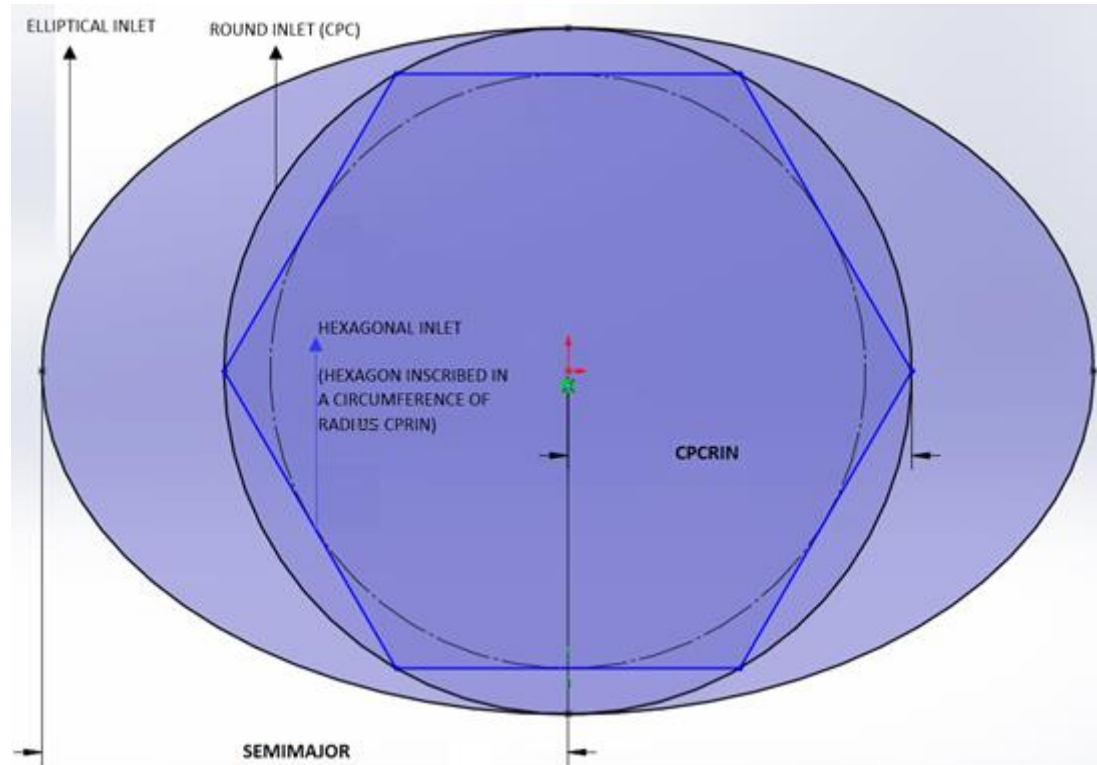
Figure 47. Different shape's inlet for the SC and variables that describe them CPCRIN and SEMIMAJOR

In the CPC case, the shape is axisymmetric and the curve can is defined by an equation. This equation gives the radius for every z value, using the acceptance angle and the outlet radius.

So in order to test the CPC shape with the ANSYS method, the same shape was designed using the equation and revolving it [17]. However, for the ellipse inlet and round outlet, the surface cannot be designed as a revolved curve, so the "Loft" function is used in SOLIDWORKS, using as reference the inlet and outlet shape. A curvature is given to the surface and some simulations are done with a 10807 cells mesh. The random subroutine was deactivated to run these simulations. In Table 11 the results are shown for several inlets shapes for March 21, 12:00 PM. First, the non-curvature shape is tested, with 1.5m semimajor's length (For all the cases the semiminor is constant and equal to 0.85 m) and the power incident is pretty lower, compared to the CPC incident power.

Table 11. Results for different elliptical inlet shapes with MIRVAL M3 as input file. March 21, 1200pm.

10^4 rays		CPC	ELLIPSE					
21-mar	Degrees out (Start constraint)	23	25	0	25	0	25	
1200PM	Degrees in (End constraint)	0	-	-	-	-	-	
	(m) SemiMajor	1.2	1.2	1.2	1.3	1.5	1.5	
Rays incident window	(%)	94.12578	93.91731	93.71249	92.38354	89.41651	79.39634	75.94823
	(W)	5502308	5495619	5483634	5405870	5253686	4685087	4481618
Rays incident with reflection	(%)	52.78692	52.60551	52.40069	51.07173	48.14042	38.21737	34.76926
	(W)	3085763	3078238	3066253	2988488	2828500	2255163	2051694
Rays incident without reflection	(%)	41.33886	41.3118	41.3118	41.3118	41.27609	41.17897	41.17897
	(W)	2416545	2417381	2417381	2417381	2425185	2429924	2429924
Rays rejected after reflection	(%)	7.63E-02	0.362008	0.566829	1.89578	5.256167	15.72906	19.17718
	(W)	4459.599	21183.09	33168.26	110932.5	308827.2	928154	1131623
INSIDE INLET	(%)	98.11012	98.20835	98.20835	98.20835	98.61066	99.03635	99.03635
	(W)	5845698	5851551	5851551	5851551	5875521	5900885	5900885
OUTSIDE INLET	(%)	1.889882	1.791645	1.791645	1.791645	1.389344	0.963653	0.963653
	(W)	112604.9	106751.6	106751.6	106751.6	82781.3	57417.33	57417.33

As the inlet is bigger in the ellipse-round case, the power incident in the window may have been expected greater than in the CPC case; however, the power incident in the window is greater in the CPC than in any of the Ellipse entrances. In fact, the power incident in the window, is greater every time that the ellipse's semimajor is decreased. Figure 48 shows how the shapes have been designed. At the left, the ellipse inlet and round outlet shape is created with no curvature. The curve at the top of this left side image stands the curve defined for the CPC. At top right, the shape is defined with 25 degrees at the start constraint, but the shape exceed the CPC curve. Therefore, in the bottom right, finally the shape is adapted to the CPC curve perfectly for the vertical plane with 23 degrees at the start constraint and 2 degrees at the end constraint. A simulation is run and the power incident in the window for this case is even lower than when the vertical plane

DAVID CEREZO AGUADO

is not matched with the CPC curvature, so the results are irrelevant and for that reason not added to the table.
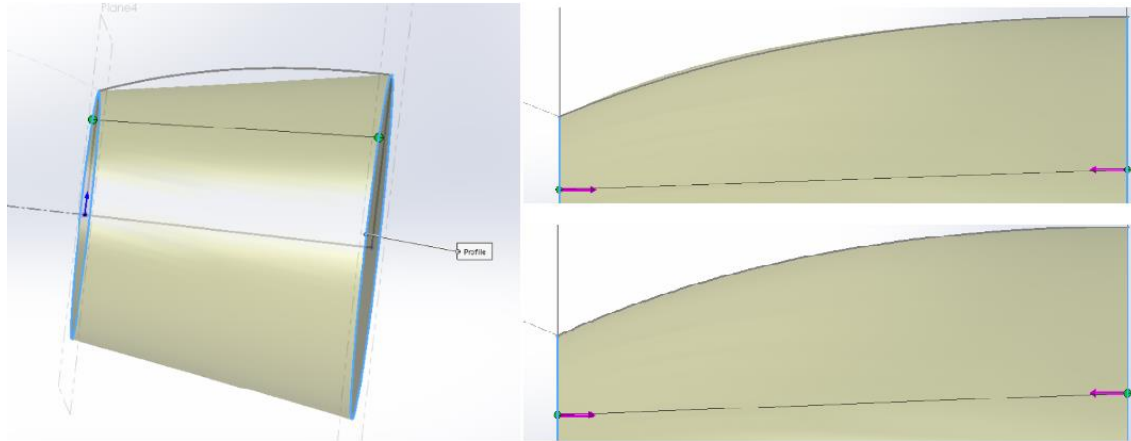
Figure 48. Design of the Elliptical entrance and round outlet when the vertical plane is matched with the CPC curvature.

It is shown in Table 11 how the power incident in the window increases progressively as the semimajor axis is decreased, while the opposite happens for the rejected rays after reflection. While the rays hitting the window without reflection are almost constant for every shape, the rays hitting the window with reflection vary significantly. This decrease is coincident with the increase in the percentage of rays rejected after reflection. In spite of the bigger inlet, the new amount of rays inside the inlet (Increasing from 98.11% to 99.03%, 98.61% and 98.20% respectively) do not compensate increase in the rays rejected. In order to check in which reflection the largest number of rays is, a new file REJ_RAYS.txt is added as output in the code, and the information obtained is shown in the Table 12.

The greatest augmentation is in the rays rejected after hitting two times in the SC, and this is reasoned because of the hit angle, which is bigger when the inlet is increased. It is necessary to remember that the CPC shape is the most efficient SC.

Table 12. Rays rejected after reflection in CPC and Elliptical inlet- round outlet

CPC		ELL-25D-1.5M	
TOTAL	16	TOTAL	4060
Reflections	Rays	Reflections	Rays
1	0	1	17
2	14	2	3835
3	2	3	149
4	0	4	15
5	0	5	3
6	0	6	1
7	0	7	0
8	0	8	1
9	0	9	0
10	0	10	0
11	0	11	0
30	0	30	39

Now, the rays are reflected to the other SC's face and rejected after one more reflection in most cases. So the CPC is a compromise solution for, in one hand, getting a big enough inlet size to accept a great percentage of the rays from the heliostat field, and in the other hand, it has not a too concave curvature which avoid that the rays are reflected to the other SC face (Figure 49).
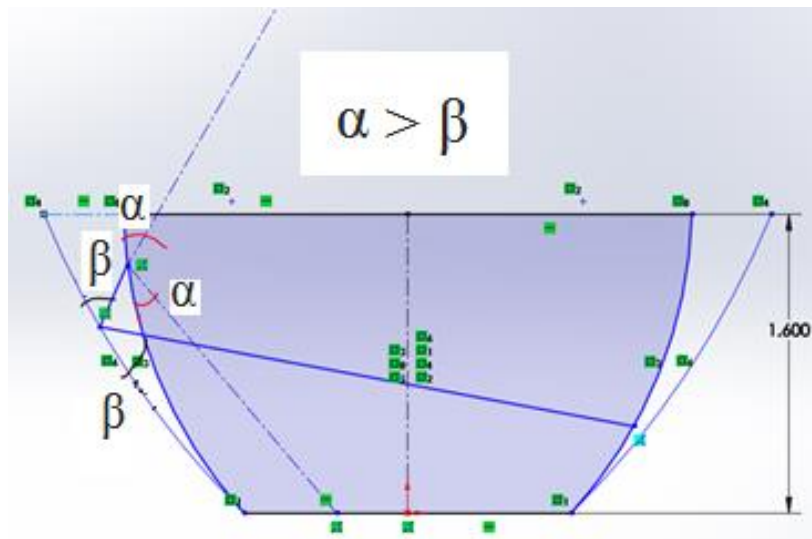
Figure 49. Scheme for the rays rejected after reflection behavior in the elliptical inlet-round outlet compared to the CPC shape.

The time at the input file tested is 1200 pm, when the sun is completely centered, so a new input file is tested, in this case the time is 800 am, on 21-March. The same four first shapes simulated at 1200 pm are tested in the Table 13 for 8:00 am. The results show how the SC behavior is the same. The power incident in the window increases each time that the semimajor axis is decreased. The problem resides again in the rays incident with reflection, due to the new more concave shape, are reflected and rejected out of the SC. At 8:00, as was expected, the difference in the power inside the inlet is greater, since the position of the sun is not that centered as 1200 pm and the power distribution in the target plane it is not so centered, and it will be more oval than round. In spite of that fact, the power incident is still lower than in the CPC.

Table 13. Results for different elliptical inlet shapes with MIRVAL P5 as input file. March 21, 800am.

10^5 rays	CPC	ELLIPSE				
21-mar	Degrees	25	25	0	25	Units
08:00AM	Semimajor	1.2	1.3	1.5	1.5	(m)
Rays incident window	94.61836	94.18457	89.70299	79.47661	77.68771	(%)
	2872105.7	2869891	2779629	2519253	2462548	(W)
Rays incident with reflection	55.199212	54.85043	50.69874	40.91401	39.12512	(%)
	1675551.9	1671343	1571003	1296894	1240190	(W)
Rays incident without reflection	39.419148	39.33413	39.00425	38.56259	38.56259	(%)
	1196553.8	1198547	1208626	1222359	1222359	(W)
Rays rejected after reflection	0.1495914	0.650602	5.418349	16.03368	17.82258	(%)
	4540.791	19824.43	167898.5	508236.3	564940.9	(W)
INSIDE INLET	90.074931	90.42001	91.95149	94.06139	94.06139	(%)
	3035463.4	3047092	3098702	3169804	3169804	(W)
OUTSIDE INLET	9.925069	9.579992	8.048508	5.938609	5.938609	(%)
	334468.02	322839.2	271229.2	200127.1	200127.1	(W)

DAVID CEREZO AGUADO

3. RESULTS

This chapter shows: the comparison of both methods (Perfect shape vs ANSYS mesh), how the main variables influence in the graphs and how the power-absorbed areas are changing during the day. In every graph *East* and *Down* are positive. All the data shown in the graphs in this chapter has been calculated with the random subroutine activated in order to get a real distribution of the power absorbed. In addition, the new meshes with a more homogenous area distribution are used.

3.1 Perfect shape vs ANSYS mesh.

It was already tested that the main powers (power incident in the window, power absorbed in reflection…) were practically identical, if the perfect shape or the ANSYS mesh were used for the calculations. In this section, it will be tested if the distribution of power absorbed in reflection in the SC is also the same in both methods.

In order to compare both methods, both shapes are divided in the same number of cells, but with a difference in the process to do it. In the perfect shape case, the shape is divided in *n* vertical divisions (north) and *phi* angle. The number of vertical divisions is set in 120 and the angle for the divisions $phi = 3°$. Then, for the perfect shape, a $120 \cdot 120$ cells mesh is created, with 14,400 quadrilateral cells. For the second method, the mesh was already defined with 14,400 triangular cells in ANSYS.

The Figure 50 shows the power absorbed distribution by the 3D CPC for both methods, at 12pm on March 21 with $3 \cdot 10^7$ number of rays. The total absorbed power is about 128kW, with a 0.2% between the results obtained from both methods. At the left, the perfect shape divided in quadrilaterals, and at the right, the ANSYS mesh divided in triangular cells. The same scale is set for both graphs, and the peak absorbed power is about $70kW/m^2$.

The power absorbed in reflection is a little percentage of the power that is hitting inside the SC inlet. The power hitting inside the SC inlet is 5,8MW versus the 0.128MW which are absorbed in the SC. Both graphs show the same spatial distribution of power absorbed. This distribution is explained at section 3.2, then it has been demonstrated the similarities

in the global values and in the spatial distribution of power absorbed obtained with both methods.
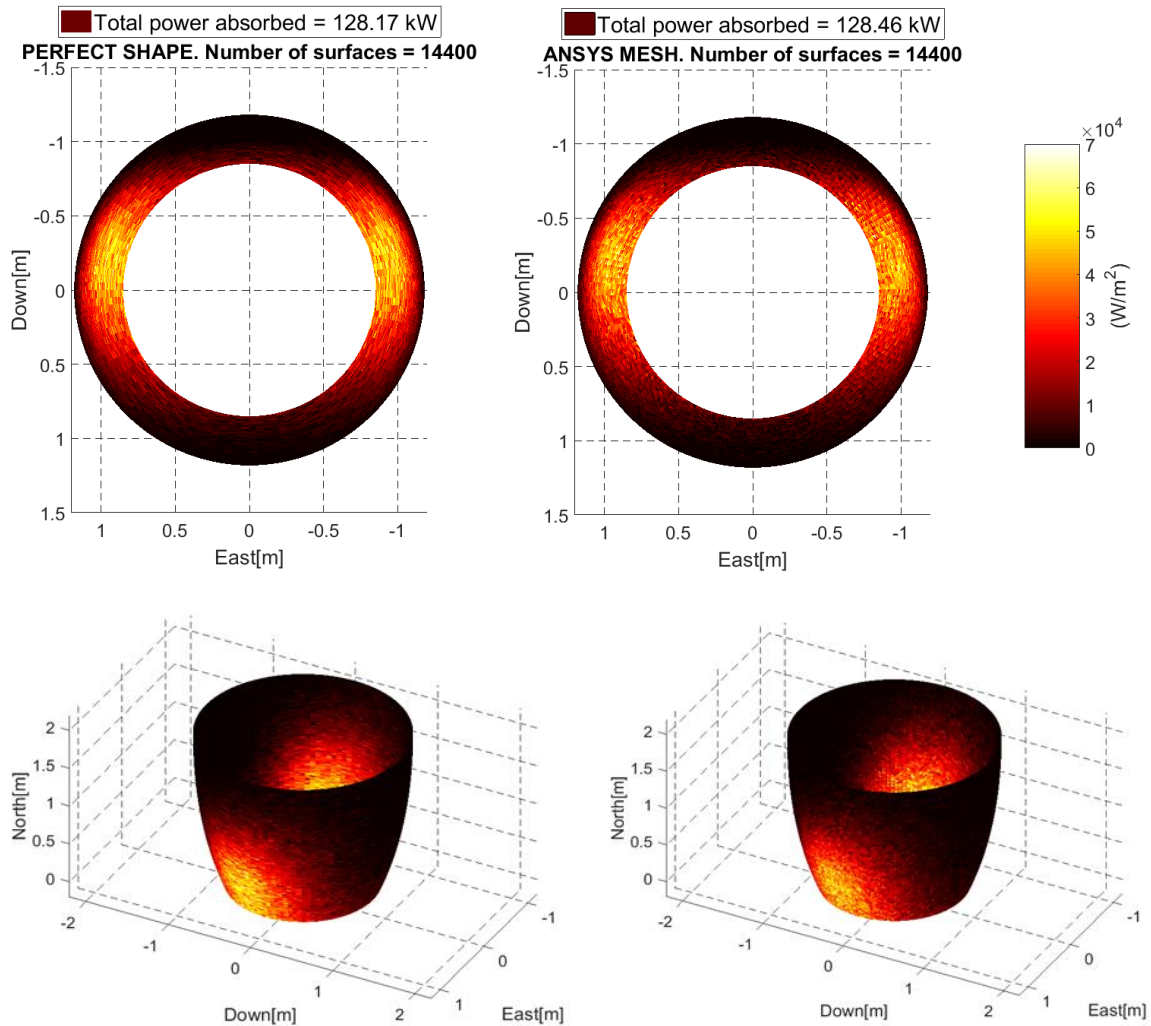
Figure 50. CPC absorbed power, March 21, 1200pm. Left: Graph obtained from the perfect CPC defined by an equation. Right: Graph obtained from the ANSYS method. Power of rays hitting inside SC inlet: 5.8 MW

3.2 Quality change when number of rays or surfaces are increased or decreased

Section 2.4.4 shows the relationship between the number of surfaces and the number of rays. There is a relation of proportionality, the more the number of surfaces is increased, the more the number of rays must be increased to keep the error constant [44]. The stability of the solution (main powers) does not only affect to the calculations, but also to

the graphs appearance. Therefore there are two methods (in addition to the option of redistribute the mesh as was explained in the last chapter) in order to get a better quality in the graphs.

First, the number of rays is increased. However, this method involves a greater simulation time every time that this variable is increased. The number of rays was set in the section in order to get the minimum number, which gives a stable response for optimizing the simulation time. The simulation time is a main variable in the ANSYS method. The Figure 51 illustrates this example.

Both graphs show the same mesh with 14,400 cells, but at the left a 10^5 rays MIRVAL file is used, and at the right $6 \cdot 10^7$ rays are used for the simulation. When the 10^5 rays file is used, the graph looks grainy and not homogenous, since the difference of power absorbed between a (any) cell and its adjacent cells is not uniform. If the number of rays is increased, the spatial distribution turns into soft and homogenous. The simulations time are 1,110 seconds when 10^5 rays are used, and 6,684 seconds when $6 \cdot 10^7$ rays are used.
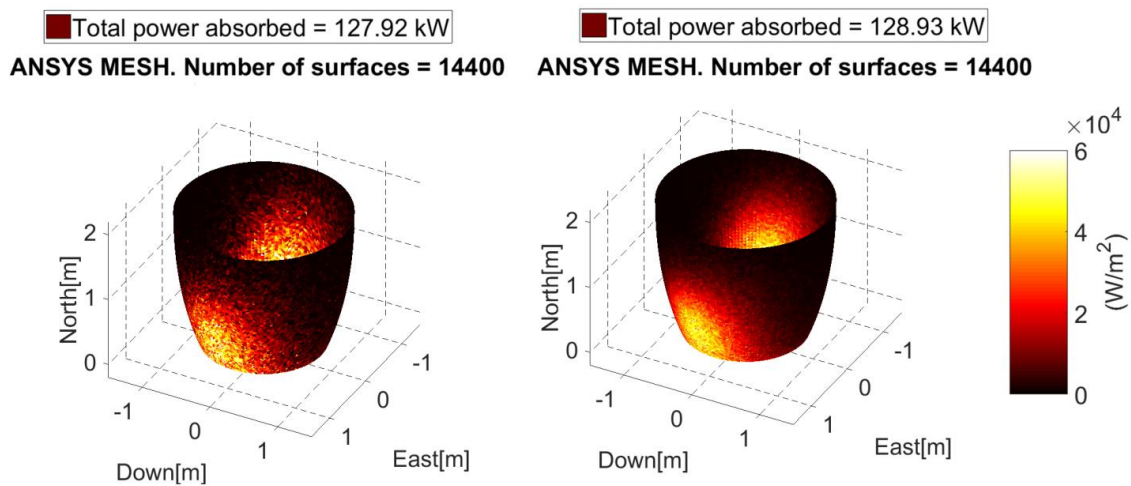
Figure 51. CPC absorbed power, March 21, 1200pm. Left: Graph obtained from the ANSYS mesh with 14,400 cells and 10^5 rays. Right: Graph obtained from the ANSYS mesh with 14,400 cells and $6 \cdot 10^7$ rays.

Second, the number of surfaces is decreased. It was demonstrated in the sections 2.4.4 and 2.6 how even when the number of cells is decreased and the cells are redistributed the results obtained are practically the same than in the original case. Therefore the best option in case of being necessary, will be decreased the number of surfaces in the mesh

in order to improve the graph quality and decrease the simulation time. For example, in the hexagonal-hexagonal case, the same MIRVAL file with $3 \cdot 10^7$ rays at 12pm on March 21 is used to get the graphs for a 21,240 and 14,400 cells mesh respectively. The Figure 52 shows both graphs.
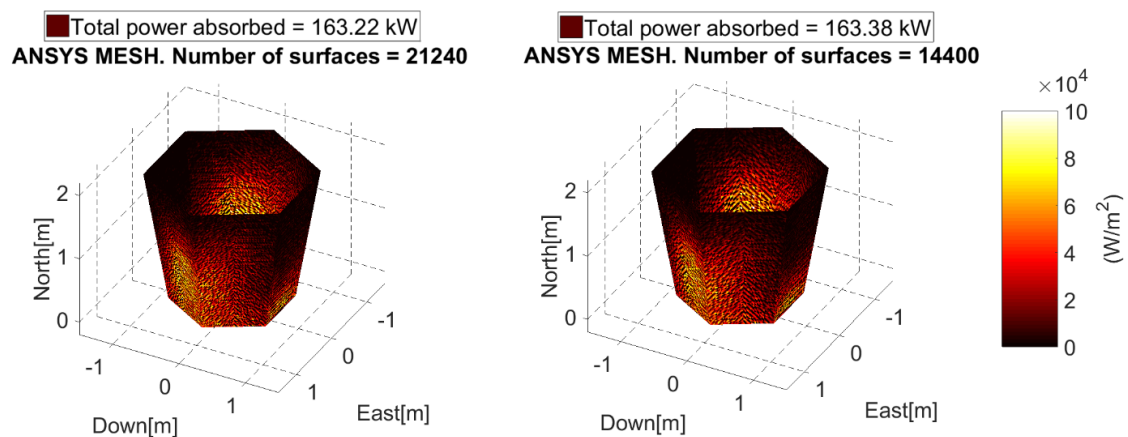
Figure 52. Hex-hex SC absorbed power, March 21, 1200pm. Left: Graph obtained from the ANSYS mesh with 21,240 cells and $3 \cdot 10^7$ rays. Right: Graph obtained from the ANSYS mesh with 14,400 cells and $3 \cdot 10^7$ rays.

Now, when the number of cells is decreased, the quality stays practically constant. Therefore, the 14,400 cells mesh will be used to accomplish the next graphs, since the same quality is gotten with a minor simulation time (6,437 seconds for the 21,240 cells mesh versus the 4,415 seconds for the 21,240 cells mesh).

3.3 Round-Round shape

This section exposes the evolution in the distribution of power absorbed in the SC during different times on the day. The Figure 53 shows the power absorbed distribution in the CPC shape at 12pm (up), 2pm (middle) and 4pm (down) on March 21, with a $3 \cdot 10^7$ MIRVAL file. The graphs at 8am and 10am are not attached because the morning should be almost a mirror image of the afternoon. The mesh has 14,400 triangular cells. The scale referred to W/m^2 in the colorbar; instead of keeping constant for the three simulations; is automatically set by MATLAB to appreciate better the power distribution in every case. The azimuth and elevation are set in 118° and 33° to appreciate better the change in the power absorbed distribution.

At 12pm the distribution of the power absorbed is the expected, concentrated in the upper part of the East and West part in the SC. The tower is facing the north and the sun is centered, so both sides of the heliostat fields are reflecting rays to the Target Plane. In addition, the heliostat field is in the ground and it is reflecting the rays up towards the target plane located in the tower at the height HTMMI previously defined in MIRVAL. The peak absorbed power is about 70kW/m^2 and the total power absorbed is about 128kW.

At 2pm, the position of the sun moves to the West, and the East part of the heliostat field reflects more rays than the West part. In the middle graph is possible to see how the East-Up part in the SC turn from yellow to red since the power absorbed is less in proportion now. In this case the peak absorbed power is about 60kW/m^2 and the total power absorbed is about 117kW. Both parameters have decreased as was expected.

From 2pm to 4pm, the sun is still moving in the West direction, and at 4pm a larger proportion of rays are reflecting from the East part of the heliostat field. Now in the East-Up part of the SC the power absorbed keeps decreasing. At 4pm the peak absorbed power is about 35kW/m^2 and the total power absorbed is about 69kW.

3.4 Hexagonal-Hexagonal shape

All the variables explained in the section 3.3 are the same in these simulations, except of the mesh. Now the hexagonal-hexagonal SC is studied. The mesh has 21,240 cells instead of 21,095 (number of cells who was used for the study of the number of rays) since the precision of ANSYS does not allow to set that exact number. The difference in the number of cells it is only a 0.22% and it was exposed in the section 2.6 how the number of cells can be increased or decreased and the result will be almost constant. The Figure 54 shows the power absorbed distribution in the hex-hex SC shape at 12pm (up), 2pm (middle) and 4pm (down). At 12pm, the largest amount of power is concentrated in upper part of the East and West part in the SC, in the same zone that it was concentrated in the round-round shape. The total power absorbed is about 163kW versus the 128kW absorbed in the round-round shape at the same time and the peak absorbed power is about 100kW/m^2.

Figure 53. CPC absorbed power, March 21, 1200pm (top) 2pm (middle) and 4pm (bottom). Graph obtained from the ANSYS mesh with 14,400 cells and $3 \cdot 10^7$ rays.

At 2pm the power absorbed is more concentrated in Up-West face because of the sun position. The peak absorbed power is still about 100kW/m^2 and the total power absorbed is about 149kW. At 4pm the proportion of power absorbed in the Up-East face decreases

as in the round-round shape. The quantity of total power absorbed decreases from 149 kW to 85 kW.
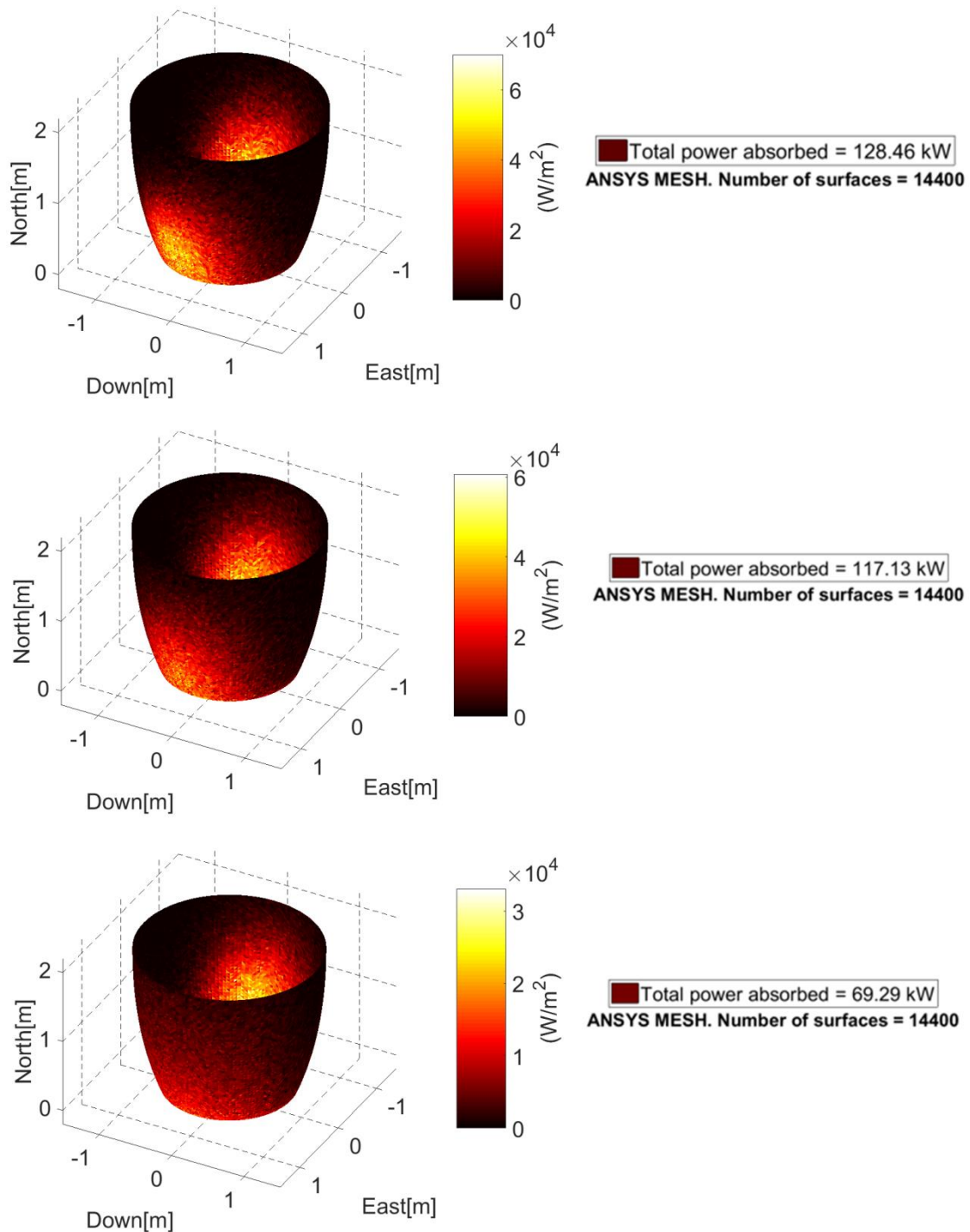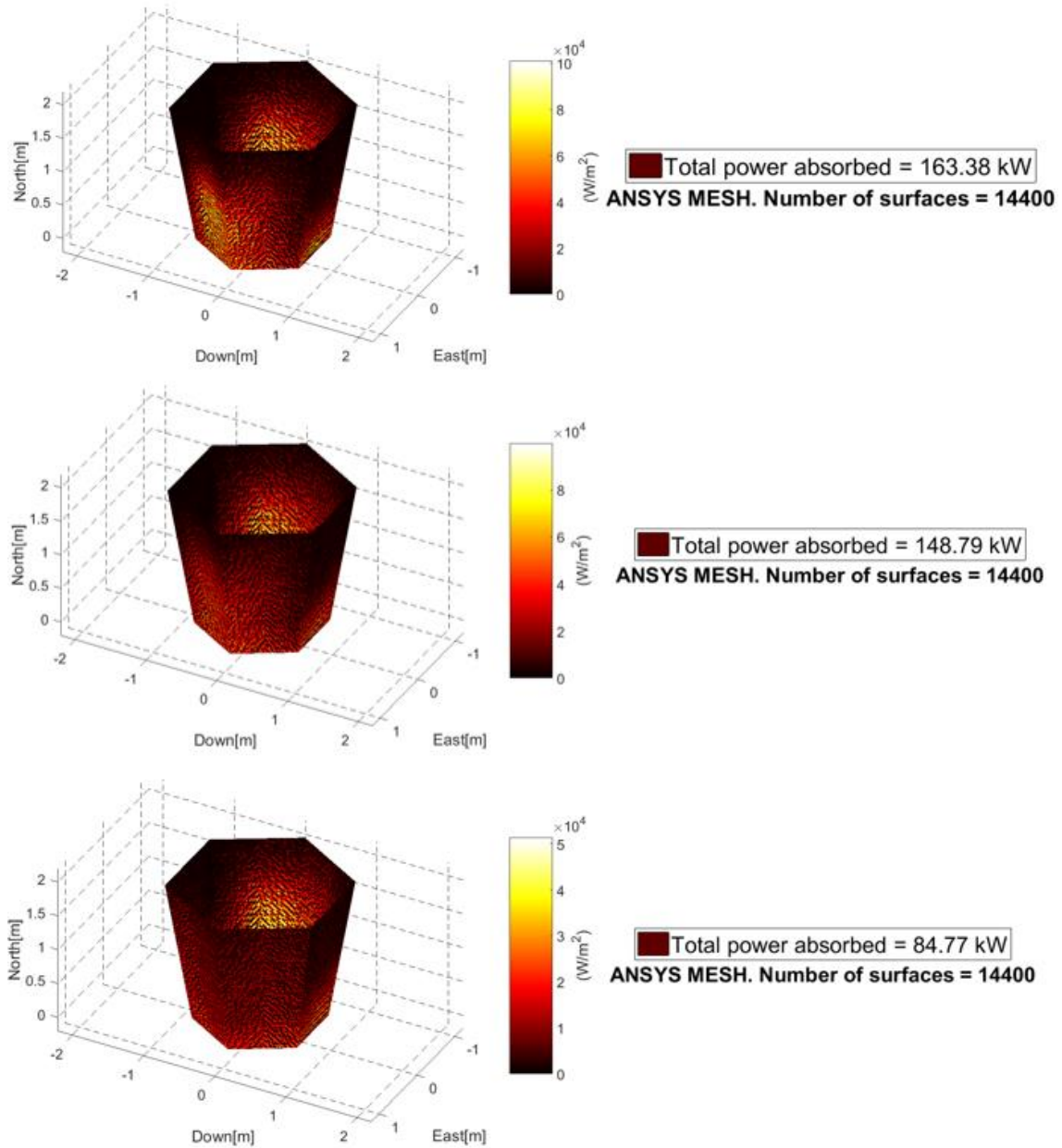

Figure 54. Hexagonal-hexagonal SC shape absorbed power, March 21, 1200pm (top) 2pm (middle) and 4pm (bottom). Graph obtained from the ANSYS mesh with 14,400 cells and $3 \cdot 10^7$ rays.

3.5 Hex-Round shape

In this section is studied the secondary concentrator with the hexagonal entrance and the round outlet. The hexagonal inlet permits add more SC in case of being necessary and the

round outlet permits a better coupling with the window, but this shape involves a more complicated manufacture.

The number of rays used for this simulation is $3 \cdot 10^7$, and the mesh is formed by 19,462 triangles. The difference with the last used meshed, are the edges, which make more difficult to set a homogenous mesh. Now, even when the triangular distribution is set in the mesh, the difference in the areas size is so much greater than in the other meshes. In the original mesh [17], the difference of size was $1.8 \cdot 10^7$, i.e. the smallest was $1.8 \cdot 10^7$ times smaller than the biggest cell. Now, with the new mesh, the difference is $1.2 \cdot 10^4$, still greater than it should be, but about 2,000 times smaller than in the original mesh. The Figure 55 shows the Area Histogram of the 19,462 triangular cells mesh.
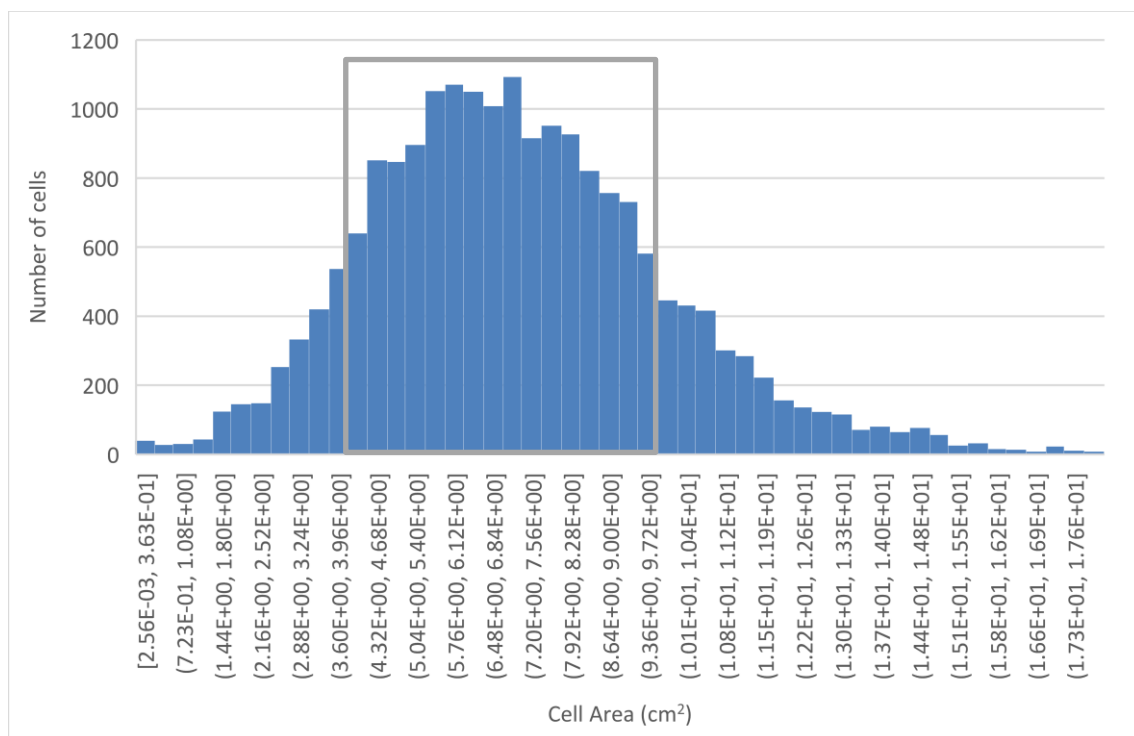
Figure 55. Area distribution in the hex-round shape with 19,462 cells mesh created by ANSYS

It is important to observe that the first bar at the left in the histogram, include a much larger area interval than the other intervals (from $2.56 \cdot 10^{-3}$ cm^2 to $3.73 \cdot 10^{-1}$ cm^2, about 150 times bigger area). For bigger areas, the difference in the interval boundaries is low in comparison. The main percentage (Grey quadrilateral at the graph) of cells have a size reasonably similar, the greatest difference is about 4 times. However, the smallest cells

have a great influence in the graph, since a single ray reaching one of those areas means a great amount a kW/m^2 because the area at the denominator is small.

The Figure 56 shows the graph obtained from the simulation of the 19,462 cells mesh on March 21 at 12pm, if the colorbar scale is set automatically by MATLAB. The peak absorbed power is about 200kW/m^2, three times more than in the Round-round shape and the double than the hex-hex shape.
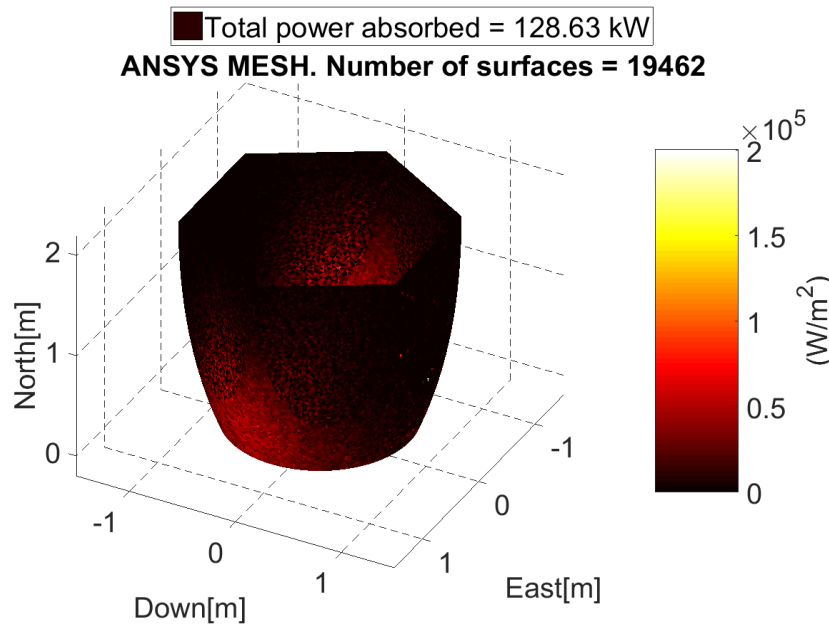
Figure 56. Hex-round SC absorbed power, March 21, 1200pm. Colorbar scale automatically set by MATLAB

In order to verify that the main problem is related with the small size cells, the Table 14 shows the Area of the cells, which have greatest values of power absorbed per square meter (kW/m^2), the power absorbed per square meter and the difference between consecutives values.

Table 14. Cells areas sort in function of the flux, and difference between consecutive values

Area (m^2)	Flux (kW/m^2)	Difference
$9.26 \cdot 10^{-6}$	200690.4	2.2
$5.84 \cdot 10^{-4}$	90711.1	1.1
$1.11 \cdot 10^{-5}$	83452.8	1.0
...	...	...

The cell that has the highest value of power absorbed per square meter is also the smallest cell in the 12,880 cells, which are hitted by at least one ray. The difference between the power absorbed per square meter in this cell is about the double respect the consecutive highest value. After this first value, the difference between consecutives values is about 1 or 1.1. Therefore, if the colorbar scale is set in the next value, the graph should be softer. The limit for the colorbar is set in 90,000 kW/m^2 since is the value of the second power absorbed per square meter highest value, and when the difference starts to decrease uniformly.
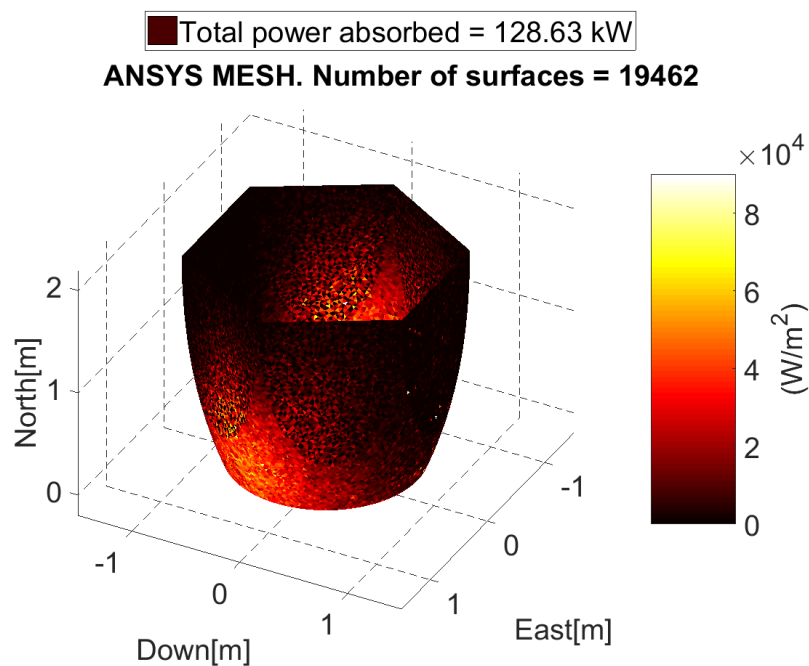
Figure 57. Hex-round SC absorbed power, March 21, 1200pm. Colorbar scale set by the author

The new graph (Figure 57) is clearer but still looks grainy and not completely homogenous. The next step consists on improving the mesh until the required quality is obtained. To create a more refined mesh the program COMSOL is used, and the mesh export with .STL system in the same way than ANSYS. The Figure 58 shows the new mesh.
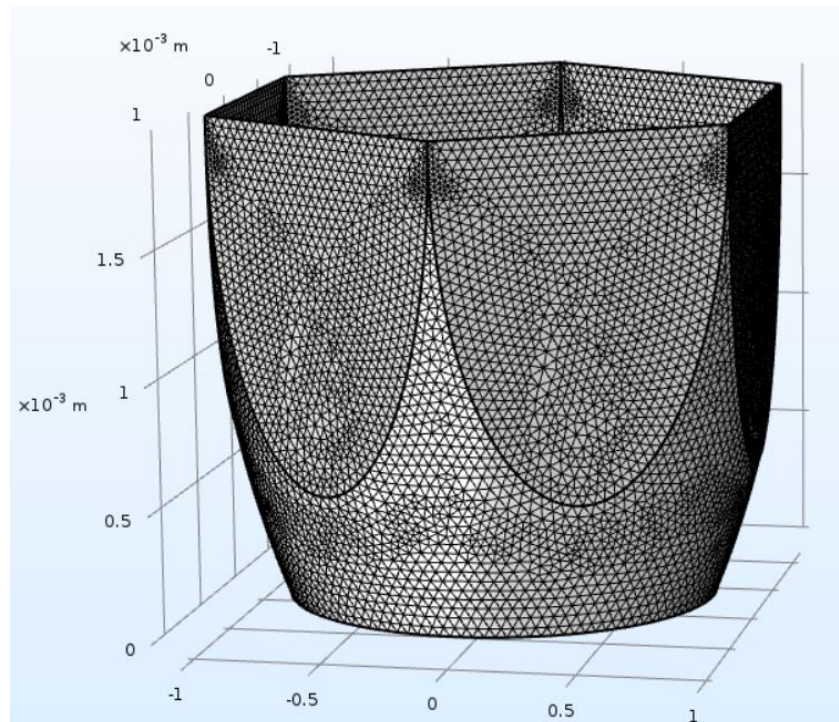
Figure 58. Hex-round mesh created with COMSOL in order to decrease the difference area factor.

In addition, a different mesh is created with a special meshing in the edges to avoid such high size differences, the difference between the biggest and the smallest area decreases ten more times (From about 10,000 to 1,000 times). For further researches, those meshes should be tested and increased the number of rays or refined the meshes if necessary.

3.6 Elliptical-Round shape

The last shape to be tested it is the elliptical inlet and round outlet and. The number of rays used for this simulation is $3 \cdot 10^7$, and the mesh is formed by 14,592 triangles. The Figure 59 shows this graph. The peak absorbed power is about 100kW/m^2 and the total power absorbed is about 140kW. The spatial distribution of power absorbed in the SC is the expected, since it is concentrated in the upper part of the East and West part in the SC. The only difference lies in the color scale, which is not clear than in other shapes. Now the contrast in the colors is not that easy to appreciate.
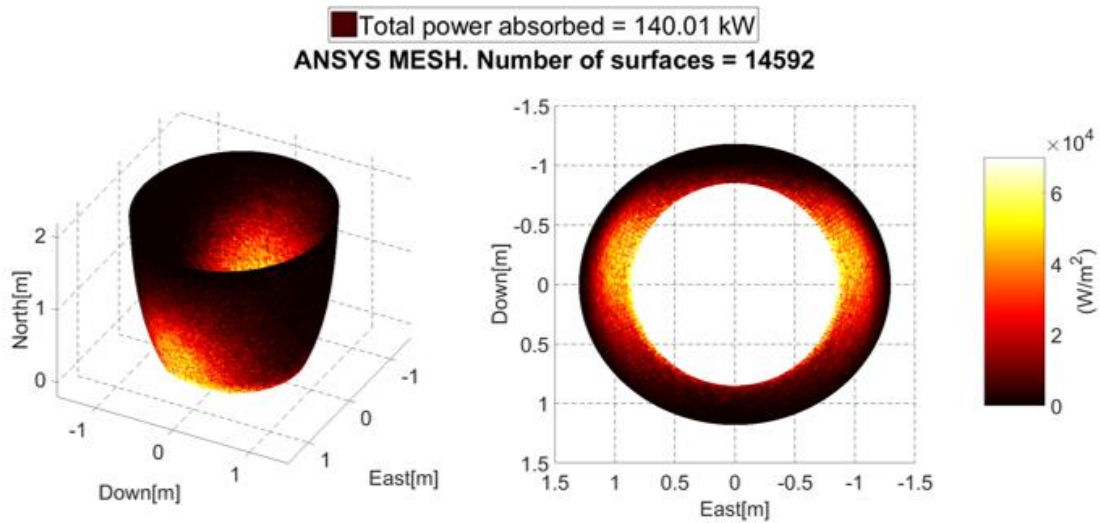
Figure 59. Elliptical-round SC absorbed power, March 21, 1200pm Number of rays: $3 \cdot 10^7$.Number of cells: 14,592

In order to test if a clearer spatial distribution is obtained with the alternatives shown in the section 3.2, the number of rays is increased from $3 \cdot 10^7$ to $6 \cdot 10^7$ and the number of cells decreased from 14,592 to 7,208. The Figure 60 shows this graph.
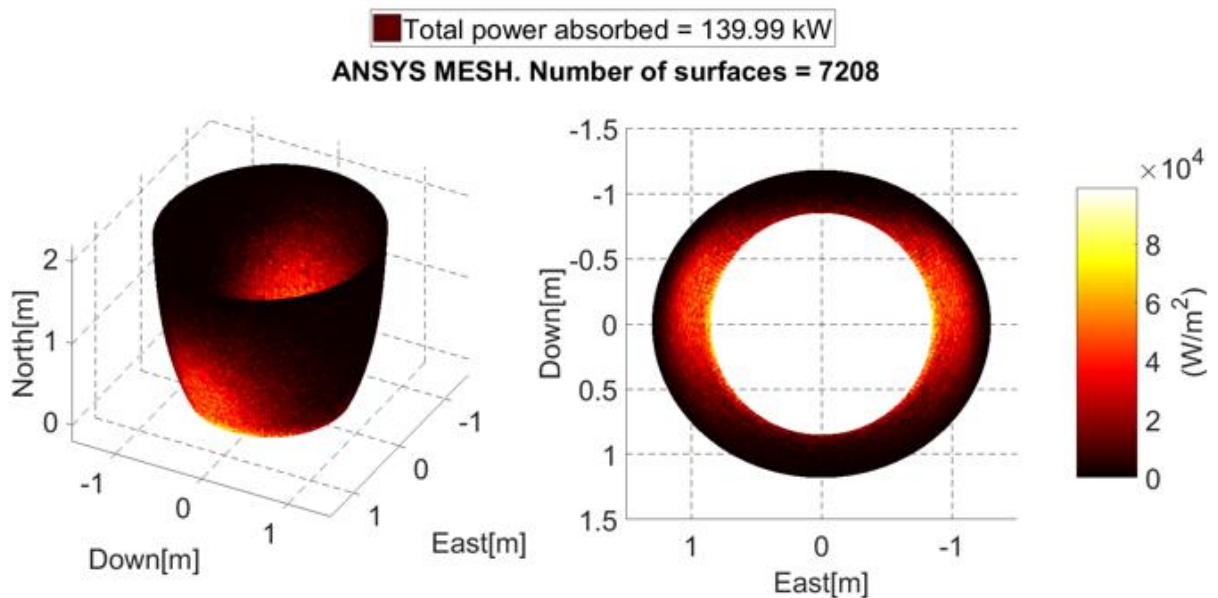
Figure 60. Elliptical-round SC absorbed power, March 21, 1200pm Number of rays: $6 \cdot 10^7$. Number of cells: 14,592.

Now the total power absorbed is still the same but the peak absorbed power is about 70kW/m^2, since the spatial distribution is more homogenous. For this reason the contrast

in the colors is more clear and the spatial distribution of power absorbed is easier to appreciate.

3.7 Different moments in the year

Finally, the round-round shape is tested for different days during the year in order to observe the progressive change in the spatial power distribution when the sun is in different relative position during three days, concretely on: December 21, March 21 and June 21. The mesh is still the same with 14,400 cells and the number of rays used in every case is $3 \cdot 10^7$. The Figure 61 shows these results. The total power absorbed decreases progressively from December to March and June respectively. In addition the peak absorbed power is increasing as it shows the colorbars. Since all the simulations are run at the same time (1200pm), all of them show a power absorbed symmetric distribution, concentrated in the upper part of the East and West part in the SC.
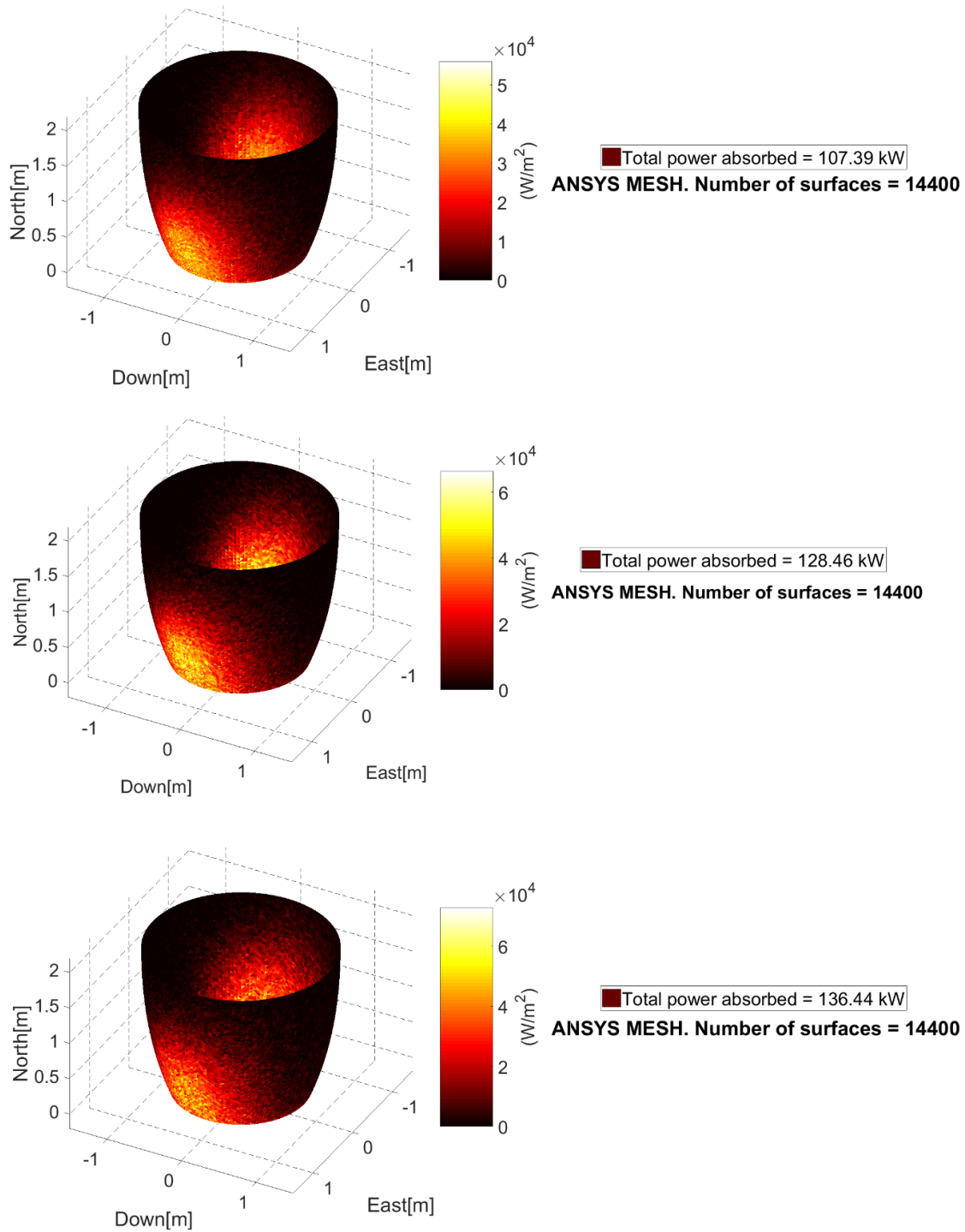
Figure 61. CPC absorbed power, 12pm, December 21 (top), March 21 (middle) and June 21 (bottom). Graph obtained from the ANSYS mesh with 14,400 cells and $3 \cdot 10^7$ rays.

DAVID CEREZO AGUADO

4. CONCLUSIONS

A method to graph the distribution of power absorbed for different secondary concentrator shapes has been developed. Despite of the previous researches have used the stability of the global powers results as the only method to calculate the quality/convergence of the solution, in this thesis has been demonstrated that when the power spatial distribution is calculated, also the maximum flux (kW/m²) must be calculated and taken into account as a main variable to define the quality of the results, since the global powers results are an average for all the mesh cells.

The number of surfaces/planes/cells can be decreased in the mesh and the global powers obtained will not vary practically. In addition, the mesh can be "redistributed" to get a more homogenous cells area proportion, and the global powers obtained will not vary practically.

Inspecting the different tables obtained, it has been decided to use $3x10^7$ rays for studying the parameter "Power absorbed" in the SC, making sure that the convergence is obtained with less than 0.6% of variation for any case. The parameter "power reaching the window" converges with a smaller quantity the rays than the power absorbed in the window. That means that it has been demonstrated how the simulations for the power reaching the window, made in previous research, with $3\cdot10^6$ rays, have a convergence with less than 0.5% of variation. However, in the calculations accomplished for the hex-hex and hex-round shapes the acceptance angle was not taken into account. This subroutine has been added to the code.

The FORTRAN code has been modified so the target plane can be bigger than the SC inlet. Therefore, it will be possible to calculate the percentage of rays, which are hitting inside and outside of the SC inlet. In addition, the global values and the spatial distribution of the power absorbed for different moments of the days and different days in the year have been calculated and graphed. Finally, the elliptical inlet implies a higher number of rays hitting inside the SC inlet, but since it has a more concave shape than the CPC, the number rays rejected after reflection increases, and, finally the power incident in the window is lower than the CPC shape.

DAVID CEREZO AGUADO

5. FUTURE WORK

5.1 Cooling system design

The model generated in this research outputs the power absorbed by each mesh element for a specific time of day. When several simulations during different times on the day are performed, (for example 12pm, 2pm and 4pm) the SC power absorbed, in different times of the day, is obtained, and it is possible to approximate the curve for the energy absorbed during the course of one full day (see Figure 11). The MATLAB code was designed to obtain the same sequence of surfaces when the "AbsorbedPlane" file and the "Shape" file are compared, creating a homogeneous output being able to work in a simple way as an input in the future. Since, in this research only a surface (zero thickness) model was studied for the power absorbed by the mesh elements, a new model has to be generated with the specified material and thickness. The temperature distribution in the new model can be calculated from the power absorbed by the zero thickness model and the properties of the defined materials. The temperature distribution from the new model can be used to calculate the need for active cooling in the SC.

5.2 Heat Transfer and Optical Model

In this and previous research only the optical effects in the SC have been taken into account to calculate the power incident on the window. The temperature of the SC cavity increases since it absorbs power during the day, so the cavity emits radiation, both to the surroundings and to the window. The model can be improved if this emission effect is included. A heat transfer and optical model can be created to combine both phenomena and get a more accurate solution since the power absorbed data is calculated with the method exposed in this thesis.

5.3 Couple the new heliostat fields and SC new designs

The heliostat field and the SC have been studied and optimized by separate calculations, since it was not possible to simulate more than one SC shape so far. Now that any shape can be simulated, it will be possible to modify both parameters (SC shape and Heliostat Field) and study the behavior in a unified way. In this thesis, the elliptical inlet has been

studied for the Sandia National Laboratory heliostat field. A possible further work related to the idea exposed in this section, would be to design a heliostat field, which instead of being aimed at only one point, is aimed at two different points on the aperture plane. There are already different heliostat fields designs for MIRVAL, accomplished in the SDSU C&SEL laboratory, which make studying the heliostat field somewhat easier.

5.4 Use energy runs for optimized the SC shape

Most of the simulations accomplished to test the SC and the heliostat field have been done for a specific time and day. If the objective is to design a SC shape which gets more transmitted power through the window, MIRVAL allows simulations to be run for the whole year. Instead of simulating 4 days in the year [Alvarez] and extrapolate the solutions for the whole year, it will be interesting to vary the main parameters and try to obtain the greatest power incident, optimizing the set of parameters. It is necessary to take into consideration that most of the parameters have been optimized for certain days of the year so far. The most intuitive example is the tilt angle explained in section 2.8.

5.5 Coupling SC and window code

In a previous research in SDSU C&SEL [Ahmet] studied the optical properties of the window in function of the material and the shape. In this and previous researches, the window is not interacting with the system. If the window is coupled in the system, and the shape and the properties taking into account (Transmissivity, reflectivity and absorptivity), not every ray which is reaching the window will be accepted in the window, but can be reflected from the window to the SC again. An interesting further work will be the coupling both codes in order to get a more accurate solution.

5.6 Integrate the program in MIRVAL

To obtain the power absorbed graphs through the ANSYS method, it is necessary to go through the following three steps.

- First, run MIRVAL to get the .FLX file with the rays hitting the target plane.

- Second, run the FORTRAN code to get the power incident upon the window and the power absorbed in the SC.

- Third, the power absorbed and the shape file are read by MATLAB.

If the FORTRAN code related to the ANSYS method is added to MIRVAL, the second step will not be necessary.

DAVID CEREZO AGUADO

6. REFERENCES

[1] A. Shahsavari, M. Akbari *"Potential of solar energy in developing countries for reducing energy-related emissions"*, Renewable and Sustainable Energy Reviews 90, 275–291, 2018.

[2] N. Kannan, D. Vakeesan *"Solar energy for future world:-A review"*, Renewable and Sustainable Energy Reviews 62, 1092–1105, 2016.

[3] A. Shahsavari, M. Akbari *"Potential of solar energy in developing countries for reducing energy-related emissions"*, Renewable and Sustainable Energy Reviews 90, 275–291, 2018

[4] J. Li, *"Scaling up concentrating solar thermal technology in China"* Renewable and Sustainable Energy Reviews 13, 2051-2060, (2009).

[5] U. Pelaya, L. Luoa,Y. Fana, D. Stitoub, M. Roodc. *"Thermal energy storage systems for concentrated solar power plants"* Renewable and Sustainable Energy Reviews 79, 82–100, 2017.

[6] E. Kabir, P. Kumar, S. Kumar, A. A. Adelodun, K. Kim, "Solar energy: Potential and future prospects", Renewable and Sustainable Energy Reviews 82, 894–900, 2018.

[7] T. Kodama *"High–temperature solar chemistry for converting solar heat to chemical fuels."* Prog Energy Combust 2003;29:567–97.

[8] M. Romero, R Buck, J. Pacheco *"An update on solar central receiver systems, projects, and technologies."* Journal of Solar Energy Engineering 2002;124(2):98– 108

[9] O. Behar, *"A review of studies on central receiver solar thermal power plants,"* Renewable and Sustainable Energy Reviews, Volume 23, July 2013, Pages 12-39

[10] P. Gauché J. Rudman, M. Mabaso W. A. Landman, T. W. von Backström, Alan C. Brent *"System value and progress of CSP."* Solar Energy Volume 152, Pages 106–139 (2017).

[11] W. Fuqianga, C. Ziminga, T. Jianyua, Y. Yuanc, S. Yongc, L. Linhuab *"Progress in concentrated solar power technology with parabolic trough collector system: A comprehensive review."* Renewable and Sustainable Energy Reviews 79 (2017) 1314–1328.

[12] A. Kribus,, M. Grijnevicha, Y. Graya and C. Caliot *"Parametric study of volumetric absorber performance"*, 2014.

[13] W.H. Stein, R. Buck *"Advanced power cycles for concentrated solar power".* Solar Energy 152 (2017) 91–105

[14] M.M. Virgen *"Power and efficiency analysis of a solar central receiver combined cycle plant with a Small Particle Heat Exchanger Receiver"*, San Diego State University, 2015.

[15] E. P. Trullen, *"Heliostat field design and optimization for a small particle solar receiver."* San Diego State University, 2015.

[16] R. Zhai, H. Liu, Y. Chen, H. Wu, Y. Yang. *"The daily and annual technical-economic analysis of the thermal storage PVC-SP system in two dispatch strategies." Volume 154, 15 December 2017, Pages 56-67.*

[17] J. Alvarez, *"Analysis of an arbitrary secondary concentrator for the Small Particle Heat Exchange Receiver"*, San Diego State University, 2016.

[18] J. P. Kotzé1, T. W. von Backström and P. J.Erens. *"NaK as a primary heat transfer fluid in thermal solar power installations"* First Southern African Solar Energy Conference, May 2012.

[19] P. Fernandez, "*Numerical-Stochastic Modeling, Simulation and Design Optimization of Small Particle Solar Receivers for Concentrated Solar Power Plants"*, San Diego State University 2013.

[20] J. Lillan. *"Extensive US project pipeline awaiting dollars and transmission."* Solar Industry, No. 4, 2010.

[21] F. Miller and A. Hunt, *"Developing the Small Particle Heat Exchange Receiver for a Prototype Test."* ASME 6th International Conference on Energy Sustainability, ESFuelCell2012-91337, San Diego, CA, July 23-26, 2012.

[22] A. J. Hunt, *"A new solar thermal receiver utilizing small particles."* In Proceedings of International Solar Energy Society Conference, 1362-66. Atlanta, GA: International Solar Energy Society, 1979.

[23] A. Hunt. *"A New Solar Thermal Receiver Utilizing a Small Particle Heat Exchanger",* 14th Intersociety Energy Conversion Engineering Conference, Boston, MA, 1979.

[24] S.J. Ruther, *"Radiation heat transfer simulation of a Small Particle Heat Exchaner Receiverusing the Monte Carlo Method",* San Diego State University, 2010.

[25] Lane, D. *"Brayton Cycle: The Ideal Cycle for Gas-Turbine Engines in Relation to Power Plants."* Oil and Gas Journal 99 (2008): 54-60.

[26] A. Z'Graggen and A. Steinfeld. *"Heat and Mass Transfer Analysis of a Suspension of Reacting Particles Subjected to Concentrated Solar Irradiation – Application to the Steam-Gasification of Carbonaceous Materials"*, International Journal of Heat and Mass Transfer, vol. 52, pp. 385-395, 2009.

[27] A. B. V. B. F. C. A. C. D. d. V. T. M. L. P. M. R. f. t. S.-1. s.-C. J.A. Aguilar, *"Design, optimization and characterization of the light concentrators of the single-mirror small size telescopes of the cherenkov Telescope Array,"* ELSEVIER, Geneva, 2014.

[28] I. Purohit, P. Purohit *"Technical and economic potential of concentrating solar thermal power generation in India."* Renewable and Sustainable Energy Reviews 78 (2017) 648–667.

[29] O. Berchtold, *"The Analysis of a Secondary Concentrator for the Small Particle Heat Exchange Receiver using the Monte Carlo Ray Trace Method,"* San Diego State University, 2014.

[30] R. Winston, J, Minano, & P. Benitez, *"Nonimaging optics."* Saint Louis, Mo, USA: Elsevier Science & Technology. (2004).

[31] M. C.-S. M. R. C. W. c. H. L. M.-A. A. García, *"Durability Of solar reflector materials for secondary concentrators used in CSP systems,"* ELSEVIER, no. 17 June, p. 13, 2014.

[32] A. Kribus, M. Huleihil, A. Timinger and R. Ben-Mair, *"Performance of a rectangular secondary concentrator with an asymmetric heliostat field",* Solar Energy Vol. 69, No. 2, pp. 139–151, 2000

[33] M.F. Modest, *"Radiative Heat Transfer."* Third edition. 2013.

[34] A.M. Mecit*, "Optical analysis and modeling of a window for small particle receiver using the monte carlo ray trace method."* San Diego State University, 2013.

[35] S. K. Park and K. Miller. *"Random number geuerators: Good ones are hard to find. communications of the acm."* Number 10. October 1988

[36] P. L. Leary, J. D. Hankins *"A User's Guide for MIRVAL-A Computer Code for Comparing Designs of Heliostat-Receiver Optics for Central Receiver Solar Power Plants",* Sandia Laboratories 1979.

[37] P. Garcia, , A. Ferriere, and J. Bezian. *"Codes for solar flux calculation dedicated to central receiver system applications: A comparative review."* Solar Energy 82, (2008): 189-197.

[38] Gui-Long Dai, X.-L. X.-C. (2011). *"Numerical investigation of the solar concentrating characteristics of 3D CPC and CPC-DC".* Solar Energy 85, 2833-2842.

[39] T. Cooper & A.Steinfeld, *"Derivation of the Angular Dispersion Error Distribution of Mirror Surfaces for Monte Carlo Ray-Tracing Applications."* ASME J. Sol. Energy Eng., 133. (2011).

[40] http://www.sandia.gov/

DAVID CEREZO AGUADO

[41] Optics of solar central receiver systems: a review. L. Li, J. Coventry, R. Bader, J. Pye, and W. Lipiński *"Optics of solar central receiver systems: a review"* Optical Society of America, 2016.

[42] R. Siegel, J. R. Howell. *"Thermal Radiation Heat Transfer."* 4th ed. New York:Taylor and Francis, 2002.

[43] H., A. Schweiger, M. Oliva, M. Costa, and C. D. Perez Segarra. *"A Monte Carlo method for the simulation of transient radiation heat transfer: application to compound honeycomb transparent insulation."* Numerical Heat Transfer B-35, (1999): 113-36.

[44] J. R. Mahan, *"Radiation Heat Transfer. A Statistical Approach."* New York: Wiley, 2002

[45] M. Spiegel, R. Schaum's *"Outline of Theory and Problems of Probability and Statistics."* New York: McGraw-Hill, 1975.

[46] A.Wang and M. F. Modest. *"Spectral Monte Carlo models for non-gray radiation analysis in inhomogeneous participating media."* International Journal of Heat and Mass Transfer 50, (2007): 3877-89.

[47] Lipinski, W., A. Z'Graggen, and A. Steinfeld. *"Transient radiation heat transfer within a nongray nonisothermal absorbing-emitting-scattering suspension of reacting particles undergoing shrinkage."* Numerical Heat Transfer B-47, (2005): 443-57.

[48] W.T.Welford. *"High Collection Nonimaging Optics."* San Diego, California 92101: Academic, 1989.

[49] M.Umair, A. Akisawa and Y. Ueda *"Optimum Settings for a Compound Parabolic Concentrator with Wings Providing Increased Duration of Effective Temperature for Solar-Driven Systems: A Case Study for Tokyo",* Energies 2014, 7, 28-42

[50] J. A. Duffie, W. A. Beckman. *"Solar Engineering of Thermal Processes",* 4th Edition, 2013

DAVID CEREZO AGUADO

APPENDIX A

Definition of the elliptical inlet in the code

In order to understand how the geometrical conditions are defined a brief explanation of the code is given in this section. The ellipse is divided in the 4 quadrants, and all the rays are transferred to the first 0-90 degrees to make the code easier. The ellipse equations integrated in the code are already exposed in the section 3.6, and the Figure 62 shows a scheme of the process.
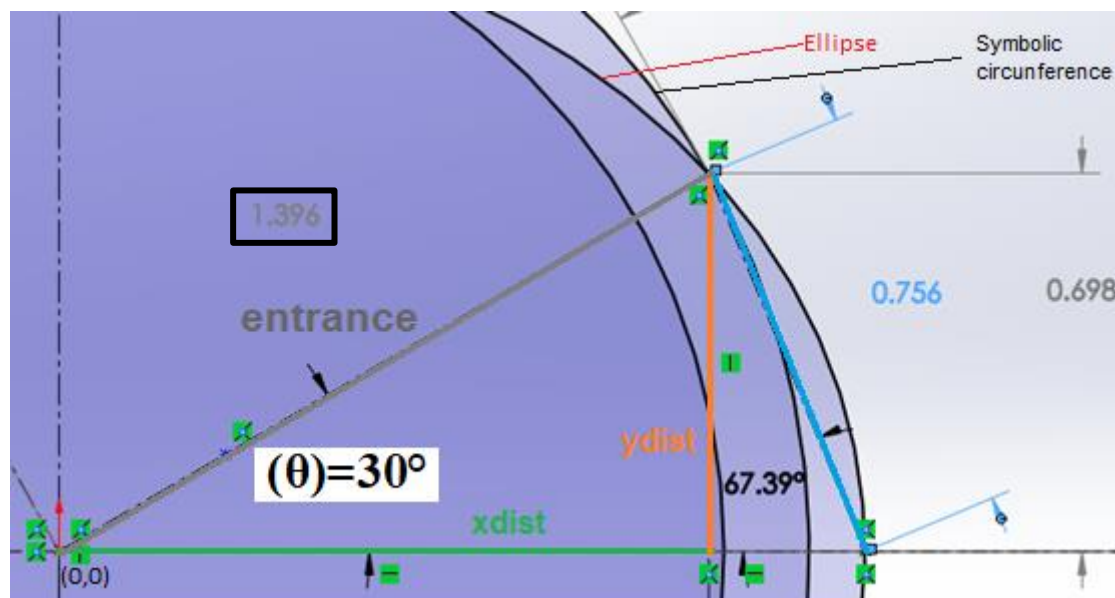

Figure 62. Measure of the main parameters in the elliptical inlet used for the code verification.

The incident ray angle is calculated with the XVAL and YVAL, which are obtained from MIRVAL. The center of the coordinate axis is "joined" with the incident ray point and prolonged until the intersection with the ellipse. Now, a "symbolic" circumference is drawn, with center in the 0,0 of the axis coordinate, and the round is defined by the intersection point before calculated with the ellipse. These successive circumferences for every ray are the successive entrances. Then, the Rimpact and the successive Rcircunferences are compared for every case to define if the rays are inside or outside of the SC inlet. The ellipse is drawn in SOLIDWORKS and the variables calculated theoretically with two different methods in order to check if the equations are well defined. The figure 60 shows the example studied. For a Semimajor and semiminor given,

a θ=30º is chosen and the main parameters are measured. Then, those parameters are calculated with the polar coordinates and the Table 15 shows the results:

Table 15. Elliptical inlet code verification trough the calculations of the entrance with polar coordinates.

Polar coordinates		
eccentricity	-	0.617378
angle	º	30
	rad	0.523599
entrance	m	1.396344

The eccentricity is calculated for a semimajor = 1.5 m and the semiminor = 1.18 m, then for the case when a ray impact with an angle θ=30º, the entrance is calculated and the value obtained (entrance = 1.396m) is coincident with the measure obtained from the SOLIDWORKS.

UNIVERSIDAD DE VALLADOLID

ESCUELA DE INGENIERIAS INDUSTRIALES

MÁSTER EN INGENIERÍA INDUSTRIAL

"Ray Trace Modeling in a Solar Secondary Concentrator with Various Inlet Shapes"

Autor:

Cerezo Aguado, David

María Teresa Parra Santos

San Diego State University

Valladolid, Julio 2018.

TFM REALIZADO EN PROGRAMA DE INTERCAMBIO

TÍTULO: "Ray Trace Modeling in a Solar Secondary Concentrator with Various Inlet Shapes"

ALUMNO: David Cerezo Aguado

FECHA: 22/06/2018

CENTRO: COMBUSTION & SOLAR ENERGY LABORATORY

TUTOR: Dr. Fletcher J. Miller

RESUMEN

Este Trabajo Fin de Máster está enfocado a las plantas de energía solar concentrada, las cuales usan heliostatos para concentrar la radiación solar en un área relativamente pequeña, con el fin de calentar un fluido. En este Trabajo Fin de Máster un concentrador secundario forma parte del sistema.

El software MIRVAL es utilizado para el trazado de los rayos desde el sol hasta el concentrador secundario. Una vez los rayos entran al concentrador, FORTRAN se utilizará para realizar los cálculos de la trayectoria de los rayos. La forma del concentrador secundario se definirá primero en SOLIDWORKS y después se creará una malla en ANSYS. La potencia absorbida en el concentrador secundario se graficará con MATLAB.

Asimismo, se creará una nueva forma de concentrador secundario la cual será añadida al código y simulada. Con varias formas de concentrador secundario, se podrá crear el óptimo en función del campo de heliostatos dado.

PALABRAS CLAVE: Energía solar concentrada, Concentrador Secundario (SC), SPHER, Trazado de rayos y MIRVAL.